8. Polymer Composites Research and Development

A. Automotive Composites Consortium Focal Project 4: Structural Automotive Components from Composite Materials

Principal Investigators: Libby Berger
General Motors Corporation
Research & Development
MC 480-106-710
30500 Mound Road
Warren, MI 48090-9055
(586) 986-1177; e-mail:libby.berger@gm.com

John Jaranson
Ford Motor Company
Vehicle Design R&A
2101 Village Road MD 3137
Dearborn, MI 48121
(313)390-5842; e-mail:jjaranso@ford.com

Technology Area Development Manager: Dr. Carol Schutte
(202) 287-5371; e-mail:carol.schutte@ee.doe.gov

Contractor: U. S. Automotive Materials Partnership
Contract No.: DE-FC26-02OR22910

Objectives

- Develop methodologies and data for each Automotive Composites Consortium (ACC) member company (Chrysler, Ford, and GM) to implement lightweight, cost-effective structural composites in high-volume vehicles.
- Guide, focus, and showcase the technology research of the ACC working groups.
- Design and fabricate structural automotive components with reduced mass and cost, and with equivalent or superior performance to existing components.
- Develop new composite materials and processes for the manufacture of these high volume components.

Approach

- Design, analyze, fabricate, and test
    1. A structural composite underbody, focusing on cycle time, structural joining of composite to steel, and using continuous oriented fibers.
    2. A second row composite seat (without an integrated restraint system) which will combine the functions of a seat and a load floor.

Accomplishments

- For the underbody, selected glass-fabric sheet molding compound (SMC) as materials and process system from 3 options, and developed processing.
- Completed full design and analysis of composite underbody, saving 11.5 kg.
- Completed fabric drape analysis of the glass-fabric SMC, and validated technique with surrogate tool.
- Demonstrated steel-to-composite weld bonding, in both quasi-static and dynamic testing.
- Designed full underbody tooling, with tool fabrication in progress.
- A composite seat structure comprising bonded composite shells of 40% glass-reinforced polypropylene has been designed. The design also utilizes bonded steel reinforcements for managing local point loads at the attachments. The design has been analyzed and optimized to meet all seat loading requirements.
- The seat design saves 23% (1.74 kg) of the weight of the steel comparator seat. The seat cushion saves 33% (1.29 kg) and the seat back assembly saves 11% (0.40 kg).

Future Direction

- Technical cost modeling for underbody manufacture and assembly into vehicle.
- Molding of full composite underbody, using matched metal tooling and glass fabric SMC.
- Design, analysis, and fabrication of test assembly for underbody, for quasi-static and dynamic testing.
- Repeat the Composite Seat cost modeling exercise with the final design and materials.
- Design and build Composite Seat molding tools and metal reinforcements, manufacture composite parts and reinforcements, and assemble seats.
- Experimental and analytical correlation for both underbody and seat.

Introduction

This project encompasses two components, a composite underbody and a lightweight composite seat, with unique goals with respect to vehicle volume per annum, physical size, materials, and technology development. They both require structural performance with reduced mass and acceptable cost, and with equivalent or superior performance to existing components. For both, our primary objective is to develop analytical and manufacturing methodologies and data for each ACC member company to be able to implement lightweight, cost-effective structural composites in high-volume vehicles

Structural Composite Underbody

The structural composite underbody is part of the USAMP Multi-Material Vehicle (MMV) project, and will follow the MMV vehicle technical specifications. The primary research outcomes of this project are:

- A 2 ½ minute cycle time (100k vehicles per year, 2 shift operation)
- Developing methods of joining and assembly of the underbody to the Vehicle
- Processes for fabricating oriented reinforcement within the time window

Phase 1 of this project was the preliminary design of the composites underbody and the selection of the materials and processes. Three material and process systems were investigated: SMC, long-fiber thermoplastic, and urethane long-fiber injection, with several subsets of each characterized. Based on the ability of each to meet program requirements and a technical cost model, glass-fabric SMC with a low-density SMC core was selected as our material and process system.

Phase 2, which is underway, is the full design of the underbody, based on a Large Rear Drive Vehicle (LRDV). This design includes:

- The whole underbody, suitable for tooling design and fabrication
- Manufacturing plan for the component
- Plan for joining and assembly to the vehicle structure
- Validation of materials, processes, and analysis methodologies and assumptions

Phase 3 will be fabrication and testing of the underbody, including correlation of analytical and experimental results.

In Phase 1, a preliminary composite underbody design was developed to replace the steel assembly from the donor vehicle. The preliminary design takes into account three proposed M&P System candidates, as well as the general vehicle packaging, and assembly and joining requirements. The vehicle level stiffness performance with the composite underbody is required to have equivalent performance to the donor, while crash performance is required to meet applicable government and industry requirements. In this design, one molded composite part replaces 16 steel components, as shown in Figure 1.

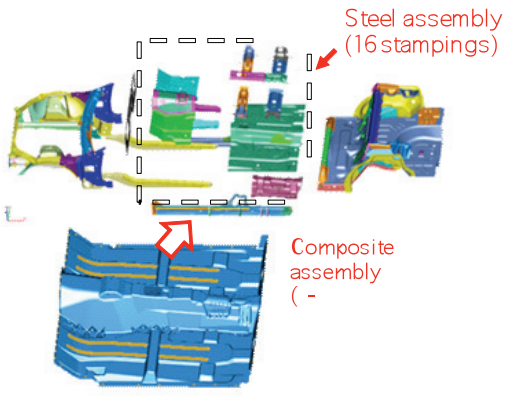

Figure 1. Preliminary composite underbody design, replacing 16 steel stampings with one molded component.

We found that our primary design driver was the 40 mile per hour Offset Deformable Barrier test. In turn, this pushed us to a strength-limited design, as opposed to stiffness-limited. This contributed to our decision to use glass-fabric reinforcement instead of carbon fabric, as the strength benefit for carbon over glass is much less than the stiffness benefit, driving the excess cost for carbon to $150/kg saved.

One major need is a methodology for structurally attaching the composite underbody to the steel body-in-white (BIW) within our cycle time. For this, we are developing composite-to-steel weld bonding.1 Quasi-static and dynamic testing and analysis are described later in this report.

Using the glass fabric SMC for this complex part will require significant fabric deformation. We have worked with the University of Massachusetts at Lowell (UML) to develop a fabric drape model to simulate the compression molding of this material. This involved experimental characterization of the material, mesoscopic modeling, and experimental verification in a small shaped part. This model was then transferred into our analysis system for verification and further modeling of components.

One point of interest which has been raised about structural applications of composites is how to ensure quality, both after the initial manufacture and through day-to-day usage, or after low-energy crash events. This will require the development of non-destructive evaluation (NDE) techniques that are low cost, robust, and easy to use.

Manufacturing a structural composite underbody and assembling it into a vehicle is a radical change in the vehicle assembly process. We are working on a scenario that will allow this assembly within a generic auto manufacturing facility. This includes technical cost models of both the component manufacture and the vehicle assembly.

Vehicle Model Development

The Phase 1 FE model was refined in Phase 2, based on updated material properties for the SMC fabric and low density (LD) SMC, the locally revised floor geometry, and detailed weld-bond joint geometry The Phase 1 and 2 models are shown in Figure 2, with the detailed joint design shown in the inset. The differences between the two models are revised material thicknesses (thinner 1.8mm minimum, and a thicker 5.15mm maximum thickness), ply orientations, and local radii (improved local strength and draping). To meet the timing for the prototype underbody mold tool, only the most severe load case, the front offset deformable barrier (ODB), was assessed and the underbody thicknesses and layups were revised to provide reasonable performance at this stage in the design. At the time when the CAD model was released for tooling, the mass status of tooled underbody design was predicted to be ~26% lighter than the equivalent baseline steel design, a savings of 11.5 kg. However, the final underbody system design and final mass is currently under development, with additional material and coupon test data being developed. The corresponding mold tool design is shown in Figure 3.

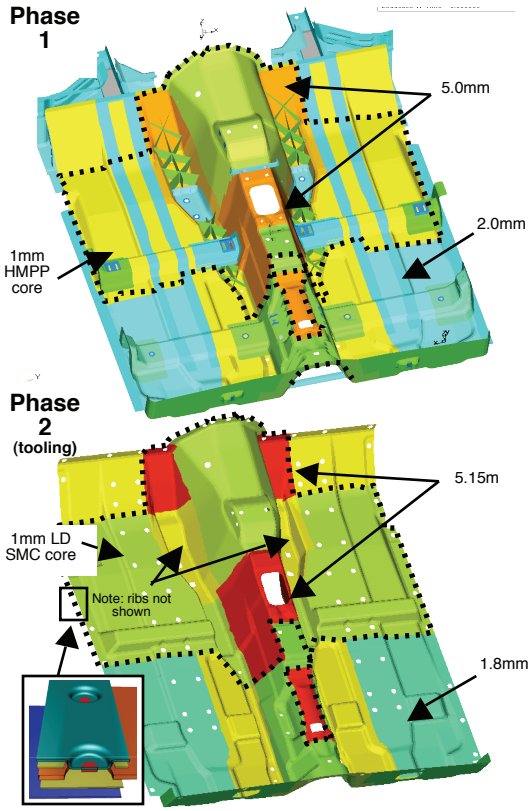

Figure 2. Phase 1 and Phase 2 model comparison

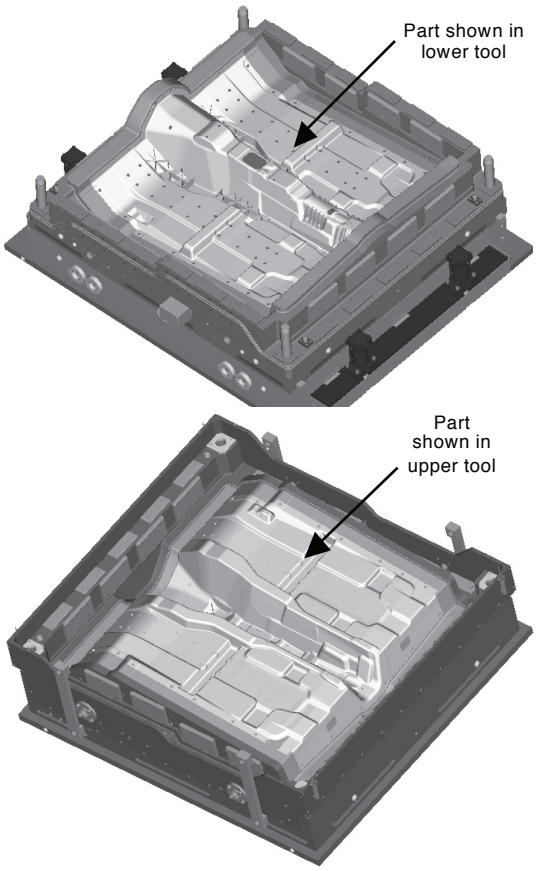

Figure 3. Underbody Tool Design (Century Tool)

Joining of Composite Underbody to Steel Frame

Weld bonding, a combination of spot welding and adhesive bonding, has been selected as the primary method of joining the composite underbody to the steel BIW. Several finite element modeling techniques are being used to evaluate the structural performance of this joint. To generate the physical test data needed to determine the key modeling parameters, quasi-static and dynamic tests were conducted.

Quasi-static tests

120mm wide super-lap shear (SLS) coupons, shown in Figure 4, were subjected to quasi-static tension at different temperatures. Three types of specimens (adhesive only, weld only and weld + adhesive) were tested at three temperatures (-40°C, 23°C, and 80°C). Figure 5 shows the average peak loads at each test condition, while Figure 6 shows the load-extension plots at -40°C, 23°C, and 80°C. The average peak load for adhesive only specimens was in the range of 30kN to40kN.

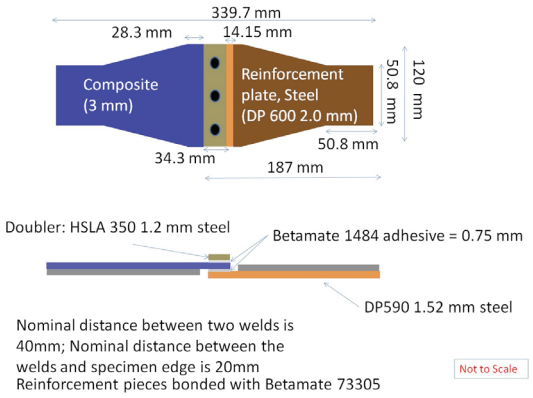

Figure 4. Composite-steel super-lap shear (SLS) weld bonded specimen

The initial failure mode appeared to be the adhesive peel and/or the composite substrate delamination at the edge of a joint or the tabs. Separation of substrates appeared immediately after the initial failure, displaying the brittle nature of the adhesive failure. For weld bonded samples, the average peak

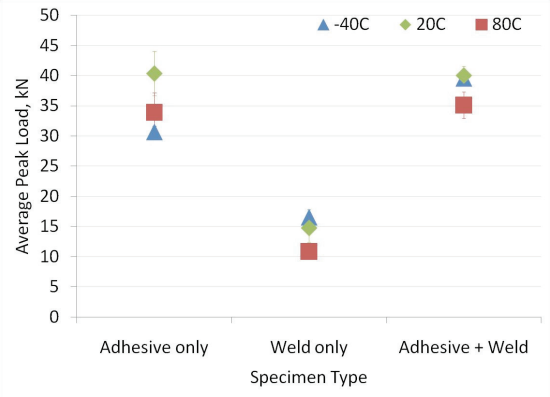

Figure 5. Average peak loads for various types of composite-steel SLS specimens tested under quasi-static loads at different temperatures

load was in the range of 35kN to 40kN. The initial failure mode was similar to the adhesive only samples; however, the presence of welds delayed the separation after the initial failure. Maximum extension for these samples was about 1.5 to 2 times greater than the adhesive only samples. The results confirm the role of weld spots as an adhesive peel stopper. Figure 6 also shows the effect of temperature on the performance of the joint. Weld bonded samples did not show any significant reduction in peak load at -40°C and showed only a slight decrease at 80°C (35kN vs. 40kN at 23°C). Thus, it was concluded that the performance of the weld bond joint was robust within the tested temperature range. In the next phase of testing, the effects of steel gage and the distance between weld spots will be evaluated.

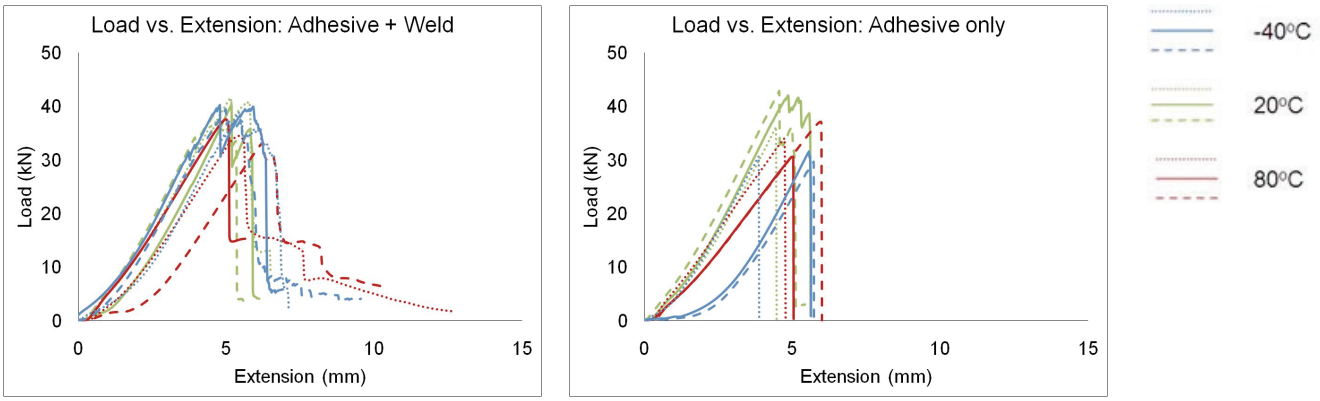

Figure 6. Load vs Extension charts for various types of composite-steel SLS specimens tested under quasi-static loads at different temperatures

Dynamic tests

Due to lack of the industry standards for the dynamic tests for a complex joint specimen such as shown in Figure 4, significant work was needed to develop test methods. This work is in progress at Oak Ridge National Lab (ORNL) and methods are being developed to run dynamic tests on Testing Machine for Automotive Crashworthiness (TMAC). The initial phase of test development used 150 mm wide SLS coupons. Both steel-steel and steel-composites specimens were tested at different speeds ranging from 0.1m/s to 6m/s. Figure 7 shows the sample chart of load vs. stroke with the still pictures captured from a video recorded in sync with the tests, using a high speed video camera (1500 fps). The initial peak and plateau seen in the chart was the result of grip slippage due to slow wedge reaction to load. The failure sequence was similar to the one observed in quasi-static tests. The first failure appeared to be localized peel in the joint due to joint rotation and localized bending, resulting in adhesive disbond

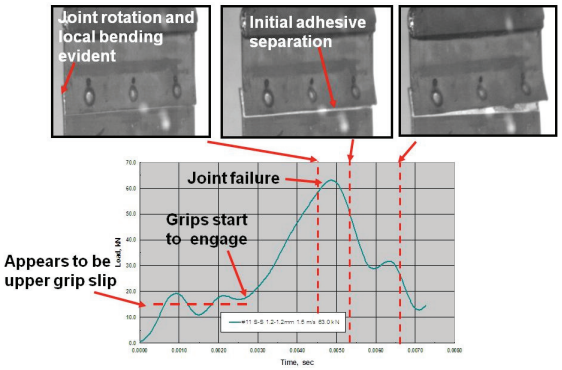

Figure 7. Load vs time chart for 1.2 mm steel-steel SLS specimens tested under dynamic load at 1.5m/s.

followed immediately by weld failure. Based on the limited initial data, it appears that the average dynamic (1.5m/s) peak loads are 20-30% higher than quasi-static peak loads for comparable 150mm wide coupons.

From the learning during the test development, the specimen geometry was revised to 120 mm wide rectangular shape with no taper to the grip area. The final testing will begin upon the completion of custom made 120mm wide grips. The test matrix includes studying the effects of test speed, steel gage, and fabrication methods. The data obtained from these coming tests will be used in structural test-analysis correlation.

Quasi-Static Joint Performance Model Development

Several FE analysis studies were conducted using LS-DYNA analysis software to evaluate the tension, shear, torsion, and four-point bending performance of the original super lap shear (SLS) coupon geometry. The objective of the studies was to (a) aid in the coupon test methodology development and (b) to develop analytical models with sufficient fidelity to capture the basic stiffness and strength response of the joints within the context of a full vehicle FE model. Details of the modeling (e.g. mesh size, constraint types, adhesive modeling, material model parameters, etc.) can have an effect on the results so that a methodology has to be established that best represents the selected materials and geometries. At present, the FE models account for elastic-plastic steel behavior, bilinear elastic-plastic weld behavior without failure, laminated composite behavior with in-plane material failure, and nonlinear adhesive behavior with failure. Composite delamination and tab disbonding are currently not comprehended in the models.

FE models were created for each test configuration and were analyzed using material property and boundary condition assumptions based on the best information available at the time. Predicted SLS coupon responses for 1.6mm thick DP590 steel and 3mm thick fabric composite substrates are compared to available test data for tension, bending, and torsion in Figure 8.

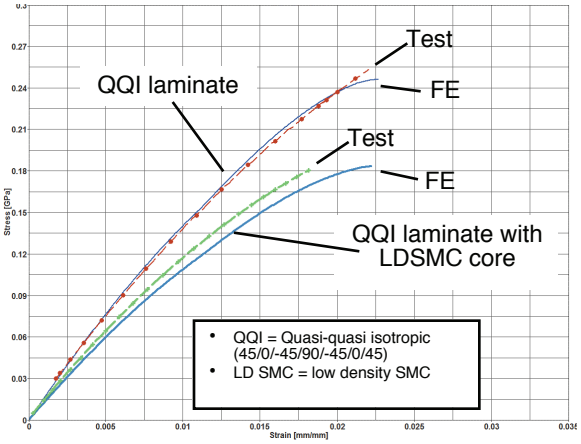

Figure 8: Tensile stress-strain response of QQI laminate with and without LDSMC core

Measured tensile test load vs. deflection data is compared to predictions in Figure 9. The results indicate a similar predicted and measured response up until the measured peak load is attained, with the analysis slightly over-predicting the peak load. Because of the element-deletion methodology used, the post-peak loads are not comprehended in the model. The inset in Figure 9 indicates the region of predicted adhesive failure and subsequent element deletion, resulting in a reduction of joint load carrying capability. The predicted failure mode was found to be consistent with the test observations.

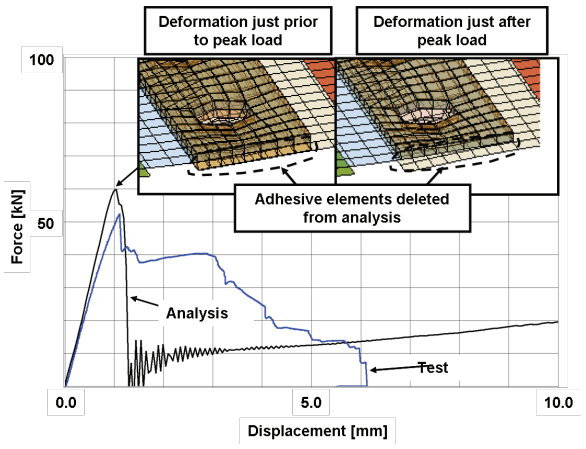

Figure 9. Tensile test vs. analysis load-deflection

Measured 4-pt bending load vs. deflection data is compared to predictions in Figure 10. The results indicate a similar response up until the measured peak load, after which the predicted load response deviates relative to the measured response, which is related to the boundary conditions on the lower rollers. In the analysis, the rollers are allowed to translate laterally,

which reduces the distance between adjacent rollers and results in a stiffening effect due to the test geometry and friction. At peak load, the model exhibits failure in the adhesive and subsequent element deletion, as indicated in the inset in Figure 10. Evidence of adhesive failure and steel substrate yielding was observed in the test samples.

Measured torque vs. angle data is compared to predictions in Figure 11. The results indicate a similar response up until the measured peak load, after which the predicted load carrying capability is reduced due to failure in the adhesive. Evidence of adhesive failure, adhesive disbonding, and steel substrate yielding was observed in the test samples.

All three tested loading conditions correlated reasonably well up to the initial peak load given the basic material assumptions, model boundary conditions assumptions, and predicted failure modes. Additional material and test data will be used to further develop and validate the modeling assumptions for future implementation in the vehicle level model.

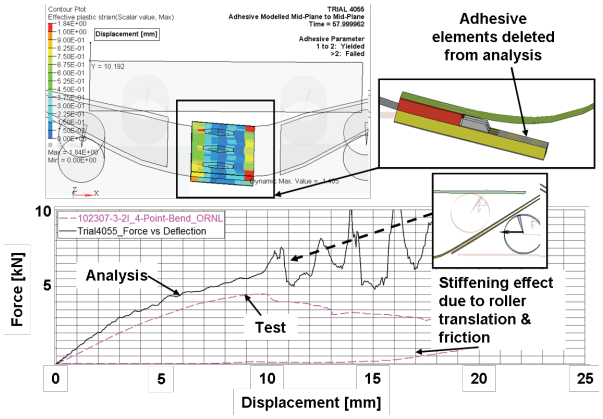

Figure 10: 4-pt bend test vs. analysis load-deflection

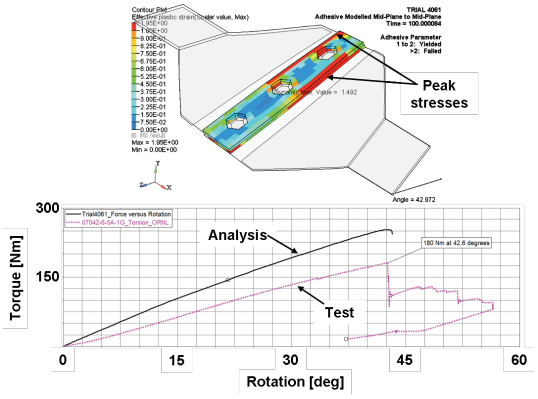

Figure 11: Torsion test vs. analysis torque-angle

Fabric Drape Analysis

The University of Massachusetts Lowell (UML) developed a fabric drape model to simulate the compression molding of fabric SMC material. The initial application of the model was to determine whether the underbody design was manufacturable using a fabric composite, before investing in tooling. The function of the model was verified by bringing the model into our analysis system to replicate the predicted results for several geometry test cases including "double dome" geometry, a surrogate tub geometry, and an initial underbody design. The drape model simulates the idealized shearing of the compounded SMC fabric and predicts shear angle and yarn tension in consideration of friction between fabric and mold surfaces. However, in its present form, the draping model does not account for yarn sliding, spreading, or fiber breakage, the importance of which have yet to be determined.

A major application of the draping model is to aid in understanding the effect of fabric shearing during molding. It is known that fabric shearing can significantly alter local stiffness and strength properties, which can in turn alter the predicted structural performance. The ability to incorporate the effect of draping on structural properties and the resulting performance will be considered in the future.

The UML fabric drape simulation was applied to a second tub component, a rear compartment for which the tooling was available, in an attempt to predict flat ply patterns to support a molding trial. Unfortunately, the simulations failed at ~80% completion due to model instability related to the severe part geometry. As a result, it was not possible to predict an accurate ply

flat pattern shape. Lessons learned from the actual tub molding trials appeared to reflect some of the observed drape modeling difficulties including wrinkles, local tearing, etc. An example of a draping simulation and estimated ply flat pattern is shown along with a physical tub perform in Figure 12. The analysis predicts local regions of high shear and potential wrinkles in regions similar to the physical perform.

In contrast to the draping simulation of the rear compartment tub, the draping simulation of the initial underbody geometry ran to nearly 99% completion indicating a more drapable geometry. Preliminary draping results were used to modify local areas in the underbody component geometry model to further reduce the indicated local regions of peak shearing and fiber tension (Figure 13). The resulting draping performance gave the team confidence to proceed with the development of the mold tooling.

The drape model will be used further to develop the individual plies and their corresponding flat patterns, and to provide a basis for including the effect of shearing on material properties and structural performance.

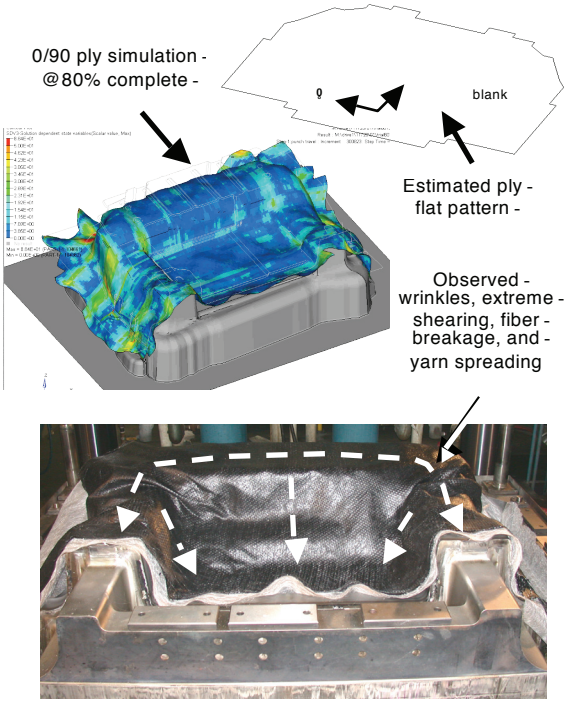

Figure 12: Tub draping simulation and physical tub perform prior to molding

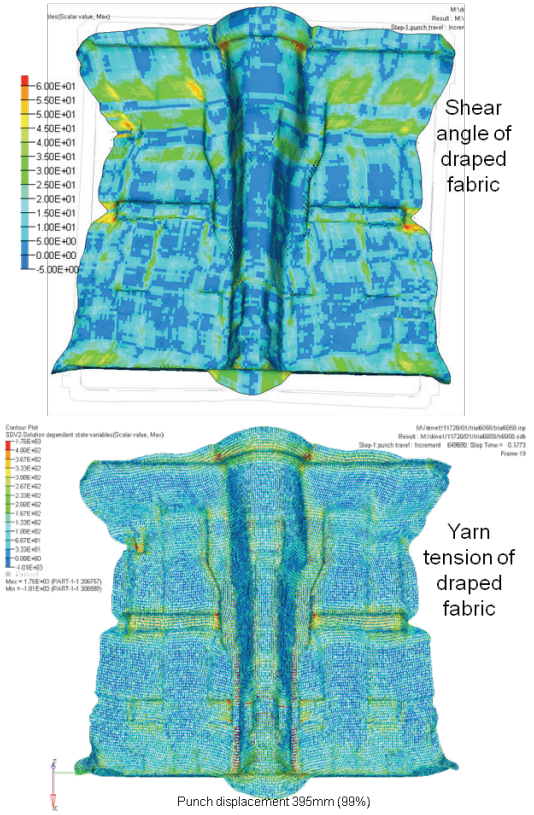

Figure 13: Predicted regions of high fabric shear and yarn tension

Experimental verification of drape analysis

As a qualitative check of the draping simulations described above, further experimental trials were performed in 2009 to evaluate the accuracy of simulation predictions for a laboratory-scale double dome forming tool. The results of this analysis were used to detect any major simulation deficiencies before proceeding with purchase of full scale tooling for manufacture of the vehicle underbody.

The geometry of the double dome forming tool is shown in Figure 14. Initial analysis was performed to predict the unformed 2-D blank shape for 0/90 and 45/-45 fiber orientations. The results of this analysis are shown in Figure 15 and Figure 16. Hence, these blank dimensions defined the shape of cutting templates used during subsequent experimental studies.

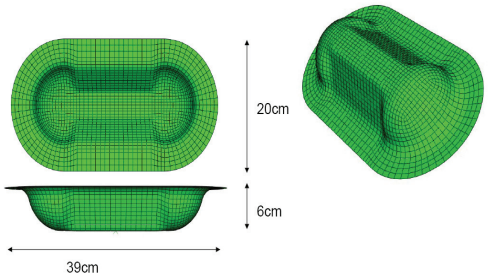

Figure 14. Double dome forming tool.

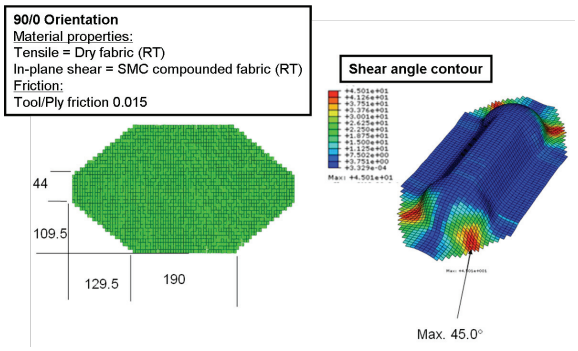

Figure 15. Blank shape predictions for 45/-45 orientation.

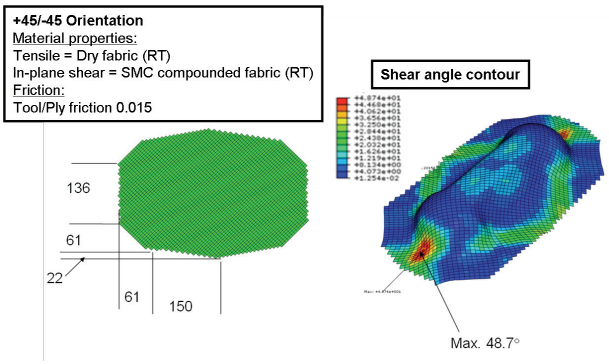

Figure 16. Blank shape predictions for 0/90 orientation.

In Figure 17, the double-dome stamping of a 0/90 sheet is shown alongside its corresponding finite element model result. The contours shown on the deformed model are the in-plane shear strains in degrees. The overall shapes of the model and the molded part are in good agreement. A zoomed-in view on one quarter of one hemisphere of the double-dome (Figure 18) confirms the good performance of the model to capture the resulting yarn orientation in the molded part. One visible difference between the model and the trial molding is that more draw-in is predicted by the model than is observed in the formed part, in particular in the width. The vertical lines shown in Figure 17 assist in seeing the relative draw-in for the model and the experiment. A close examination of the molded parts shows a very large spacing between the yarns on the lateral low sheared zone of the double dome rim. This observation implies that the yarns in the fabric have slipped more than expected, resulting in less fabric draw-in in the actual forming of the part in comparison to that seen in the model. The rim of the punch acted as a “binder” which did not allow the fabric outside the rim to be drawn into the mold. If this “binder effect” had been known before the molding trials, then a “binder” could have been incorporated into the model to account for this phenomenon. The same visual comparison was done for the -45/45 orientation (Figures 19 and 20). The draw-in distance comparison looks better in this case than in the previous fabric orientation.

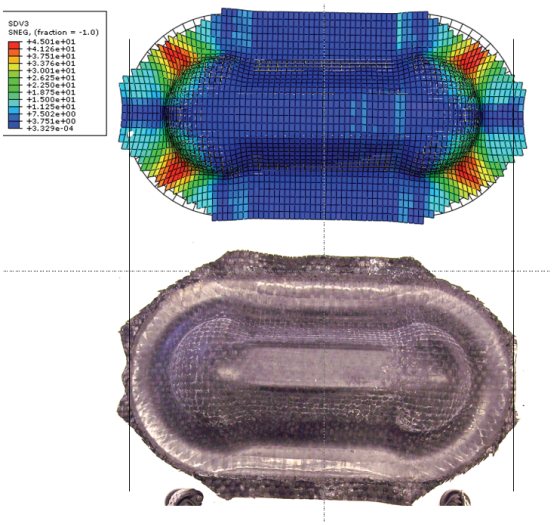

Figure 17. Comparison between simulation and formed component for a 0/90 orientaion.

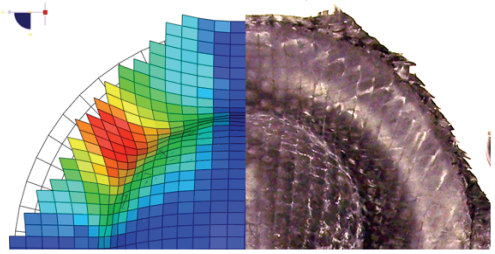

Figure 18. Overlay of numerical simulation on formed part for 0/90 orientaion.

Using an optical method, a measurement of the experimental in-plane shear angles was explored to perform a quantitative comparison between the simulation and the experimental parts. Trials showed that such an optical measurement of the in-plane shear angles was possible. However, because this measurement was beyond the scope of the present study, it was not pursued in detail.

In general, the drape model predictions for the SMC woven fabric show good agreement with experimental results. However, it was observed from the molding experiments that the slipping of the yarns was significant within the rim of the part, leading to some differences between the experiment and the simulation in terms of shear angles and draw-in distances in this region. Nevertheless, no major deficiencies in the modeling technique were discovered. This provided additional confidence that the layup proposed for the underbody tool was feasible. Consequently, the underbody team proceeded with the design and purchase of a tool set for molding of this component.

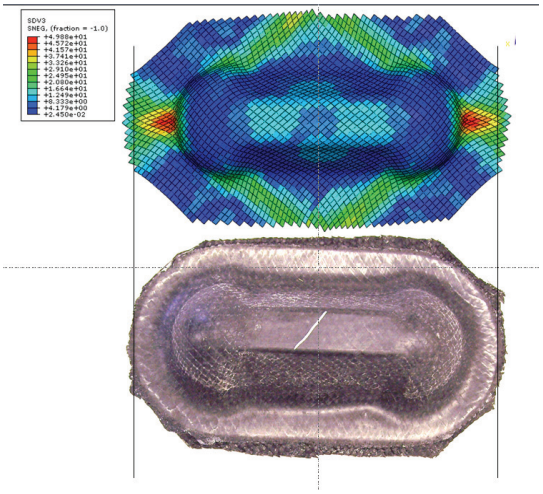

Figure 19. Comparison between simulation and formed component for a 45/-45 orientation.

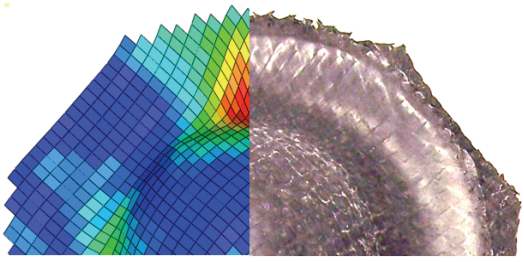

Figure 20. Quarter of hemisphere detail of experimental-simulation comparison of the final shapes for 45/-45 fabric orientation.

Non-Destructive Evaluation

In the 2008 Annual Report for this project, vibrothermography and thermal wave imaging were identified as means of inspecting flaws in weld bonded joints, and may be means of manufacturing inspections. Our work this year has centered on detecting damage to the composite from durability or impact concerns. This will require a low-capital cost appropriate for small, independent collision shops, as well as an understanding of what level of damage is significant for vehicle performance. This investigation is in two parts: detecting impact damage to the surface, and detecting structural damage from durability or impact.

Our first attempt at this was molding test plaques using two different fluorescent compounds imbedded between fabric layers near the center of the material thickness. The intent was to investigate if pre-loading/damage could be detected just using a UV light to search for the imbedded florescent agent. The plaques were subjected to flexural loading to near failure and drop ball point impact. However, neither fluorescent agent was detectable after damage.

A second round of testing utilized a fluorescent penetrant wiped onto the test surface after flexural preconditioning. Again, the flexural loading was not detectable, since no surface cracking occurred until sample failure.

Next, a 2-inch steel ball was dropped 96 inches (13.17 J delivered) onto the supported test plaque. In normal light the cracking is hardly visible, appearing as a minor dent (see Figure 21). However, drop ball impact was detectable with the surface-applied fluorescent dye. Figure 22 shows the impact surface under UV light after a fluorescence dye application.

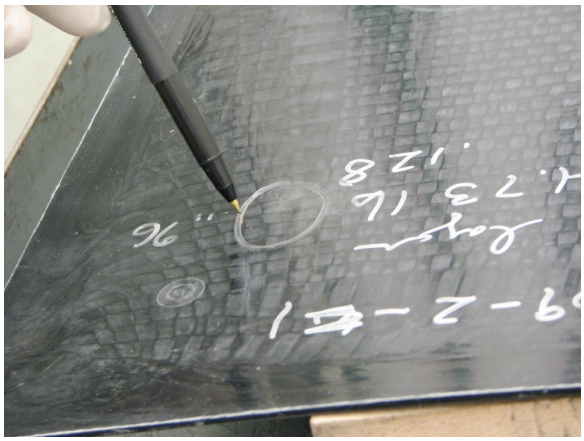

Figure 21. Impact site of 96-inch height ball drop, under normal light

Figure 22. Impact site of 96-inch height ball drop, under UV light

Surface cracks were detectable for impacts down to a 60-inch drop height (8.23 J delivered). In addition, all drop ball impacted samples (in the tested range) showed some indication of sub-surface damage using vibro-thermography or sonic infra red imaging. The fluorescent dye applied to the surface method promises to be a simple, inexpensive method of identifying point impact damage. Our continuing work in NDE involves quantifying the level of damage from pre-loading in a flex configuration, and developing NDE methodologies for this damage.

Underbody Conclusions and Next Steps

A glass-fabric SMC structural composite underbody has been designed, which saves a predicted 11.5 kg mass, and replaces 16 stamped-steel components with a single molded component. Matched metal tooling is being fabricated for the underbody, and molding will begin first quarter of 2010. The material has been developed, and processing in a large, complex part has been trialed with a surrogate

tool. Fabric drape analysis has provided guidance in the design and fabrication. Composite-to-steel weld bonding has been developed, with dynamic testing underway. Non-destructive evaluation of impact damage has been demonstrated, and measurement of damage limits is ongoing. Full underbody assembly test scenarios are being developed, and test assemblies will be fabricated and tested. Experimental and analytical results will be correlated and necessary redesigns made for a fully functional composite underbody.

Lightweight, Low-cost Composite Seat

The primary objective is to develop materials, processes and designs to yield a light-weight, low-cost composite seat structure. Second row outboard stand-alone seats are the target applications with volumes up to 340k units per year. Only the back frame, cushion frame, and the pivoting recline/folding joint will be included in the scope. The project will investigate predominately glass fiber reinforced composites due to cost considerations, but will consider local reinforcement with carbon fiber and other materials including metal in order to achieve a 30% weight save versus the components being replaced. Both thermoset and thermoplastic matrix material will be included. A design achieving a 50% weight savings utilizing carbon fiber reinforced composites is also being developed.

Results from the comparator seat teardowns and testing have been used to develop average weights for a conventional steel seat frame that is used for comparison with the composite seats.

Design Progression

The composite seat design has progressed through three phases of optimization and refinement. The Phase 1 design shown in Figure 23 below is a chopped-carbon-fiber-reinforced nylon composite with localized reinforcing patches of directional carbon fiber. It is a single shell design with ribs for local reinforcement. The seat back is assumed to have a grained surface that removes the need for a close-out trim panel.

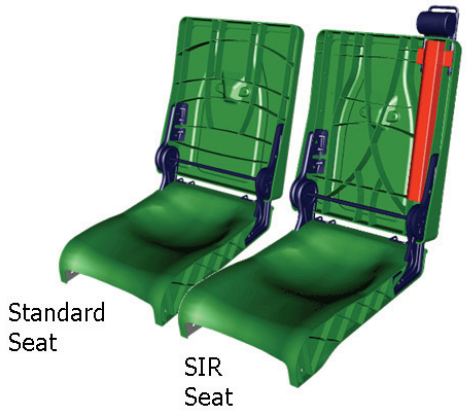

Figure 23. Phase 1 Seat Design

Figure 24. Phase 2 Seat Design

The Phase 2 design shown in Figure 24 is also chopped-carbon-fiber-reinforced nylon. However, it utilizes an adhesively bonded, twin shell design to increase the section properties of the design and to reduce the weight. In addition, the Phase 2 design does not rely on localized patches of directional carbon fiber for reinforcement, and it does not have the requirement for a Class A appearance on the seat back.

The basic design philosophy for the composite parts does not change for the Phase 3 design of the seat. It is a further optimization of the Phase 2 design in carbon fiber/nylon and an optimization of the basic design for glass-filled polypropylene. There is also change in the

attachment design of the seat to the riser. The bolted connections are now in vertical shear, rather than in compression/tension as in Phase 1 and 2. This allows more efficient design of the composite parts and the local metal reinforcements. The Phase 3 base design is shown in Figure 25. The adhesive bonding paths are also shown in Figure 26.

Additional optimization of the Phase 3 design in carbon/nylon was not carried out. The cost per mass saved value did not look favorable. Focus was shifted to the glass/polypropylene version of the Phase 3 design. This version of the seat was taken to a final design for tooling. Additional load cases were included such as headrest, child seat tethering, and knee loading, which added additional detailed structural changes and additional steel reinforcements. The results of these changes are seen in Figure 27.

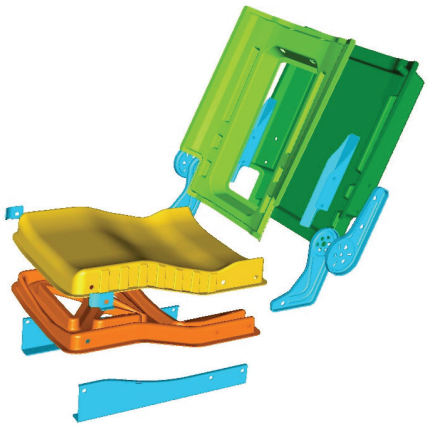

Figure 25. Phase 3 Seat Base Design

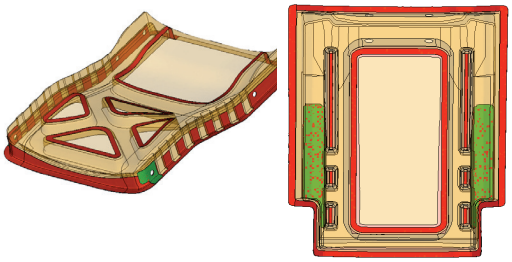

Figure 26. Adhesive paths and reinforcements

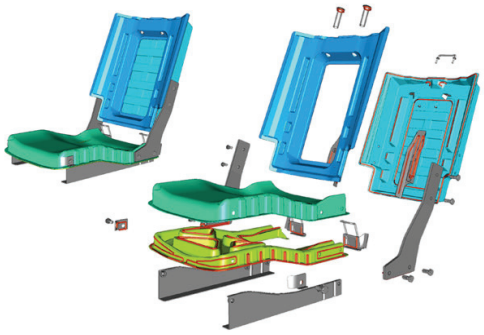

Figure 27. Final composite design – Exploded View

While these changes tended to add weight to the design, thickness optimization of the molded composite parts took weight back out of the seat design. The final thickness distribution of the composite parts can be seen in Figure 28.

Based on the CAE analysis, the final design meets or exceeds the requirements of the following load cases:

- Front and Rear Impact
- Cargo Retention
- Headrest (FMVSS 202A)
- Seat Belt Pull (FMVSS 207/210)
- Child Seat (FMVSS 225)
- Knee Loading

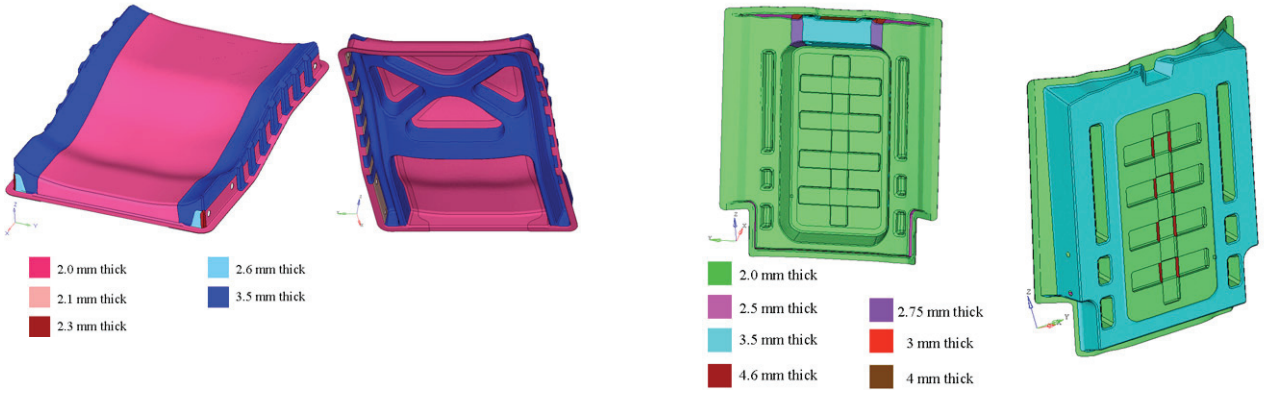

Figure 28. Final composite design – Thickness distributions

Weight Status

The Phase 1 seat design achieves a weight savings of 24% (1.8 kg) for the complete carbon-reinforced seat. The Phase 1 design was hindered by lack of effective section modulus and needed excessive thickness and ribbing to meet the functional requirements in addition to costly directional carbon fiber patches.

The Phase 2 design improved the weight savings to 49% (3.6 kg) for the complete seat. The implementation of a bonded two- shell construction allowed significant improvements in the effective geometric section modulus which allowed reduction in material thickness. The Phase 2 design however, never fully met the structural requirements, particularly in the seat cushion fame, and needed further optimization. The Phase 2 design still was only done in expensive carbon fiber reinforced nylon composite.

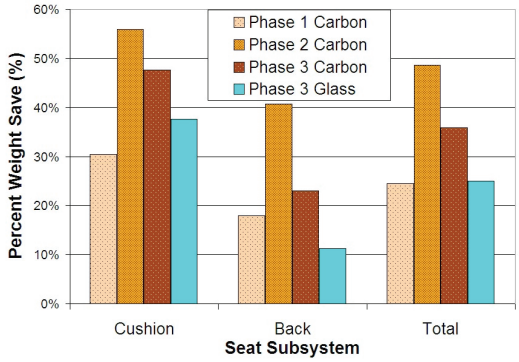

Figure 29. Composite seat weight status

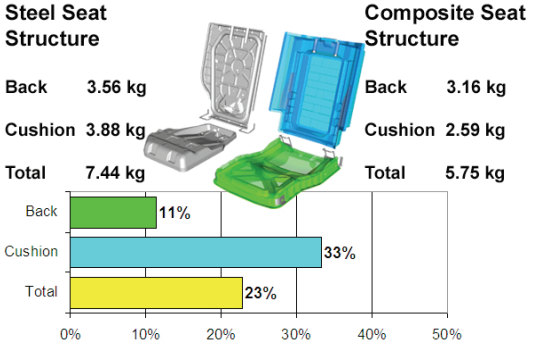

Figure 30. Weight comparison – steel vs. final composite design.

The Phase 3 design addressed the structural shortcomings of the Phase 2 design through further design optimization and by changing the load path between the seat and the seat riser. Phase 3 also introduced glass-filled polypropylene as a means to reduce cost. The carbon reinforced nylon Phase 3 base design achieved a weight savings of 36% (2.67 kg) for the complete seat, and the glass-reinforced polypropylene seat achieved a 25% (1.9 kg) weight save. The details of the weight status with a breakdown of seat back, cushion, and total can also be seen in Figure 29.

As mentioned earlier, the design of the carbon seat did not offer favorable weight savings per dollar and was not optimized further. The glass/polypropylene design was optimized and further load cases applied. The final design results in an overall weight savings of 23% (1.7kg) compared to the steel comparator seat. Details of the weight breakdown are shown in Figure 30.

Next Steps

Future work includes repeating the cost modeling exercise with the final glass design and materials. Molding tools will be designed and built in order to manufacture the composite parts. In addition, the metal reinforcements and brackets and the foam pads will be prototyped to allow build-up of complete seats for testing. Molding trials will commence by the end of the first quarter in 2010.

The completed seats will then be tested for verification of the design. Detailed test plans will be developed.

Presentations/Publications/Patents

L. Berger, H. Fuchs, "Automotive Composites Consortium Structural Composite Underbody," Society of Plastics Engineers Automotive Composites Conference and Exhibition, Troy, MI, 9/16/2009.

J. Sherwood, "Mesoscopic Finite Element Simulation of the Compression Forming of Sheet Molding Compound Woven-Fabric Composites," Society of Plastics Engineers Automotive Composites Conference and Exhibition, Troy, MI, 9/16/2009.

D. Jauffres, et. al., "Mesosocopic finite element modeling of woven reinforcements applied to sheet molding compound forming simulation," Proceedings of the 17th International Conference on Composite Materials. Edinburgh, UK, 2009

References

1 J. P. Fuchs, et al, "Automotive Structural Joint and Method of Making Same," US Patent Application 12119084, 5/12/2008.

B. Composite Underbody Attachment

Principal Investigator: Barbara J. Frame
Oak Ridge National Laboratory (ORNL)
P.O. Box 2008, Oak Ridge, TN 37831-6053
(865) 576-1892; e-mail: framebj@ornl.gov

Team Members:
Donald L. Erdman and Vlastimil Kunc, Oak Ridge National Laboratory

Hannes Fuchs
Multimatic Engineering Services Group
19790 Haggerty Road, Livonia, MI 48152-1076
(734) 591-0773; email: HFuchs@multimatic.com

Technology Area Development Manager: Dr. Carol Schutte
(202) 287-5371; e-mail:carol.schutte@ee.doe.gov

Field Technical Monitor: C. David Warren
(865) 574-9693; e-mail: warrencd@ornl.gov

Contractor: Oak Ridge National Laboratory (ORNL)
Contract No.: DE-AC05-00OR22725

Objective

- Develop a method to predict the effects of environmental exposures and mechanical loadings on the durability of a composite-adhesive-metal (i.e., multi-material) joint. The focus application for this project is the joining of a polymer-matrix composite (PMC) underbody to an automotive body structure.

Approach

- Develop and validate the analytical models and tools capable of predicting multi-material joint performance and durability under multiple loading scenarios.
- Generate an experimental database on the multi-material joint's performance and durability under various loading and environmental conditions to support and validate the modeling approach.
- Establish and define the bounds of validity for the methodology.
- This project is a collaborative effort on the Composite Underbody project (Focal Project 4) between the Automotive Composite Consortium (ACC), Multimatic, Inc and ORNL.

Milestone, Metrics and Accomplishments

- Milestone: Develop and demonstrate durability testing of multi-material joint specimens using super lap shear weld-bonded coupons (completed by July 2009)
- Conducted finite element analyses of types and magnitudes of stresses experienced by weld bonded "super lap shear" specimens under various load conditions.

- Initiated tensile fatigue testing of super lap shear specimens fabricated both with and without spot welds at ambient, 80°C and -40°C. These data will be used for the joint model validation and development effort.
- Prepared test fixtures and equipment to evaluate weld bonded specimens via cantilever bending and torsion test methods. Torsional loading produces high combined peak peel and peak shear stresses in the joint, while bending results in higher peak peel stresses and lower peak shear stresses. Both type load cases are expected in the automotive body structure.
- Conducted preliminary cantilever bending and torsion tests with composite-to-steel weld bonded specimens. Necessary refinements/modifications to the test methodologies were identified.
- Conducted failure analyses of weld bonded composite-to-steel torsion specimens using infrared (IR) thermography method. IR thermography has the potential to provide information on failure mechanisms of joint structures where details of the failure may be obscured by the outer facings of the specimen.
- Identified an available "rear compartment tub tool" for the manufacture of the composite portion of the multi-material joint specimens that will be evaluated in the second phase of this project.
- Designed grips and generated software drive files to enable dynamic (high strain rate) tensile tests of joint specimens using the Test Machine for Automotive Crashworthiness (TMAC). The TMAC is part of the ORNL User facility. These tests are important to understanding the effects of dynamic loading on the performance of composite-to-steel joints in an automotive application.

Future Direction

- Complete tensile fatigue tests of super lap shear specimens fabricated both with and without spot welds at ambient, 80°C and -40°C. These data will be used for the joint model validation and development effort. Milestone: September 2010.
- Complete modifications of super lap shear specimen geometry and test methodology to enable evaluation of joint durability via cantilever bending and torsion test methods. Milestone: March 2011.
- Conduct dynamic tensile tests of composite-to-steel joint specimens using the TMAC. Testing shall be conducted and scheduled at the discretion of the ACC.
- Evaluate validity of durability analytical models with weld bonded specimen test data and make modifications to models as appropriate (Multimatic, Inc.)
- Design specimen, tests, fixtures, and equipment for evaluating multi-material joint durability using three-dimensional (3D) composite molded from "rear tub tool." Milestone: September 2011.
- Continue validation and development of durability analytical models using test data from rear compartment tub specimens as input. (Multimatic, Inc.)

Introduction

The objective of this project is to develop a methodology to predict the effects of environmental exposures and mechanical loadings on the durability of a composite-adhesive-metal joint. The focus application is joining a PMC underbody to an automotive body structure and validating the assembly's long-term durability and performance.

Technologies for attaching/joining PMC parts with other metallic components enable the widespread integration of composites into a predominantly steel vehicle's design and manufacture. This design strategy requires reliable technologies for joining components made of dissimilar materials. Issues associated with joint design include long-term reliability (durability) and ease of assembly (manufacturing cost). Multi-material joining also requires an understanding of the compatibility of the joined members and means of attachment (adhesives, fasteners, etc.) under long-term service conditions.

Attempts have been made to characterize performance of such load-bearing joints in aerospace as well as some automotive applications in the past. However, those earlier results were specific to the geometries, materials, and joining techniques studied. Generic tools for predicting the performance of any composite design do not exist. Consequently, the joint and materials to be used in the PMC underbody must be studied for this particular application.

Because original equipment manufacturers need to minimize the number of developmental prototypes, validated modeling tools must be created to allow them to predict the durability of composite structures with the same level of confidence as metal structures if they are to implement composite structures in vehicles intended to be produced in high volume using common program timing. This project is a step toward achieving that goal.

This project will validate the basic methodology for building computer-aided engineering (CAE) models capable of predicting the durability of composite-to-steel joints. Additional work will be required to expand the models to other types of multi-material joints. However, the tools developed as part of this project will be available for other joint designs, including other material combinations. An additional objective is to characterize the durability performance of the fabric reinforced sheet molding compound (SMC) in combination with the weld bond joint geometry.

Approach

This project is a collaborative effort between the ACC, Multimatic, Inc and ORNL on the Composite Underbody project (Focal Project 4). The key work elements include: (1) design of the multi-material joint tests; (2) material characterization; (3) test article manufacture; (4) mechanical performance of joint specimens for durability; (5) synergistic durability from multiple environmental stressors, and (6) CAE model validation and development. Test-program specifics will be determined based on an analysis of an underbody design project.

The underbody geometry will be simplified to allow extraction of test data representative of the performance of this type of multi-material joint, and a methodology for coupon-level testing of combined environmental and mechanical loading on the joint will be developed. Necessary size and scaling techniques to interpret test results will be established. CAE modeling will be conducted to aid in the design of the test specimens to best replicate real-life joint exposures and to allow for accelerated testing of environmental stressors and joint design due to differing load histories. The validity of existing automotive CAE durability tools for this application will be evaluated. Inputs for model validation and development will be based on test results obtained as part of this project and previous research on similar materials.

As part of this approach, experimental durability test data derived from tensile, bending, and torsional coupon tests, along with appropriate material durability data, will be generated by ORNL and the ACC and will be used by Multimatic, Inc. to develop the appropriate modeling techniques for this project. This, followed by testing and correlation using data derived from a larger structural specimen subjected to two unique loading conditions that produce different types of stress concentrations in the joint will provide a high level of confidence in the validity of the models.

Contributions from the project team are expected to include the following:

ORNL: Project lead, test method development, durability testing, TMAC dynamic tension testing

ACC: Technical consultation regarding automotive industry needs and requirements, material characterization, test specimen fabrication

Multimatic, Inc.: Joint finite element (FE) analyses, CAE model validation and development

Milestone, Metrics and Accomplishments

Deliverables include a composite-to- steel joint coupon-testing protocol, test data, CAE model validation results, and final report. Recommendations to improve the methodology (testing and analytical) will be proposed as deemed appropriate.

ORNL Milestones:

- Develop and demonstrate durability testing of multi-material joint specimens using super lap shear weld-bonded coupons (completed by July 2009)
- Complete tensile fatigue tests of super lap shear specimens fabricated both with and without spot welds at ambient, 80°C and -40°C. These data will be used for the joint model validation and development effort. (September 2010).
- Complete modifications of super lap shear specimen geometry and test methodologies to enable evaluation of joint durability via cantilever bending and torsion test methods. These test methods will enable bend and torsion durability data to be generated for joint model validation and development effort. (March 2011).
- Design specimen, tests, fixtures, and equipment for evaluating multi-material joint durability using three-dimensional (3D) composite molded from "rear tub tool." The durability data produced in these tests will be the final confirmation in this project of the developed joint model(s) validity and applicability. (September 2011).

Durability Modeling (Multimatic, Inc)

Durability modeling of metal structures is well established in the automotive industry; however, the applicability of those models to composite-metal structures has not yet been established. Durability data generated as part of this project will be used to determine what modeling techniques are appropriate for predicting the durability of composite-metal joints.

A two-step approach will be used to validate the suitability of the vehicle level finite element (FE) modeling techniques selected: (1) coupon level models will first be developed to determine the most suitable FE material models for the composite, steel, adhesive, and spot welds and for the FE types and element connection strategies needed to achieve good correlation with experimental test data, and (2) the FE modeling strategies developed from the coupon level data will be employed in the modeling of a larger structural component. The correlation of the modeling results for this structural component with experimental durability data will validate the modeling strategy's applicability to a more complex structure.

To determine what coupon level test data is necessary to develop confidence in the FE modeling techniques selected, analyses of the types and relative magnitude of stresses that result when the weld bonded joint geometry is subjected quasi-statically to tensile, four-point-bend, torsional and guided (rail) shear loads were conducted. Table 1 summarizes the peak adhesive stresses at each loading condition and metal thickness evaluated.

Results indicate that the metal adherend thickness and loading condition have a significant influence

on the peak joint stresses and adhesive stress distribution. The data also shows that the tensile and guided shear loading conditions generally result in low peak peel and high peak shear stresses. Torsional loading produces high combined peak peel and peak shear stresses, while four-point-bend results in higher peak peel stresses (particularly for the thinner metal adherend) and lower peak shear stresses.

Table 1. Peak adhesive stresses as a function of loading condition and metal adherend thickness. Data is provided courtesy of Multimatic Incorporated.

Load Case		Dominant Adhesive Stresses (Approximate Peak Values) [MPa]			Comments
		Peel	XY Shear	YZ Shear	
Tension	0.70 mm GMW2	2	20	15	Generally low peel, high XY, and moderate YZ shear stresses
	1.20 mm HSLA350	8	23	12	
	1.60 mm DP 590	13	23	3	
Guided Shear	0.70 mm GMW2	2	18	20	Generally low peel, high XY and YZ shear stresses
	1.20 mm HSLA350	2	18	20	
	1.60 mm DP 590	10	20	10	
Torsion	0.70 mm GMW2	25	20	18	High combined peel and shear stresses
	1.20 mm HSLA350	25	20	20	
	1.60 mm DP 590	27	13	20	
Bending	0.70 mm GMW2	29	7	2	High peel and low shear stresses
	1.20 mm HSLA350	15	3	3	
	1.60 mm DP 590	5	3	1	

Expectations are that experimental durability test data derived from tensile, bending, and torsional coupon testing, along with appropriate material durability data, should be sufficient to develop the appropriate modeling techniques for this project. This, followed by testing and correlation using data derived from a larger structural specimen subjected to two unique loading conditions that produce different types of stress concentrations in the joint will provide a high level of confidence in the validity of the models.

Tensile and Tensile Fatigue Test

The super lap shear weld bonded coupon, shown in Figure 1, was developed by General Motors for evaluating weld bonded metal joints. Since a significant amount of joint characterization has already been conducted using this geometry, this coupon was selected for the first phase of durability testing of a composite-to-steel joint. Several prototype composite-to-steel weld bonded specimens were provided by the ACC to verify that the ORNL tensile testing equipment and fixtures are suitable for these type specimens, as well as determine what type failure mode results from tensile fatigue.

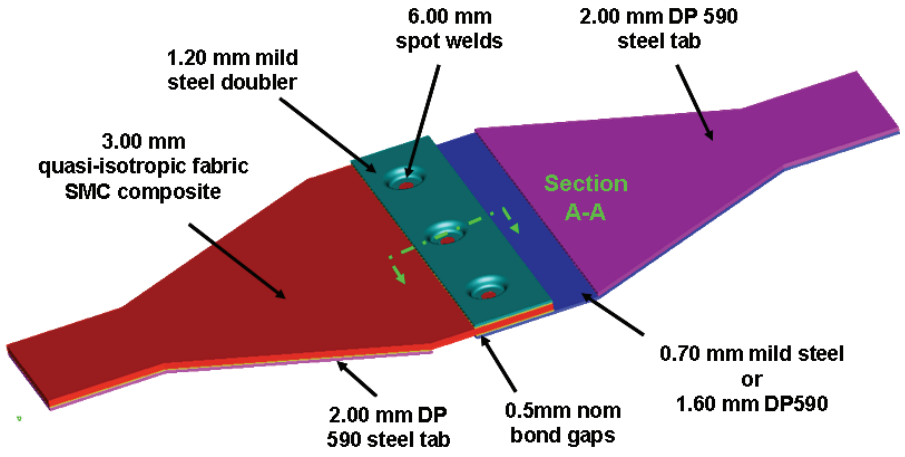

Figure 1. Super lap shear test weld bonded coupon developed by General Motors.(Image is courtesy of Multimatic Incorporated.)

Figure 2 shows a weld bonded coupon installed in an ORNL mechanical test machine and oven set-up. Plots of the quasi-static tensile results from testing two specimens at ambient temperature are shown in Figure 3. The quasi-static tensile test failures were initially in the joint region, and are identified by the initial load reductions visible on the tensile load versus test machine stroke plots.

Figure 2. Super lap shear weld bonded specimen installed in ORNL mechanical test machine and oven.

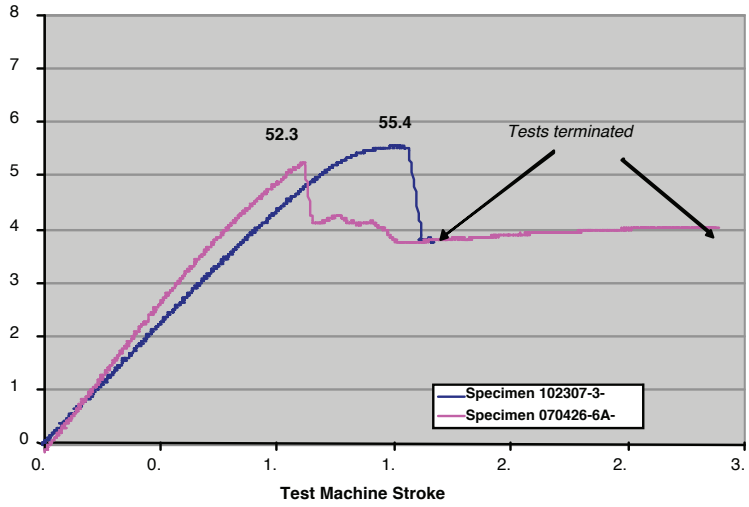

Figure 3. Quasi-static tensile data for two super lap shear weld bonded coupons (tensile load versus test machine stroke).

The specimens continued to "hold together" following initial failure and maintained lower loads via the spot welds. Continued tensile loading of the specimens resulted in the spot welds tearing through the composite laminate at the pre-drilled hole perimeters (see Figure 4) similar to what might be observed by loading a hole with a pin in a bearing test.

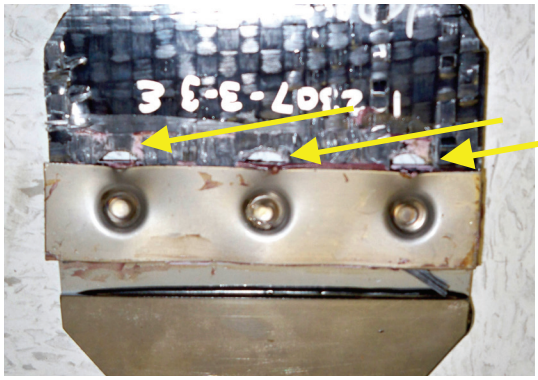

Figure 4. Weld bonded coupon tested in tension. Initial failure was within joint followed by spot welds tearing through composite at perimeters of holes.

Post-failure examination of weld bonded specimens tested under tensile fatigue conditions indicated that these failures also initiated within the weld bonded joint. Therefore this test method should provide acceptable data for development and validation of joint durability models.

One fatigue sample was instrumented with a thermocouple inserted into a hole drilled into the adhesive bond line between the composite and steel tab. The sample was tested to over 10 million cycles at a frequency of 3 Hz without failing. Joint temperature rise measured during the fatigue test was on the order of 2-3°C.

Tensile fatigue testing of ACC-provided composite-to-steel super lap shear specimens has been initiated and is in progress. The specimens were manufacture using the same fabric SMC material that has been selected for the ACC composite underbody, including the same layup, thickness and fiber volume fraction. The test matrix includes specimens prepared with and without weld spots (adhesively bonded only). Results of tests conducted at ambient temperature are plotted in Figure 5. All fatigue tests were conducted with a stress cycle R factor of 0.1 and a frequency of 3 Hz.

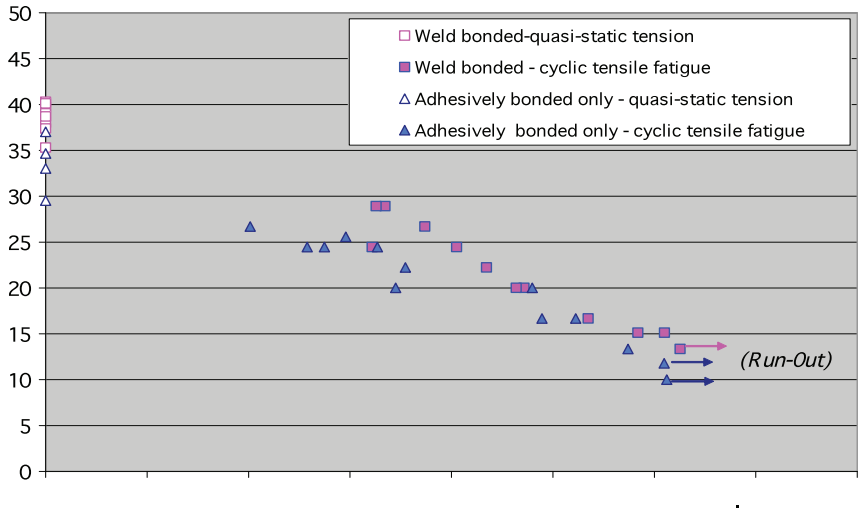

Figure 5. Quasi-static tensile and tensile fatigue results for composite-to-steel specimens fabricated with and without weld spots (adhesively bonded only).

This testing will generate coupon-level durability data needed for this project's model development and validation efforts. In addition, the data will also provide important joint durability information on design hardware to the automotive community.

Cantilever Bend Test and Torsion Test Method Development

Plans are to modify and adapt the basic components of the super lap shear specimen so that it may be used to evaluate the weld bonded joint configuration via both bending and torsional loading. Data derived from these tests will be used to validate that the joint durability models are appropriate for prediction of durability performance under these load conditions.

Initial trials conducted with weld bonded specimens using a four-point-bend test fixture were unsatisfactory because of the relative instability of the un-restrained specimen in the fixture, and the fact that joint failures were not achieved even after large vertical displacements.

A cantilever bend test set-up was therefore devised in which one side of the weld bonded joint coupon is fixed (clamped) while the other side is loaded (see Figure 6). Because movement of the specimen in the test machine is confined to bending at or near the weld bonded joint only, the cantilever bend test provides a more stable method for conducting bend fatigue tests than the four-point-bend test.

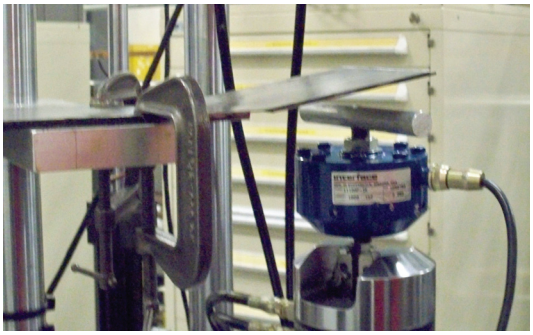

Figure 6. Cantilever bend fatigue test set-up for composite-to-steel weld bonded coupons.

Cantilever bend fatigue tests have been successfully demonstrated with industry-provided composite-to-steel weld bonded specimens. These were low amplitude fatigue tests in which the maximum fatigue load was set at a level below the yield threshold for the steel adherend. After testing for millions of cycles, none of the specimens showed detectable signs of peel or other damage at the weld bonded joint.

To evaluate joint durability, the cantilever bend test method requires careful consideration of the specimen geometry and materials of construction in order to prevent prematurely failing the composite or steel adherends. Plans are to evaluate specimens fabricated with thicker steel adherends and without the spot welds (adhesively bonded only) to determine if joint failures can be reliably produced with this test method.

Quasi-static torsion tests were conducted with weld bonded composite-to-steel specimens in a MTS AT (Axial-Torsional) test machine (see Figure 7).

Figure 8 is a close-up of cracks visible at a corner of weld bonded joint specimen tested to failure. In addition to localized damage in the vicinity of the joint, the composite-to-steel weld bonded specimens experienced a variety of other failure mechanisms that included composite delamination, yielding of the steel adherend, debonding of the reinforcement tabs, grip-induced damage to the composite, etc. This is an issue because in a load controlled fatigue test, these non-joint related failures will result in a premature test termination, rendering the cycles-to-failure data invalid for characterizing joint durability.

The challenge with this torsion test method will be whether the surrounding specimen structure can be made sufficiently robust so that the first detectable failure mode will be in the joint. Plans are to evaluate specimens fabricated with thicker steel and stronger composite adherends, and joined without the spot welds (adhesively bonded only).

Figure 7. Torsion test of composite-to-steel weld bonded coupon in MTS Axial-Torsional test machine.

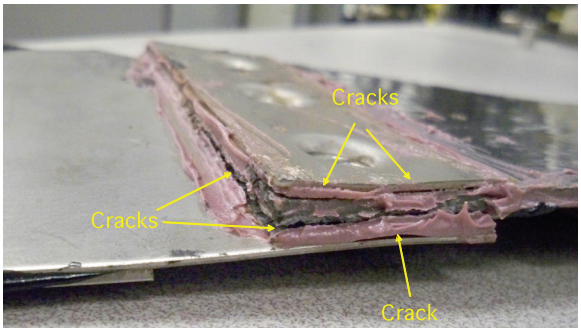

Figure 8. Cracks visible at corner of composite-to-steel weld bonded joint that had been loaded in torsion.

Infrared Thermography Inspection of Weld Bonded Coupon

A series of weld bonded composite-to-steel specimens that had been tested in torsion were examined at ORNL using infrared (IR) thermography in order to identify failure locations and mechanisms. The objective was to determine if the first torque reductions recorded in the plots of torque-versus-rotation were due to failure in the joint or to some other degradation of the coupon.

In this investigation, a weld bonded composite-to-steel specimen was torqued to its maximum rotational capacity in order to generate visible cracks in the joint (see Figure 8). Other damage in this specimen also included yielding of the steel adherend, surface cracks in the composite that initiated at the laminate edges and in the vicinity of the grips, and delamination within the composite wall thickness initiating at the corner of the steel reinforcement tab (see Figure 9).

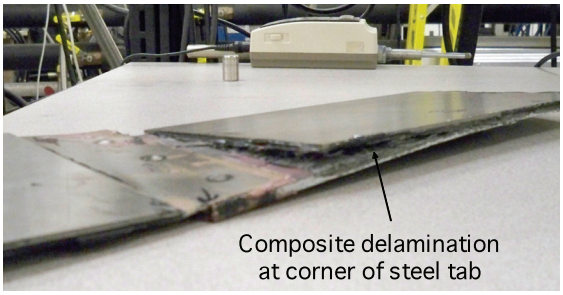

Figure 9. Composite delamination at corner of steel reinforcement tab of weld bonded torsion specimen.

Figure 10 is the IR thermography image of the torsion test specimen shown in Figures 8 and 9. The composite delamination beneath the steel tab is visible as the darker region in Figure 10. Damage in the joint region was not detectable in this analysis, although it can be concluded that despite the high torsional loading, the spot welds did not fail.

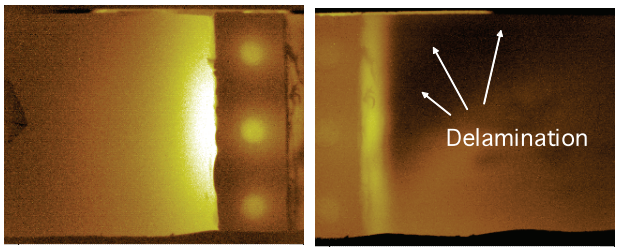

Figure 10. IR thermography image of weld bonded torsion specimen shown in Figures 8 and 9.

Torsion test specimens were also loaded until just past the first reduction in measured torque was recorded, at which point the tests were terminated. The specimens showed no visible evidence of damage or source of the initial failure when they were removed from the test machine for inspection.

Figure 11 is an IR thermography image of one of these specimens that shows the same composite delamination beneath the steel tab as the specimen taken to a higher torque load (Figure 10). The results suggest that the initial torque reductions during testing were a result of a composite delamination beneath the steel tab. Damage in the joint region was not detectable in these analyses.

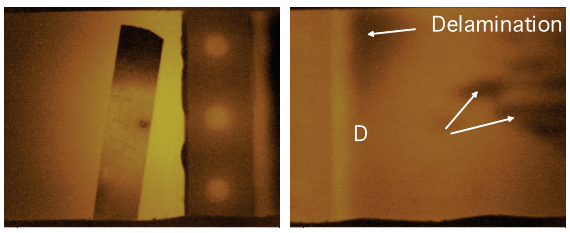

Figure 11. IR thermography image of weld bonded torsion specimen in which testing was interrupted following first recorded torque reduction.

The IR thermography image in Figure 11 also shows some defects that are believed to be discontinuities (debonds) in the adhesive between the steel tab and the composite adherend and/or flaws in the composite. An IR thermography image taken of a comparable specimen that was not tested (as-manufactured) shows the same features (see Figure 12). The data suggest that these debond features are an inherent part of the as-manufactured specimen and not a result of the torsional loading. These debonds were not detected in the bond layer between the steel adherend and the steel tab on the other side of the weld bonded joint.

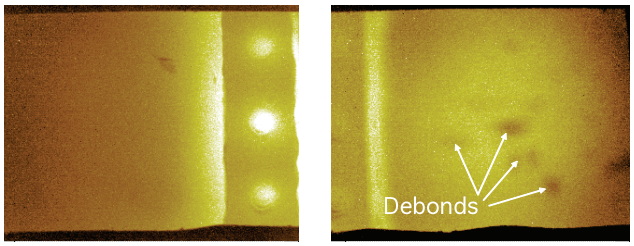

Figure 12. IR thermography image of an as-manufactured weld bonded specimen.

IR thermography may provide a means to assess the quality and uniformity of weld bonded, composite-to-steel assemblies. It has the potential to provide information on failure mechanisms for test specimens and structures where details of the failure (composite delaminations and cracks, weld nugget fractures, etc.) may be obscured by the outer facings of the specimen. Further work will be required to develop an IR thermography technique that can elucidate details of the weld bonded joint integrity through the multiple material layers.

TMAC Dynamic Tension Testing

Preparations are being made to conduct dynamic tension testing of composite-to-steel specimens using the TMAC. These tests are important to understanding the effects of dynamic loading on the performance of composite-to-steel joints in an automotive application.

Preliminary tension testing conducted with the super lap shear geometry weld bonded specimens showed that the existing TMAC grips did not fully engage in most of the tests, resulting in significant slippage and pullout of the specimen during loading. Although it was possible to produce several joint failures during these tests, results also indicated that the tapered width geometry of the super lap shear specimens was inappropriate to transfer load to the joint consistently. A decision was therefore made to modify the specimen geometry to constant width, and to increase the width of the specimen that is clamped by the grips from 50.8-mm (2-in.) to up to 120-mm (4.7-in.) wide.

Wider, higher capacity grips were designed and are being fabricated to accommodate loading to ~130 kN (30 kip) without specimen slippage. Design and fabrication of the new grips is being funded by ORNL.

A deficiency identified in earlier tensile testing trials involved synchronization of the TMAC data collection with high speed video. As previously configured, triggering needed to be done manually when the TMAC was run in tension, vastly increasing the time needed to record, and consequently decreasing the video resolution. In initial trials, most of the failures seemed to take place between one frame and the next so that the actual failure sequence could not be precisely determined.

The TMAC manufacturer (MTS) was contacted regarding this issue and technical support determined the required changes that needed to be made to the drive files. These changes were incorporated by ORNL staff and new drive files that run the TMAC in tension at high rates were generated. The drive files were executed without any specimen loaded in the machine and it was demonstrated that the triggering/timing issues were resolved.

Rear Compartment Tub Tool

Durability test data from single-load case (tensile, bending, and torsional) coupon tests will be used initially in this project to develop the appropriate modeling techniques for composite-to-steel joints. This, followed by testing and correlation using data derived from a larger structural specimen subjected to two unique loading conditions that produce different types of stress concentrations in the joint will provide a high level of confidence in the validity of the models. Plans are that the composite component of that larger structural specimen be molded using an existing rear compartment tub tool.

Use of the existing tool for molding the composite was identified as a low cost way to obtain a surrogate (underbody) part for this project. This component will be used to provide the composite portion of the structure used in sub-structural level testing in the second phase of the project. Composite tubs molded with the tub tool should possess many of the 3D features of the composite underbody design, including the flanges and corner details. Figure 13 is a photograph of a composite section molded using this tool.

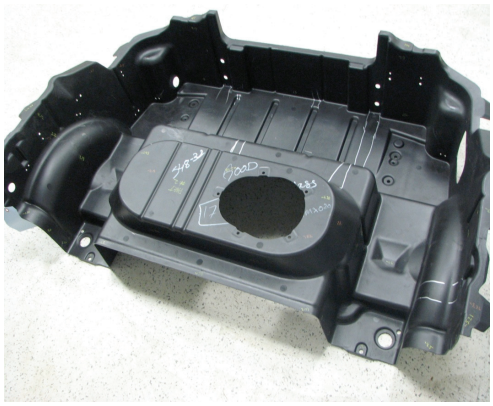

Figure 13. A composite section molded using the rear compartment tub tool.

Design of the tub-tool test specimens is on hold pending results of the super lap shear coupon tests and model validation work.

Summary and Future Plans

To determine what coupon level test data is necessary to develop confidence in the FE modeling techniques selected, analyses of the types and relative magnitude of stresses that result when the weld bonded joint geometry is subjected quasi-statically to tensile, four-point-bend, torsional and guided (rail) shear loads were conducted by Multimatic, Incorporated. Results indicate that the metal adherend thickness and loading condition have a significant influence on the peak joint stresses and adhesive stress distribution. The data also show that the tensile and guided shear loading conditions result in low peak peel and high peak shear stresses. Torsional loading produces high combined peak peel and peak shear stresses, and four-point-bend results in higher peak peel stresses (particularly for the thinner metal adherend) and lower peak shear stresses. All three load conditions (tension, bending and torsion) are expected to occur in the automotive body structure.

Composite-to-steel weld bonded specimens were tested to verify that the ORNL tensile test equipment and fixtures are suitable for these type specimens, as well as determine the type failure mode that results from tensile fatigue. The quasi-static tensile test failures are initially in the joint region. The specimens continue to "hold together" after initial failure and maintain some load via the spot welds. Post-failure examination of specimens tested in tensile fatigue indicates that the failure also initiates within the weld bonded joint. This is significant because this tensile fatigue test method should provide acceptable data for the development and validation of joint durability models. (Milestone completed by July 2009).

Tensile fatigue testing of ACC-provided composite-to-steel super lap shear specimens has been initiated and is in progress. The specimens were manufacture using the same fabric SMC material that has been selected for the ACC composite underbody, including the same layup, thickness and fiber volume fraction. Test matrix includes specimens prepared with and without weld spots (adhesively bonded only). This testing will generate coupon-level durability data needed for this project's model development and validation efforts. In addition, the data will also provide important joint durability information on design hardware to the automotive community.

A cantilever bend test set-up was devised in which one side of the weld bonded joint coupon is fixed (clamped) while the other side is loaded. Because movement of the specimen in the test machine is confined to bending at or near the weld bonded joint only, the cantilever bend test provides a more stable method for conducting bend fatigue tests than the four-point-bend test.

Low-amplitude cantilever bend fatigue tests have been demonstrated with composite-to-steel weld bonded specimens for millions of cycles. In these tests, none of the specimens showed detectable signs of peel or other damage at the weld bonded joint.

Quasi-static torsion tests were conducted with weld bonded composite-to-steel specimens in a Materials Test System MTS Axial-Torsional test machine. In addition to localized damage in the vicinity of the joint, the composite-to-steel weld bonded specimens experienced a variety of other failure mechanisms.

To evaluate joint durability, the cantilever bend and torsion test methods will require careful consideration of the specimen geometry and materials of construction in order to ensure that the primary failure is in the joint. Plans are to evaluate specimens fabricated with thicker steel adherends and without the spot welds (adhesively bonded only) to determine if joint failures can be reliably produced with these test methods.

Weld bonded composite-to-steel specimens that had been tested in torsion were examined at ORNL using infrared (IR) thermography in order to identify initial failure locations and mechanisms. The objective was to determine if the initial reductions observed in the plots of torque-versus-rotation were due to failure in the joint or to some other degradation of the coupon. IR thermography has the potential to provide information on failure mechanisms for test specimens and structures where details of the failure (composite delaminations and cracks, weld nugget fractures, etc.) may be obscured by the outer facings of the specimen. It may also be used to assess the quality and uniformity of weld bonded, composite-to-steel assemblies.

The IR thermography results suggest that the initial failures included delamination of the composite beneath the steel reinforcement tab. Damage in the joint region were not detectable in these analysis, although it may be concluded that even under high torsional loading, the spot welds did not fail. Further work will be required to develop an IR thermography technique that can elucidate details of the weld bonded joint integrity through the multiple material layers.

Preparations were made to conduct dynamic tension testing of composite-to-steel specimens using the TMAC. These tests are important to understanding the effects of dynamic loading on the performance of composite-to-steel joints in an automotive application. Drive files to run the TMAC in tension at high rates have been generated and tested. Wider, higher capacity grips were designed and are being fabricated to accommodate loading to ~130 kN without specimen slippage. The super lap shear specimen geometry is being modified to be constant width, and to increase the width of the specimen that is clamped by the grips from 50.8-mm to up to 120-mm wide.

Use of the existing tool for molding the composite was identified as a low cost way to obtain a surrogate (underbody) part for this project. This component will be used to provide the composite portion of the structure used in sub-structural level testing in the second phase of the project. This tool also replicates many of the significant geometric features of the composite underbody. Design of the specimens based upon this component is on hold pending results of the super lap shear coupon tests and model-validation work.

Future plans and milestones for this project include:

Complete tensile fatigue tests of super lap shear specimens fabricated both with and without spot welds at ambient, 80°C and -40°C. These data will be used for the joint model validation and development effort. (September 2010).

Complete modifications of super lap shear specimen geometry and test methodologies to enable evaluation of joint durability via cantilever bending and torsion test methods. These test methods will enable bend and torsion durability data to be generated for joint model validation and development effort. (March 2011).

Design specimen, tests, fixtures, and equipment for evaluating multi-material joint durability using three-dimensional (3D) composite molded from "rear tub tool." The durability data produced in these tests will be the final confirmation in this project of the developed joint model(s) validity and applicability. (September 2011).

Acknowledgements

The project team would like to acknowledge and thank Ralph Dinwiddie and Hsin Wang at ORNL for conducting the IR thermography examinations and analyses presented in this report.

C. Development of Next-Generation Programmable Preforming Process

Principal Investigator: Robert E. Norris Jr.
Oak Ridge National Laboratory
P.O. Box 2008; Oak Ridge, TN 37831-6053
(865) 576-1179; e-mail: norrisrejr@ornl.gov

Primary Participants:
R. D. Lomax, F. Xiong, Ken Yarborough - Oak Ridge National Laboratory
J. Dahl, G. Smith, P. Blanchard - Ford Motor Company

Technology Area Development Manager: Dr. Carol Schutte
(202) 287-5371; e-mail:carol.schutte@ee.doe.gov

Field Technical Monitor: C. David Warren
(865) 574-9693; e-mail: warrencd@ornl.gov

Contractor: Oak Ridge National Laboratory (ORNL)
Contract No.: DE-AC05-00OR22725

Objectives

- Develop the next generation of low-cost fiber-preforming technologies based on programmable, robotic-controlled, directed chopped-fiber processes for the application of
  1. reinforced thermoplastics,
  2. hybrid glass-carbon, and
  3. low-cost carbon fiber (CF).
- Develop the supporting technologies required to successfully implement the process technology including
  1. preform characterization (e.g., permeability, areal-density uniformity) and
  2. perform-process modeling for process-effects analysis.
- Conduct parametric process studies to investigate fundamental process effects and establish process-property relationships.
- Conduct requisite molding investigations—experimentally and through modeling—to elucidate the relationship between preform characteristics and moldability.

Approach

- Use and expand the base-research, programmable, robotic preforming system for development and evaluation of advanced capabilities (e.g., new chopper designs). Demonstrate capabilities to automotive suppliers and other potential end users.
- Use a highly instrumented and controlled research molding capability to isolate and investigate the effects of process variables on moldability and mechanical properties.

- Develop new or enhance existing severing technologies to facilitate the implementation of low-cost carbon-reinforced thermoplastics and hybrid glass-carbon products.
- Benchmark and incorporate process modeling in experimental work to guide parameter selection and to provide tools for longer-term implementation of preforming and related technologies.

Accomplishments

- Completed extensive characterization of the ORNL-upgraded Wolfangel chopper throughout a wide rage of potential operating speed ranges while mounted on a test stand. Utilized characterization experience to identify likely fiber handling impediments to running the Wolfangel chopper on the preforming robot at the high output speeds targeted for demonstration and developed and implemented system improvements during the course of this activity. Demonstrated capability to run at target outputs on this stand for extended time periods.
- Modified system hardware and controls to mount the upgraded Wolfangel chopper on the robot. Demonstrated capability for chopper to meet output targets in short operating runs on the robot in making preforms representative of the liftgate application. Preform uniformity and capability to run for extended periods without hanging and/or jamming (process durability) issues are being addressed at the close of this reporting period.
- Continued working with in-situ-blended polypropylene and hybrid blends of commercially available industrial grades of CF and glass fiber making additional blending improvements with air jet entanglement. Even with improvements, molded panels are not yet adequate for extensive characterization, at least partially due to inadequate charge heating capabilities.
- Identified a promising combination of IR and convective charge heating system and conducted successful experiments at the vendor, Wisconsin Infrared. Worked with the vendor to identify an economical path forward consisting of modifying a system they manufacture commonly in a convection configuration by adding IR at a reasonable cost. This combination IR and convection oven was procured in late FY2009 and is being installed for operation in early FY2010. This will facilitate compression molding of traditional thermoplastics and sheet molding compounds with thermosets as well as work with in-situ blended materials. Although the focus of this approach is to facilitate evaluation of alternative material combinations, especially looking at hybrids, in situ blending may prove economically attractive as well. Since the variety of forms of commingled materials is extremely limited, this allows evaluation of materials not available at all in commingled form and in a much broader array of blending alternatives.
- Completed electrical installation of the refurbished urethane injection system procured in late FY 2008 to enable evaluation of various materials/forms in liquid molding processes, including hybrid blends and natural-fiber preforms, and early evaluation of lower cost CF. Machine startup and initial operations are anticipated in FY 2010 depending on funding availability.

Future Direction

- Utilize upgraded chopper to fabricate preforms for the Automotive Composites Consortium (ACC) Composite Seat Focal Project 4 program and evaluate technical and economic feasibility of this process for that application utilizing sample test panels as well as evaluation of the demonstration articles.
- Complete installation and checkout of the new IR/convective charge heating system as a more industry-representative and effective means of heating and transferring blanks of reinforcing fibers mingled with thermoplastic fibers into the press for compression molding. Continue improvements in preforming and molding through studies with hybrid carbon and glass

reinforcement and polypropylene materials blended in situ at the preforming machine. Expand to consider various other product forms including forms with low-cost CF as available.

- Evaluate durability of coated and uncoated chopper blades in cutting carbon fiber and capability for this system to chop other challenging material forms such as pre-impregnated DRIFT and in-situ blended materials utilizing the Wolfangel chopper in the preforming machine.
- Complete checkout and initiate operations with the refurbished urethane injection system as an alternative pathway for evaluation of hybrid blends and other materials and processes.
- Continue working with the Automotive Composites Consortium to identify and execute more applications-related work utilizing preforming and associated processes.
- Continue developing and implementing tools for more-effective characterization of process variables and effects on final products. Although currently on hold, evaluate preform process models relative to physical preform characteristics and expand model capability as funding is available for this activity.

Introduction

Polymer-matrix composite materials offer a number of benefits in lightweighting of automotive and heavy vehicles, including greater stiffness and strength per unit weight than conventional materials, easier formability, less corrosion susceptibility, the ability to tailor properties to specific load requirements, and enhanced noise and vibration damping. However, widespread implementation of CF composites, which are among the materials with the greatest weight-saving potential, will require lower-cost materials and manufacturing processes than are currently available. Advanced preforming processes offer opportunities to facilitate the widespread use of carbon composites.

Advanced preforming processes offer opportunities to facilitate the more widespread use of composites in general and specifically composites utilizing carbon fiber as carbon fiber becomes available in appropriate forms and at acceptable cost. Robotic-controlled, programmable, directed-fiber preforming processes have demonstrated exceptional value for rapidly preforming large, glass-reinforced, automotive composite structures. Due to their unique features and flexibility, and to their inherent low-scrap rate, they are among the most viable candidate processes for making affordable carbon-fiber preforms for a variety of structural automotive components. The Automotive Composites Consortium (ACC) has successfully demonstrated preforming in both Focal Projects 2 and 3 and the technology has been used in production of the General Motors (GM) Silverado pickup box and the Aston Martin Vanquish body-side.

Analyses have indicated a potential for greater than 60% weight savings for a CF-intensive body-in-white under the assumption of a thickness design constraint of 1.5 mm. The analyses also indicated the potential for saving an additional 15% if the thickness constraint is reduced to 1 mm. Unfortunately, evidence suggests that 1.5 mm may be a practical limit for liquid molding. However, thermoplastics preforms, in which the reinforcing fiber and matrix (in the form of thermoplastic fiber during deposition) are both deposited in the preforming step, offer a potential path to obtaining thinner sections and, consequently, additional weight savings as well as greater potential for recyclability. Hybrid-fiber preforms that can effectively take advantage of concurrently utilizing carbon and glass fibers offer another potential benefit in terms of economics and property enhancement and may be a good route for actually introducing more carbon fiber at somewhat lower quantities than necessary for all-carbon components in automotive applications.

Preforming Developmental Approach

The objective of this project is to advance directed-fiber preforming processes to effect a further reduction in vehicle weight—relative to metals and conventional glass-fiber composites—while maintaining the economical advantages of net-shape preforming. The project is pursuing three focus areas corresponding to three materials systems: reinforced thermoplastics, carbon fiber, and hybrid glass-carbon fiber. Each focus area consists of four main tasks: (1) materials development, including introduction and evaluation of alternative and/or new fiber product forms and binders; (2) machine development, particularly new severing technology; (3) process development, for example, to control areal-density uniformity and preform anisotropy; and (4) supporting technologies development, including modeling and characterization techniques. This project will also include developing a deeper understanding of fundamental aspects of the process and their effects on preform quality and mechanical properties in the molded part. To summarize, this project will support, augment, and facilitate the current and future research activities undertaken in related ACC projects.

A research-focused preforming system has been installed in the polymer composites laboratories at ORNL to serve as the base for hardware and associated technology developments. A number of combinations of reinforcing fibers, binders, and/or matrix fibers have been obtained to establish materials baselines for comparison with and advancement of previous P4 work conducted by ACC. The P4 machine is currently being used to build preforms for evaluation using the Twintex product (glass fiber commingled with thermoplastic fiber to serve as the matrix), glass impregnated with thermoplastic resin using the Direct Reinforcement Fabrication Technology (DRIFT) process, and various forms of carbon and glass reinforcement in alternate independent and hybrid forms. Although the near-term focus is on demonstrating advances with glass fiber and existing industrial grades of CF, the long-term goal is to establish the groundwork for large-scale introduction of low-cost CF for significant impact in automotive lightweighting. Project activities are shared with the automotive industry through collaboration with the ACC; as appropriate, results are published and demonstrations will be conducted for potential suppliers and other interested organizations to promote technology implementation.

High-Speed Chopper Development and Demonstration

The ACC Materials and Processing working groups had initiated work with Ecole Polytechnique Fédérale de Lausanne (EPFL) in Switzerland to study processing effects and material properties of commingled glass and thermoplastic fibers leading to cost-model comparisons of various thermoplastic-composite processes. The focus of this work has been on the Twintex materials produced by Saint-Gobain Vetrotex, incorporating glass and polypropylene fibers, but the basic evaluation process can be extended to a variety of materials and processes based on this concept. With the support of EPFL and an ACC representative, ORNL fabricated a large number of preforms from Twintex using various fiber lengths and preform thicknesses along with variations in preforming compaction station time and air temperature variables. Material properties of the ORNL preforms molded by EPFL are competitive with similar materials such as Glass Mat Thermoplastics (GMT) and, in some cases, significantly improved. EPFL analysis indicated economics can also be attractive versus some of these competitive processes at improved chopping speeds in the 12 to 15 kg/minute range[1], leading to our focus on demonstrating the technical and economic feasibility of higher-speed chopping processes.

ORNL and the ACC have been collaborating on evaluating and upgrading a prototype chopper unit from Wolfangel. The Wolfangel chopper allows chopping at two distinct fiber lengths, determined by blade spacing in either the inside or outside half of the cutter wheel, which is then controlled by pneumatically switching the positioning of the cutter roller with respect to the fiber stream passed through the cutter. The P4 chopper allows selection of an infinitely variable fiber length within a relatively wide range, but use of more than two lengths within a single production operation has been

very rare. The Wolfangel chopper was designed to process up to 5 tows of fiber at a maximum at what amounts to ~8.3 kg/min with 1,870 tex Twintex tows. For comparison, the P4 chopper is designed to process 2 tows at speed that would translate to ~2.3 kg/min. We were able to run 2 tows through each tube of the P4 chopper, which would effectively double the throughput, but this was difficult to sustain and certainly could not be exceeded with the current configuration. To achieve the target output with the Wolfangel chopper would require processing more tows at a time, speeding up the peripheral speed, or combinations of both. Initial efforts established actual capabilities for this chopper utilizing operational requirements for the preforming environment as described below.

A generic liftgate part envelope as shown in Figure 1 was chosen as a realistic article that could be manufactured with these materials and processes and where high output would be advantageous as shown in the earlier study. Representative chopper-control signals including the abrupt starts and stops the chopper is required to make in coordination with rapid robot movement and indexing across the part profile were captured from the P4 machine using a LabView program. A second LabView program was used to operate the chopper independently of the robot while still simulating chopper operation required for liftgate preform manufacturing. Control signal form is shown in Figure 2.

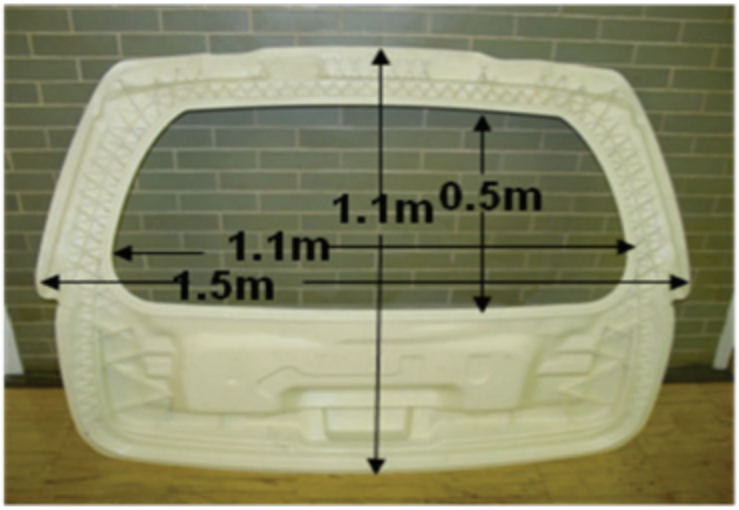

Figure 1. Approximate liftgate dimensions used in simulation program.

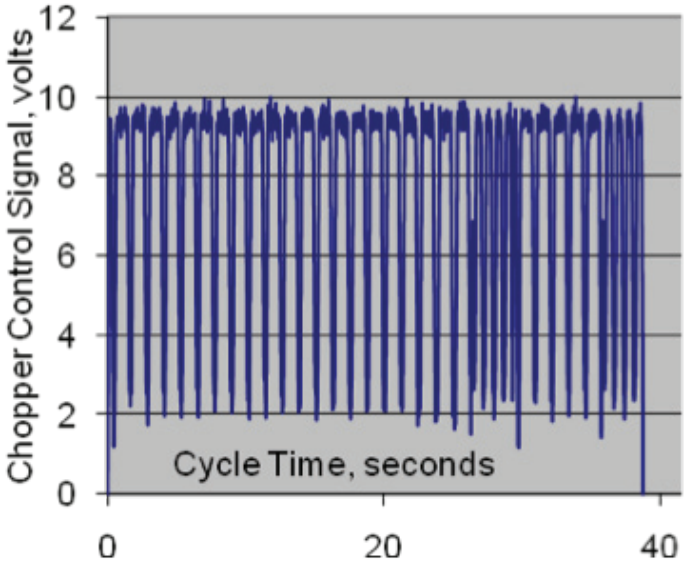

Figure 2. Chopper control signals in simulation program.

Utilizing this program, the chopper limits were characterized in a larger set of “realistic” chopping trials conducted at ORNL with ACC support. Although rated higher, we were typically able to achieve only about 4-5 kg/min in chopping with the Wolfangel chopper before the motor stalled due to torque limitations. However, it appeared practical to modify the chopper with a significantly larger motor and changes to other hardware to improve torque and speed and to be able to process more tows.

The chopper system was upgraded and then the system was characterized and conditions tweaked in extensive trials throughout a wide rage of potential operating speed ranges while mounted on the test stand. Initial trials approached output targets, but the chopper motor/head interface was inadequate for the higher torque and additional side loading added to increase the cutter/roller interface pressures beyond the original allowance for 4 bar actuating pressure, resulting in hardware failure. The insufficient hardware was upgraded and subsequent trials demonstrated the chopper to be capable of achieving more than 18 kg/min instantaneous output when using 9 tows. Very good severing was achieved at these conditions when using 10 bar air pressure on the cutter/rubber roller interface for the 1-inch cut length, while the 3-inch length at these conditions was largely, but not completely, cut. When the tow is not completely severed, the polypropylene is typically the material not fully cut. This is not considered a significant issue as the polypropylene is actually melted and flows to become the composite matrix in subsequent operations.

This trend toward better cutting at the shorter length was essentially replicated for all conditions at which any difference was noted. As expected, improved severing was achieved at higher air pressures for essentially all speeds regardless of the number of tows being processed. Also expected was the finding that cutting quality decreased with increasing the number of tows being simultaneously cut. However, we unexpectedly found that cutting quality actually improved with increased speed regardless of the number of tows being cut or interface pressure.

This characterization experience was utilized to identify likely fiber handling impediments to running the Wolfangel chopper on the preforming robot at these high output speeds and system improvements have been developed and implemented during the course of this activity. The high speeds and large numbers of tows traversing through the system are taxing; more difficult problems are encountered with the fiber inertia involved with the rapid starting and stopping of the fiber associated with the robot starting and stopping at the end of each pass. A variety of changes such as employing a number of hardened fiber guides in the system, utilizing an air ejection system at the chopper output (as shown in Figure 3, and the use of funnels to manage the fiber “whipping” out of the spool were implemented to mitigate speed and inertia problems. With hardware changes and operational experience, capability to run at target outputs on this stand for extended time periods was demonstrated.

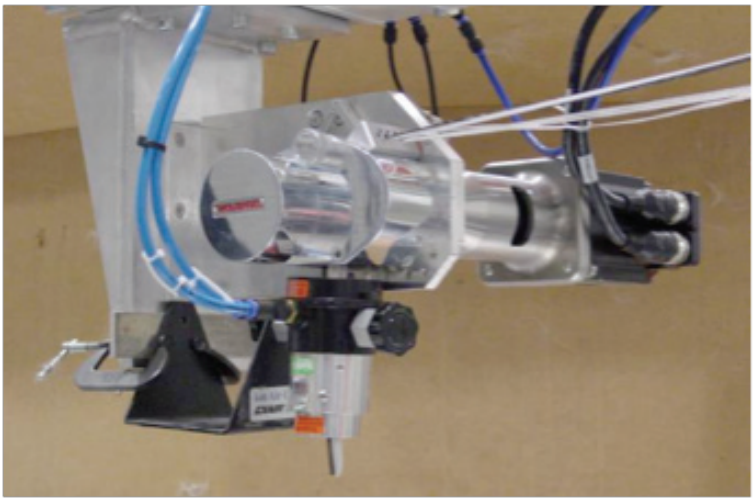

Figure 3. Upgraded chopper with air ejection system at the bottom.

Taking advantage of this background, system hardware and controls necessary to mount the upgraded Wolfangel chopper on the robot (Figure 4) have been completed and the chopper has now been characterized in making representative liftgate preforms and other test sections.

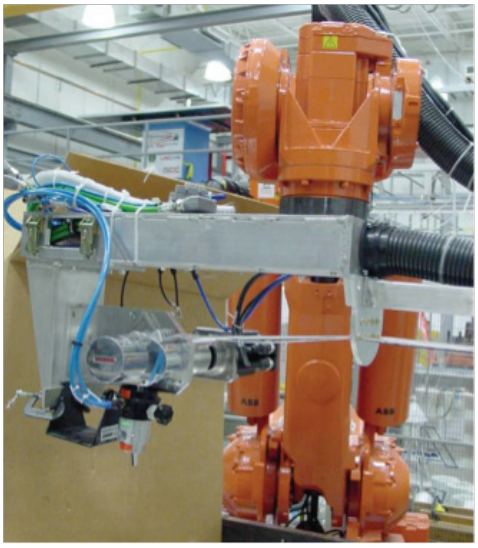

Figure 4. Wolfangel chopper mounted on robot.

As previously mentioned, fiber inertia causes problems in working with the chopper mounted on a stationary stand. These problems are exacerbated with abrupt movements of the robot with an increased number of fiber pathways turns and the length of unsupported spans in the distance between the fiber spools and the chopper. A number of additional changes have been made and others continue to be implemented to improve the fiber delivery to the robot. Among the changes is implementation of an “air braking” mechanism developed internally from related hardware (Figure 5) to maintain tension close to the spools and use of fiber spreading and ceramic eyelets to guide fibers (Figure 6).

Figure 5. Air braking mechanism to mitigate fiber inertia problems.

Figure 6. Fiber guides utilized to provide spacing and to mitigate tangling with 9 tow deposition.

With the combination of the system upgrades and process tweaking as previously described, we were able to meet the objective of 12-15 kg/min deposition rate and demonstrate capability to deposit a complete liftgate preform (Figure 7) in the 30 seconds assumed in the earlier process comparison and economic study. Our capabilities exceed the deposition rate assumed for the

upper limit of a single robot/chopper system and the lower end of a dual system as assumed in this study. It also met a DOE Joule Milestone for this project.

Figure 7. Representative liftgate preform experiment.

The ACC Focal Project 4 Composite Seat baseline design utilizes glass fiber with a polypropylene matrix. As ORNL and the ACC are implementing plans for the Next Generation Preforming effort to take on some of the application demonstration work, ORNL will provide preforms for evaluation in the seat project manufactured from the current Twintex baseline material and utilizing the existing preforming screens and upgraded chopper. The first goal is to demonstrate technical feasibility for this product form for this application before working towards optimizing robot and chopping speeds and preform quantities per cycle specifically related to this application. ORNL will collaborate with the ACC in evaluating this product form as well as the economics involved in this process.

In Situ Blending to Evaluate Hybrid Carbon and Glass Compositions

Because it is believed that hybrid-fiber preforms can effectively take advantage of concurrently using carbon and glass fibers and offer potential benefits in terms of economics and property enhancement, ORNL has obtained standard, lower-cost CF alternatives from Zoltek and Toho to evaluate in conjunction with glass- fiber reinforcement previously acquired from Owens Corning. ORNL has also procured polypropylene fiber from Fiber Science to serve as the composite matrix in initial trials to evaluate and demonstrate in situ blending of these hybrid blends at the preforming machine.

A number of preforming and molding experiments has been conducted to establish the equipment setup requirements and process parameters necessary to evaluate these hybrid blends. As previously established in cutting the Twintex materials, the polypropylene is more difficult to completely sever than the carbon- or glass-fiber reinforcement, although it is less abrasive to the cutter blades themselves. Due to current polypropylene product availability (typically only in very small tow sizes) and the desire to maintain the capability to adjust the mix ratios to a large degree, the polypropylene was combined by the vendor to a larger tow size, which was still about half the size in terms of cross-sectional area of the smaller glass and carbon tows on hand. Currently, the only packaging found immediately available was configured for outside unwind of this product versus the inside unwind configuration that works best for preforming. These limitations necessitated use of a multiple position creel to facilitate

processing and mitigate entanglement. Not being intermixed on a filament-to-filament basis with the reinforcement fibers (as with the Twintex), the polypropylene tends to "fuzz" a little more in handling than the Twintex leading to a significant amount of fiber wraps around the chopper feed rollers resulting in chopper jams and blade breakage forcing pauses in operation to clear the jams and/or to replace blades. We are currently evaluating how the upgraded chopper performs in chopping these materials (Figure 8). Initial indications are that the chopper can chop the materials, although we do not yet have adequate data to determine if cutting is

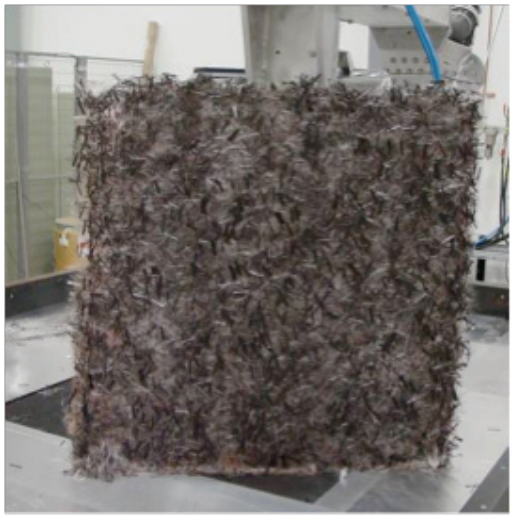

Figure 8. Hybrid carbon, glass, and polypropylene preform manufactured with upgraded chopper.

more consistent; the increased speed and capability to process a larger number of tows are not necessarily a target objective at this point.

Molding experiments indicate that we are approaching an acceptable preforming/molding process but that the distribution of the polypropylene is not uniform through the thickness of the panel. We have made significant improvements in mixing the polypropylene fiber with the reinforcing glass and carbon fiber, but we have difficulty in demonstrating how these improvements translate into molded panels worthy of extensive characterization. We believe that to get to the next step in evaluating molded panels; we need to resolve limitations with the process we have been using for this preliminary work in heating charges immediately prior to molding.

In reviewing literature and vendor materials, we determined that an appropriate method for our experimental work allowing significant flexibility in processing would be to use a combination of infrared (IR) and high air flow convection heating. We identified Wisconsin Infrared, a division of Wisconsin Oven, as having products closest to our projected targets and being able to customize those products at a reasonable cost to more fully meet those needs. We contacted them and sent samples for their initial evaluation. With positive response on those initial specimens, we set up and conducted experiments with them where they demonstrated that indeed this combination of IR and convection would work well for our specimens. With this success, they proposed modifying a

Figure 9. Combination IR and convection oven. (IR section surrounds conveyor entrance at right.)

system they manufacture commonly in a convection configuration by adding IR at a reasonable cost. This system (Figure 9) was procured in late FY 2009 and is being installed and operational parameters developed in early FY 2010. This will facilitate compression molding of traditional thermoplastics and sheet molding compounds with thermosets as well as work with in-situ blended materials.

Although the current focus of this work is using polypropylene for demonstration purposes, the concept should be applicable to other thermoplastic materials, including polyester and nylon. (Due to recent interest in nylon, we have obtained nylon samples for initial evaluation in blending experiments. Although higher molding temperatures are required, it is believed that nylon might actually be more amenable to the blending process and be less "fuzzy" in processing.) If successfully demonstrated, in situ blending would offer greater flexibility for manufacturers to tailor-blend ratios in-house to specific product needs without long lead times, inventory requirements, or dependence on the limitations of product variety from suppliers as is the case with the Twintex product manufactured by Saint-Gobain Vetrotex. Once we achieve adequate techniques for blending and molding, we can turn our attention to optimizing carbon fiber product forms for usage with various thermoplastic matrices and for specific applications making use of surface treatment technologies under development in related projects.

It is believed that regardless of whether the in situ blending process itself proves adequate for high-quality, thermoplastic matrix parts, the technology being developed could prove advantageous in blending glass and carbon reinforcement to a level adequate for use of hybrid reinforcement and could likely be extended beyond thermoplastics and applied to thermosets in sheet molding compounds or to preforming for structural reaction injection molding (SRIM). This could have a significant impact on DOE and ACC goals as hybrids would appear to be an effective route for actually introducing more CF at somewhat lower quantities than necessary for all-carbon components in automotive applications and an effective means of reducing the component cost in CF by using only the minimum amount that is needed.

During this period, we have completed electrical installation of the refurbished urethane injection system purchased earlier to establish SRIM capability for evaluation of various materials/forms in liquid molding processes, including hybrid blends and natural-fiber preforms, and early evaluation of lower cost CF. Machine startup and initial operations are anticipated in late FY 2010 depending on funding availability.

Summary and Conclusions

The Next-Generation Programmable Preforming Process project is continuing to build on past development and application of directed-fiber preforming processes, namely those of the baseline P4, to extend the process to new material systems. Developments are expected to facilitate the use of lower-cost CF-reinforced thermoplastics and glass-carbon hybrid materials as effectively as with the current state-of-the-art glass-fiber technology. Using these materials is expected to lead to further reductions in vehicle weight in a more cost-competitive scenario than is currently possible.

EPFL and ACC evaluations of a large number of ORNL-fabricated preforms from the commingled Twintex product have been both technically and economically encouraging, especially if 12-15 kg/min chopping output can be achieved with the modified Wolfangel chopper. With the combination of the system upgrades and process tweaking as previously described, we were able to meet the objective of 12-15 kg/min deposition rate and demonstrate capability to deposit a complete liftgate preform in the 30 seconds assumed in the earlier process comparison and economic study. Our capabilities exceed the deposition rate assumed for the upper limit of a single robot/chopper system and the lower end of a dual system as assumed in this study. It also met a DOE Joule Milestone for this project.

Additional blending improvements with air jet entanglement were achieved in working with in-situ-blended polypropylene and hybrid blends of commercially available industrial grades of CF and glass fiber making. Even with these improvements, molded panels are not yet adequate for extensive characterization, at least partially due to inadequate charge heating capabilities. A promising combination of IR and convective charge heating system was identified and successful experiments at the vendor were conducted. This system was procured in late FY 2009 and is being installed and operational parameters developed in early FY 2010. This will facilitate compression molding of traditional thermoplastics and sheet molding compounds with thermosets as well as work with in-situ blended materials.

Although the focus of this approach with in-situ blending is to facilitate evaluation of alternative material combinations, especially looking at hybrids, the in-situ blending process may prove economically attractive as well. Since the variety of forms of commingled materials is extremely limited, this allows evaluation of materials not available at all in commingled form and in a much broader array of blending alternatives.

We will continue working with the Automotive Composites Consortium to identify and execute more applications-related work utilizing preforming and associated processes. As appropriate, we will continue developing and implementing tools for more-effective characterization of process variables and effects on final products. Although currently on hold, we will evaluate preform process models relative to physical preform characteristics and expand model capability as funding is available to support this activity.

Collectively, the technologies under development in this project will advance low-cost processing on two fronts. First, they will provide the opportunity to use additional materials in the net-shape preforming process, which is expected to lead to additional weight reduction and/or better performance. Second, they will provide the requisite tools to evaluate the effects of process parameters on the utility and performance of preforms and molded parts.

Presentations/Publications/Patents

1. S. T. Jespersen , F. Baudry, D. Schmäh, M. D. Wakeman, V. Michaud, P. Blanchard, R. E. Norris, J.-A. E. Månson, “Rapid Processing of Net-Shape Thermoplastic Planar-Random Composite Preforms”, Applied Composite Materials (2009) 16:55–71.

2. S. T. Jespersen , F. Baudry, M. D. Wakeman, V. Michaud, P. Blanchard, R. Norris, J.-A. E. Månson, “Consolidation of Net-shape Random Fiber Thermoplastic Composite Preforms”, Polymer Composites, published online March 2009.

3. S. T. Jespersen , F. Baudry, M. D. Wakeman, V. Michaud, P. Blanchard, R. Norris, J.-A. E. Månson, “Flow Properties of Tailored Net-Shape Thermoplastic Composite Preforms”, Applied Composite Materials, published online September 2009.

References

1. M. D. Wakeman, G. Francois, J-A. E Manson, “Cost Modeling of Thermoplastic P4 Process Technology”, Progress Report 1 for the Automotive Composites Consortium, Ecole Polytechnique Fédérale de Lausanne, April 2006.

D. Advanced Materials and Processes of Composites for High Volume Application

Principal Investigator: Daniel Houston
Ford Motor Company, Manufacturing & Processes Department
2101 Village Road, Dearborn, MI 48121
(313)323-2879; e-mail: dhousto2@ford.com

Technology Area Development Manager: Dr. Carol Schutte
(202) 287-5371; e-mail:carol.schutte@ee.doe.gov

Field Project Officer: Aaron D. Yocum
(304) 285-4852; e-mail: aaron.yocum@netl.doe.gov

Contractor: U.S. Automotive Materials Partnership
Contract No.: DE-FC-26-02OR22910 through the DOE National Energy Technology Laboratory

Objective

- Develop and demonstrate high-volume manufacturing (molding) technologies germane to automotive production.
- Collaborate with suppliers to develop low-cost – high volume molding processes that enable production of minimal weight components.
- Explore new thermoplastics materials and processes affording enhanced material properties and new automotive applications.
- Assure reproducible quality of molded automotive components.
- Develop and document new test methods where required to fully understand material performance.

Approach

- Develop manufacturing processes for carbon-fiber SMC amenable to cost-effective high volume structural, semi-structural and Class-A automotive applications.
- Optimize carbon fiber SMC properties, improve consistency of properties, and optimize manufacturability of SMC.
- Experimentally validate a finite element model capable of predicting BLRT (Bond Line Read Through).
- Develop BLRT work with new OEM Tier-1 supplier for future implementation.
- Initiate direct compounding of automotive thermoplastic polymers to reduce cost and increase performance benefits offered over conventional long fiber injection or compression molding.

Accomplishments

- Six carbon fiber SMC molding trials were completed, mechanical properties generated, fiber spreading apparatus fabricated and de-bundling equipment investigated.
- Metallographic investigation was conducted to determine value of fiber spreading.
- Completed five BLRT experiments: The first experiment in FY09 was a screening experiment to determine whether the relationship between the material and process factors in assemblies made with a pliable mastic adhesive would correlate with that seen in assemblies made with adhesives. The second was an experiment to investigate the relationship between BLRT severity and a) the SMC formulation used for the inner panel, b) the SMC formulation used for outer panel, and c) and inner panel thickness on BLRT severity. The third experiment completed, investigated the impact of molding small "standoffs" into the inner panel on BLRT severity. The fourth experiment investigated the relationship between bond cell cure temperature and BLRT severity. The fifth experiment investigated relaxation of BLRT-induced distortions over time and after simulated prime and paint bakes.
- Conducted exploratory studies for direct compounding of thermoplastic polymers. Materials characterized for tensile and impact properties. Results indicate positive response of materials.

Carbon-Fiber SMC

The objectives of this project are to develop high performance, cost-effective, carbon-fiber

SMC materials and associated processing techniques for high-volume automotive components. The technical emphasis is to optimize properties, improve consistency of the properties, and to optimize the manufacturability of the compound. The project assumptions are that the materials could be used for all current structural and Class-A SMC applications; that deviations from the current SMC compounding and molding processes, and equipment are minimal; and that the thickness of the new materials will be moldable in the range of 1.0 to 3.0 mm. The development will initially be focused on structural applications.

The project has established a joint working relationship with a Tier-1 automotive glass SMC supplier, Continental Structural Plastics (CSP), to leverage their production knowledge. A CSP laboratory scale SMC compounder has been upgraded to provide carbon-fiber chopping and compounding capabilities.

To address the concern of commercial viability of the resulted technology, the project will attempt to utilize lower cost carbon fibers for the development. A low-cost carbon fiber manufacturer, Zoltek, has agreed to work with CSP supplying appropriate carbon fibers and developmental sizing systems suitable for resins ideal for automotive applications.

For initial development, Zoltek conducted short beam shear tests using CSP provided vinylester resins to identify a baseline material system. The results indicated that the combination of Panex 35 50K carbon fibers with -11 sizing and CSP vinylester resin blend performed best, as compared with the benchmark epoxy resin (Figure 1).

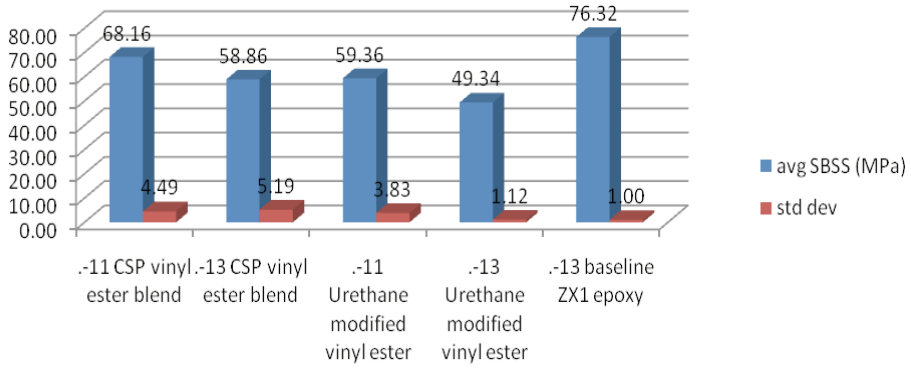

Figure 1. Fiber sizing and resin selection

A number of compounding trials were subsequently conducted by varying resin viscosity, fiber content, and compaction pressure using this recommended baseline system. For comparison, a standard commercial 12K carbon fiber was also included in these compounding trials. Low tensile properties were obtained from all the evaluated systems, including those made with 12K fibers, likely due to poor or marginal fiber wet-out inside the fiber bundles. The Tier-1 supplier noted above (CSP) is currently engaged with a tier-2 material supplier and the ACC to improve the fiber wet-out and design a manufacturing process. In an attempt to improve fiber wet-out, the compounds were molded before full maturation under higher pressure (2800 psi vs. the standard 1000 psi), lower temperature (125°C vs. 150°C), and longer time (5.5 min vs. 1.5 min). The efforts, however, have not resulted in significant improvement in properties. Examination of fracture surfaces seems to suggest failures occurring between fiber bundles (Figures 2 and 3).

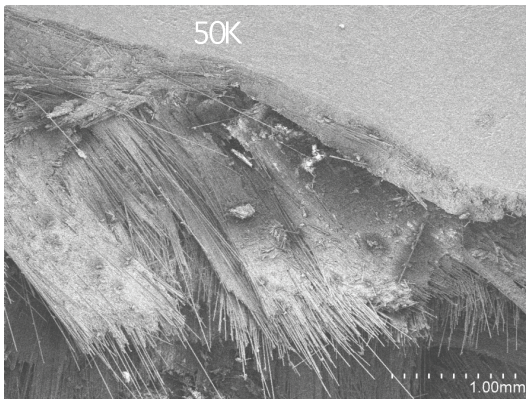

Figure 2. 50K Carbon Fiber SMC Fracture

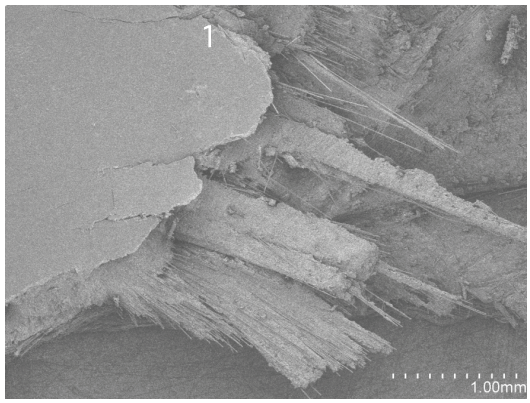

Figure 3. 12K Carbon Fiber SMC Fracture

Additionally, a density measurement across molded plaques shows a higher variation than commercially available carbon fiber SMC (Figure 4). The variation is explained by the presence of large and likely dry fiber bundles in the SMC resin matrix. It is well known that local homogeneity is critical to the tensile properties, especially strength, of composite materials.

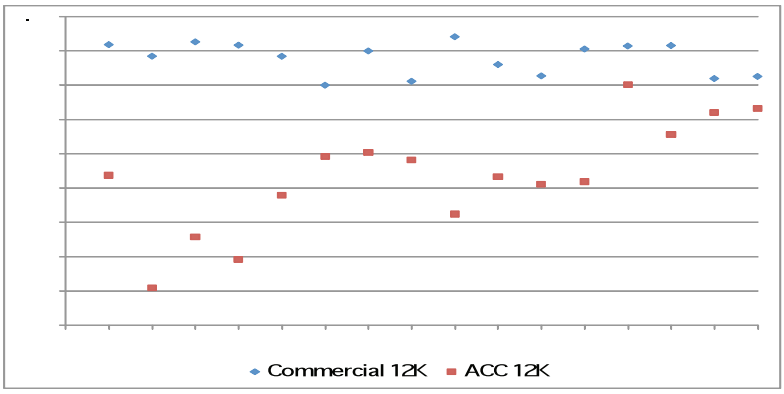

Figure 4. Higher Density Variations

The results have thus shifted efforts of the project into finding low cost methods to de-bundle the carbon fibers. One method looked at was an “air knife”. Basically, a jet of air was blasted onto the carbon fiber bundle just before it was pulled into the chopper. To determine the effectiveness of this concept, a designed experiment consisting of 36 tests was carried out using processing factors and factor levels given below (Table I).

Table I. Designed Matrix for Air Knife Carbon Fiber De-bundling

Factor	Levels	Values
Spool Number	3	1, 2, 3
Nozzle_Diameter (inch)	3	0.0625, 0.125, 0.1875
Air_Pressure	2	Low, High
Chopper_Speed (rpm)	2	20, 80

The results of this designed experiment showed that the nozzle diameter is the only factor that is statistically significant in de-bundling the 50K carbon fibers (Figure 5). The current design of the “air knife”, however, can only reduce the mean bundle size of 50K fibers to approximately 12K, which is still too large to produce a homogenous composite material. Industry literature seems to indicate the concept would perform better with a complete redesign allowing the air jet to impact the fiber bundle when it is not under tension.

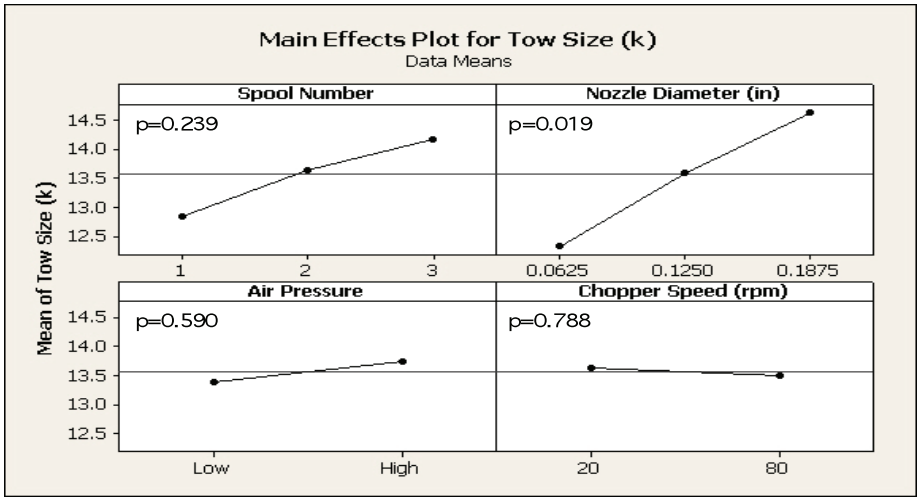

Figure 5. Designed Experiment Results of Air Knife De-bundling

In addition to improving the simple air knife design, the project is currently evaluating several other mechanical and pneumatic fiber de-bundling concepts. Additional work with other resin systems and fiber sizing’s are also underway.

Future Direction

In 2010 it is planned to modify the carbon fiber chopper to combine several de-bundling concepts. In addition to spreading the bundles prior to chopping, we will also investigate de-tensioning the bundle while simultaneously impacting it with an air jet. An alternative chopper will also be tested along with other resin systems and fiber sizings.

Bond-Line Read-Through

Phase 2

The BLRT team manufactured five sets of assemblies in FY09. All of the SMC panels used in these experiments were molded by Meridian Automotive Systems at their Shelbyville, IN plant. The assemblies in the first four experiments were bonded with assistance from Meridian. The first of these four experiments was completed at Meridian’s Shelbyville, IN plant. The last three experiments were

completed at Meridian's Rushville, IN facility. The assemblies bonded in the first three experiments were 24"x24" assemblies described in previous reports. Those assemblies were bonded using the ACC BLRT project bond fixture and press described in those reports. That equipment was moved from Shelbyville to Rushville between the first and second FY09 experiments. The fourth and fifth experiments were completed using small "lab-scale" assemblies. These assemblies were built specifically for generating data to compare to the modeling results in Phase 3 of the project. A photograph of a "lab-scale" assembly is provided in Figure 6. The substrate used in these assemblies was cut from 24"x24" assembly outer panels. A new bond fixture was built by EMC2 in Sterling Heights, MI to bond these assemblies. The fourth experiment was completed in Rushville. All of the equipment was moved to EMC2 in July after the Shelbyville and Rushville facilities were closed. The final experiment was then completed at EMC2.

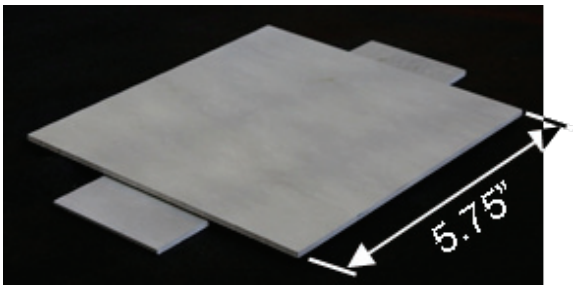

Figure 6. Example of a "Lab-Scale" Assembly

The first experiment in FY09 was a screening experiment to determine whether the relationship between the material and process factors in assemblies made with mastic would correlate with that seen in assemblies made with adhesives. The second was an experiment to investigate the relationship between BLRT severity and a) the SMC formulation used for the inner panel, b) the SMC formulation used for outer panel, and c) and inner panel thickness on BLRT severity. The third experiment completed, investigated the impact of molding small "standoffs" into the inner panel on BLRT severity. The fourth experiment investigated the relationship between bond cell cure temperature and BLRT severity. The fifth experiment investigated relaxation of BLRT-induced distortions over time and after simulated prime and paint bakes.

Mastic Experiment

The factors included in the mastic screening experiment are summarized in Table 2. The experimental design used in this experiment was a quarter-fractional factorial design with three replicates. All assemblies were made by bonding an SMC inner panel of the standard configuration to the appropriate outer panel.

Table 2. Factors Included in the Mastic Screening Experiment

Factor	Low Level	High Level
Bond Gap	1 mm	8 mm
Flange Coverage	25-50%	75-100%
Dob Spacing	50 mm	150 mm
Outer Panel Material	2.5 mm SMC	0.8mm 210 BH Steel
Mastic	A	B
Squish and Expand	No	Yes

A 0.8mm steel thickness was chosen so that the section stiffness of the steel outer would be closer to that of 2.5mm thick SMC outer. The team was concerned, however, that 0.8mm thick 210 bake hardenable steel would be too stiff and no read-through would be visible on these assemblies. To increase the opportunity to observe read-through in assemblies made with mastic, one half of the experiment was replicated using 0.7mm thick 210 bake-hardenable steel for the outer panel. All the steel used in this experiment was obtained from blanks acquired from Ford Stamping Operations. These larger blanks were cut down to the size needed for BLRT assemblies and then electro-coated with Ford's standard service part electro-coat prior to bonding at Ford's service parts facility in Brownstown, MI.

Since mastics do not cure until exposed to temperatures used to cure e-coat in production, the inner and outer panels were bonded using epoxy adhesive around the outside of the assembly. The mastic dobs were applied by hand using molds, and then the 2K epoxy adhesive was dispensed around the outer perimeter of the inner panel. The inner panel and outer panel were put into the press and cured at the desired bond gap. Since an 8mm tall bead of epoxy adhesive cannot be dispensed, 1" wide pieces of SMC were bonded around the outer edges of the inner panel for the assemblies with an 8mm bond gap. Two pieces of 2.5mm thick SMC were bonded sequentially, each with a 1mm bond gap. There was then a 1mm bond gap between the inner panel "frame" and the outer panel when the assembly was bonded.

The mastic materials will not cure until exposed to a minimum of 171°C for 10 minutes, so the assemblies were shipped to a Ford Research & Engineering facility where they were baked in an oven at 180°C for 30 minutes to cure the mastic. The assemblies were then sent to ACT Test Panels, Hillsdale, MI for painting. Unfortunately, there was no measureable deformation in these assemblies after painting. This result was disappointing as mastic can cause read-through in production situations. Future modeling work in Phase 3 may be used to predict the conditions that will cause BLRT with these materials.

SMC Density & Inner Panel Thickness Experiment

In the next experiment, the formulation used to mold the SMC inner and outer panels was varied, as was the inner panel thickness. This experiment was a full factorial experiment with three replicates. The format and detailed results of this experiment were published in [1].

The assemblies made with outer panels molded from the mid-density SMC formulation did not have a true Class "A" surface. The waviness in those panels could not be filtered out of the data, causing the BLRT data to be confounded. Nevertheless, statistical analysis of the BLRT scores found that 80% of the variation in the data could be explained by a prediction equation consisting of a) the CLTE (Coefficient Linear Thermal Expansion) of the outer panel, b) the interaction between the CLTE of the outer panel and the CLTE of the inner panel, c) the bending stiffness of the outer panel, and d) the interaction between the bending stiffness of the outer panel and the bending stiffness of the inner panel.

Standoff Experiment

The third experiment in FY09 was an experiment to collect data on the impact that standoffs molded in the bond-line on the inner panel have on BLRT severity in the assembly. 0.5mm tall standoffs were cut into the ACC BLRT inner panel tool by JATCO Machine & Tool in Pittsburgh, PA. The standoffs added to the inner panel tool replicated those that had been found to cause read-through on the Dodge Viper roof in production.

The format and detailed results of this experiment were published in [1] and [2]. The addition of standoffs to the inner panel was found to have a significant impact on BLRT severity, even before a statistical analysis of the data was completed. Statistical analysis of the data from the assemblies as bonded found that 98% of the variation in the data could be explained by a prediction model that included all four of the main effects and five interactions. The magnitude of BLRT severity, specifically

the peak curvature values, dropped after painting in these assemblies. Statistical analysis of the data after painting, however, showed that the relationship between factors and interactions and BLRT severity after painting were the same as those after bonding.

Cure Temperature Experiment

The fourth experiment in FY09 was completed to establish the relationship between the temperature at which the adhesive was cured and BLRT severity. This was the first experiment that made use of the smaller "lab-scale" assemblies. The data from this experiment was collected specifically to use in the validation of the finite element (FE) model being developed in Phase 3 of this project. The format and detailed results of this experiment were published in [2] and [3].

There was minimal distortion in the assemblies bonded with urethane, regardless of the temperature at which the assemblies were cured. BLRT severity increased with increasing bonding temperature in the assemblies bonded with epoxy. Assemblies were also bonded with the outer panel side of the fixture at a lower temperature than the inner panel side of the fixture. This strategy was shown to reduce BLRT.

BLRT Relaxation Experiment

The fifth experiment in FY09 was completed to determine whether BLRT severity changes with time. This experiment made use of the smaller "lab-scale" assemblies. Since the urethane assemblies built in the cure temperature experiment did not exhibit measureable BLRT, assemblies were only made with epoxy adhesive in this experiment. Since both SMC and adhesives are viscoelastic materials, a few assemblies were made with steel substrate in this experiment to provide data for a non-viscoelastic substrate. The format and detailed results of this experiment were published in [3] and [4].

In addition to the data discussed in those papers, the assemblies were exposed to the bake conditions that a production part would experience in the priming process at a part supplier plant. Data was then collected on the assemblies over a six week period. Once that data had been collected, the assemblies will be exposed to the bake conditions that a production part would experience in the priming and painting processes in an OEM assembly plant. Data will then again be collected over a six week period. This data collection process was underway at the end of FY2009.

BLRT-induced distortions were found to become less severe over time in the SMC-epoxy assemblies. Conversely, these distortions were found to increase slightly over time in the steel-epoxy assemblies. These changes, however, were fairly small, so were difficult to quantify when attempting to extract peak curvature values. Using a modified version of the BLRT algorithm for converting the curvature maps to BLRT severity scores clearly showed these changes.

Phase 3

Modeling Overview

A modeling activity was initiated at the start of CY09. The objective of this activity is to develop a finite element (FE) model capable of predicting the occurrence and severity of BLRT before manufacturing physical components. Preliminary modeling work using linear elastic material properties was completed in FY09 and implementation of nonlinear adhesive material properties was started at the beginning of FY10.

Linear Elastic Material Model Assumptions

A finite element analysis (FEA) based approach was used to study deformations induced by accelerating the cure of adhesives at elevated temperature. Detailed three-dimensional FEA models were developed for several configurations including an outer panel with an adhesive bead and two sizes of drops, a bonded panel assembly, and a bonded panel assembly with stand-offs in the bond-

line. A finite element mesh was created for each model such that element boundaries were aligned parallel and/or perpendicular to bond lines to facilitate comparison of predicted responses with measured curvature or profilometer / CMM displacement data. A typical FE model is shown in Figure 7.

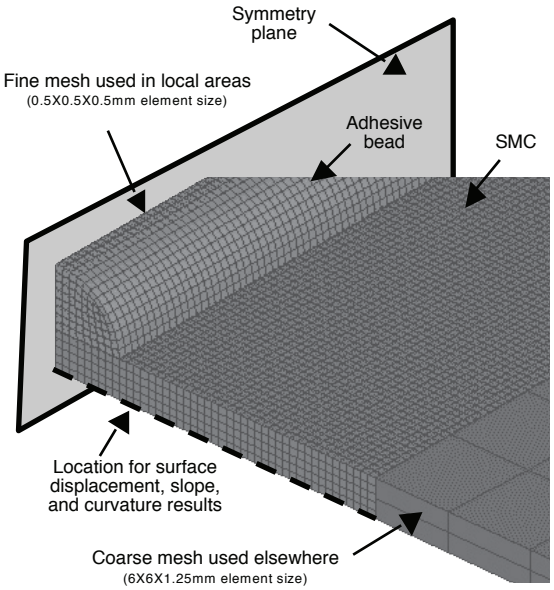

Figure 7. Representative FE Model Detail for an SMC outer panel with an adhesive bead

All modeling studies assumed an idealized elevated-temperature adhesive cure. The problem was solved using a steady state thermo-elastic analysis with the nonlinear geometry option enabled. In the analysis, the panel was assumed to be stress-free at the adhesive cure temperature, and the structural response was predicted for an isothermal cool-down to ambient temperature. A combination of estimated and published values for SMC and adhesive material properties were assumed at the early stages of the study (see Table 3).

Table 3 Material Properties for SMC and Adhesives

Property	Units	SMC	Urethane	Epoxy
E_0	Gpa	10.6	0.364	
E_{90}	Gpa	1 .		
E_Z	Gpa	6.0		
Poisson's Ratio				
ν	–	0.25	0.49	0.49
ρ	g/cc			.
Inplane	1 - /°C			
$CLTE_{Normal}$	1 - /°C	80.0		.

The displacement of the surface was an output of the FE analysis. The associated slopes and curvatures were estimated by taking the first and second derivative of the displacements, respectively, with respect to the position using a simple finite difference scheme. A more detailed description of the analysis method and results can be found in [5]. An example of the results from the analysis is shown in Figure 8. The predicted surface displacement, slope, and curvature results are compared in Figure 8 for the case of an SMC outer panel with an applied epoxy or urethane adhesive bead. The results illustrate a larger negative peak curvature for an applied epoxy bead than for an applied urethane bead. Higher peak curvatures correspond to more severe BLRT. The relationship shown in Figure 8 was in agreement with experimental observations.

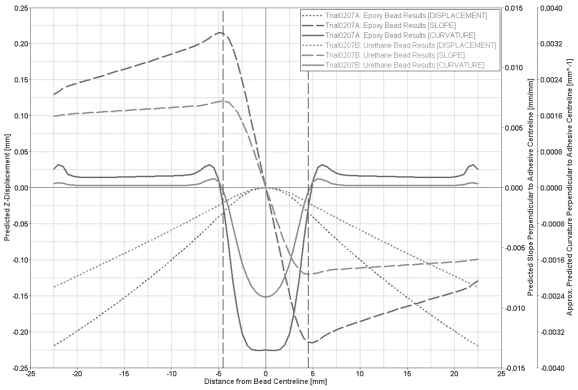

Figure 8. Predicted responses for an SMC outer panel with epoxy and urethane adhesive bead

Predicted surface curvature profiles for the assemblies in which bond standoffs were molded into the bond flanges were found to correlate well with the measured surface curvature in the corresponding experimental assemblies (the third experiment in FY09). A detailed description of the modeling results can be found in [2]. As an example of those results, Figure 9 shows a comparison between predicted and measured curvatures for an SMC assembly with stand-offs in the bond flange bonded with urethane adhesive. The predicted results were derived from a localized ¼-symmetry model of a large stand-off near the center of the panel (see Figure 9 inset). The results indicate that the analysis correctly predicted the character of the curvature response, while tending to over-predict the magnitude of the peak curvatures. The model predicted higher BLRT severity for assemblies bonded with urethane adhesive than that for assemblies bonded with epoxy adhesive. This relationship was the same as that seen in the experimental assemblies and explained those experimental observations. Those experimental results had initially appeared to contradict previous observations (e.g. Figure 8); however, investigation of the modeling results demonstrated that the urethane adhesive will cause more BLRT-induced deformation than the epoxy adhesive in assemblies where the cross section of the adhesive bead is inconsistent along its length (e.g. when there is a standoff in the bond flange).

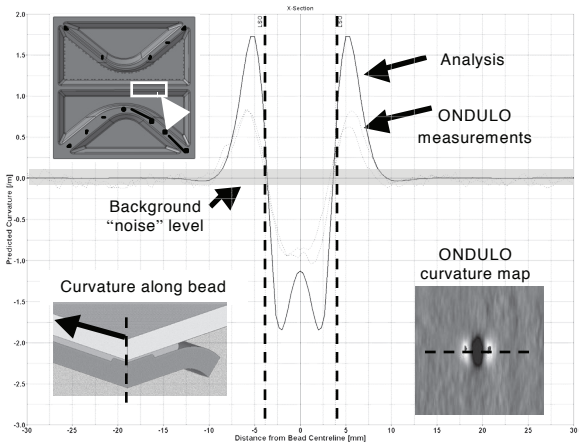

Figure 9. Predicted and measured curvatures for a urethane bonded SMC assembly with "large" stand-offs

Nonlinear Material Model Assumptions

In the absence of detailed material properties, additional studies were conducted using assumed adhesive material properties to assess the potential effects of nonlinear elastic-plastic stress-strain behavior and viscoelastic stress relaxation effects. The results of those studies were promising in that the character of the curvature response was anticipated to remain unchanged while the peak curvatures were reduced. Thus, incorporation of nonlinear adhesive material

effects is expected to improve the correlation between the experimental results and the ability to predict BLRT. This will be the focus of further investigations.

Future Direction

This project is anticipated to be finished by the end of CY2010. Five experiments are planned for FY2010. In the first and third, the larger assemblies that mimic a closure panel construction will be built. The first experiment will evaluate several design strategies for dealing with manufacturing variation in a way that minimizes squeeze-out and, hopefully, does not create distortions in the surface due to contact between the inner and outer panels. The third experiment will determine whether the relationships between material and process factors and BLRT severity are still valid when a hot air impingement bond fixture is used rather than electrically heated bond fixture. Lab-scale assemblies will be built in the second and fourth experiments. The second experiment will investigate whether the BLRT severity after priming and painting processes is dependent upon the amount of time the assembly is allowed to relax prior to being subjected to those processes. The fourth experiment will be used to validate the FE models' prediction of the effect of bead shape on BLRT severity. The fifth experiment will be a final model validation experiment. The data for a current service part that exhibits BLRT will be analyzed using the BLRT FE modeling approached developed in this project and design changes to reduce BLRT severity will be identified. The team will then make those changes to the part/tooling and build new assemblies. The BLRT present on the assemblies prior to the changes will be compared to that after the changes were made to demonstrate the applicability of all this work to an actual part.

BLRT Modeling Work

To improve the quantitative correlation between the predicted BLRT-induced distortion and the measured distortion, the project team has initiated material testing to characterize viscoelastic and nonlinear stress-strain material properties. Once the material data is available, the material models will be updated. The resulting revised FE model predictions will then be compared to the experimental data to assess the improvement in the predictive capability of the analytical models when more precise material characterization is incorporated. The initial viscoelastic characterization of an epoxy adhesive was well underway at the time of this writing and the early results of modeling assemblies made in the fourth and fifth experiments completed in FY09 appear promising. Incorporation of the updated material models appears to significantly improve the correlation between the predicted and measured peak curvatures [4]. Modeling efforts are underway to further refine the initial analytical viscoelastic epoxy material model and to implement material models for a polyurethane adhesive and a second epoxy adhesive. As noted above, additional test-analysis correlation studies will be conducted in FY2010 to validate the modeling approach. Upon successful validation, the procedures and data shown in this project to be necessary to accurately predict the severity of these distortions will be introduced to the supply base to use in the design of production components.

Presentations/Publications

1. Fernholz, K.D., Lazarz, K., and Wang, C.S., SPE Automotive Composites Conference, Troy, MI, Sept 15-16 (2009).

2. Fernholz, K.D., Fuchs, H., Deslauriers, P., Lararz, K., and Wang, CS, COMPOSITES 2010, Las Vegas, NV, February 9-11 (2010).

3. Fernholz, K.D., and Lazarz, K, The Adhesion Society 33rd Annual Meeting, Daytona Beach, FL, Feb 21-24 (2010).

4. Fuchs, H., Fernholz, K., Deslauriers, P., J. Adhesion (submitted).

5. Fuchs, H., Deslauriers, P., SPE Automotive Composites Conference, Troy, MI, Sept 15-16 (2009).

D-LFT Project

Direct compounding of thermoplastic polymers has become widespread within the automotive supply base due to the cost and performance benefits offered over conventional long fiber injection or compression molding. By integrating the compounding of raw materials into equipment at the Tier 1 supplier, intermediate process steps are avoided and new possibilities for tailored composite solutions are created. Furthermore, direct compounding reduces the extent of fiber length attrition, leading to improved material properties and thus improved component performance.

Exploratory Study

Preliminary studies focused on identifying shortcomings of existing polyamide formulations and determining if key hurdles needed to be overcome for processing these materials by extrusion compression. The pre-compounded materials listed in Table 4 also provided a set of benchmark data to be used as targets for future materials development.

Table 4. Pre-compounded, injection molding grade pellets for benchmarking study

Material	Glass Fiber Length	Glass Fiber Content	Polymer Type
DuPont Zytel® 70G30HSLR BK099	~3 mm	30 wt%	Polyamide (PA) 66
DuPont Zytel® 75LG40HSL BK031	12 mm	40 wt%	Polyamide (PA) 66
DuPont Zytel® 75LG50HSL BK031	12 mm	50 wt%	Polyamide (PA) 66
DuPont Zytel® HTN51LG50HSL BK083	12 mm	50 wt%	Polyphthalamide (PPA)

Equipment

Processing studies were performed at the National Composites Center (NCC) in Kettering, Ohio. The facility provided access to a 400 ton hydraulic down acting compression molding press and a 150mm, 36:1 L/D, single screw compounder-extruder. Both of these units were manufactured by C.A. Lawton. An aluminum plaque mold measuring 240 x 595 mm was used to produce panels for subsequent testing.

Results

Baseline properties were established for each of the material grades by excising samples from molded flat panels. Figure 10 shows the test sample layout on the flat panels for each of the tests performed. As the degree of anisotropy in these panels was expected to be significant, testing was performed in both directions (0° or flow/extrusion direction and 90° or cross-flow/ cross-extrusion direction) relative to the molded flat panels.

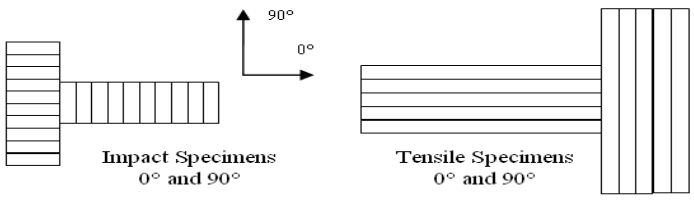

Figure 10. Test Specimen Layout on Flat Panel (not to scale)

Impact Testing

Notched Izod impact testing was performed according to ASTM D256, Test Method A [6]. Specimens were cut from molded flat panels and subsequently notched using a Testing Machines Inc. Model 22-50 Notching Cutter. All specimens were conditioned in a vacuum oven at 45°C for 24 hours. Testing Machines Inc. Model 04-02-03 Monitor/Impact tester was used to conduct impact testing and record data. A total of 10 specimens were tested in both the 0° and 90° panel directions (Table 5).

Table 5. Dry As Molded Impact Test Results

Notched Izod Impact Strength, Dry As Molded (kJ/m²)								
Material	Zytel® 70G30HSLR BK099		Zytel® 75LG40HSL BK031		Zytel® 75LG50HSL BK031		Zytel® HTN51LG50HSL BK083	
Sample Direction	0°	90°	0°	90°	0°	90°	0°	90°
Mean	9.8	6.0	24.5	15.1	34.4	22.3	22.3	15.2
σ	0.6	0.9	2.6	2.1	6.2	5.8	4.4	3.3
COV (%)	6	16	11	14	18	26	20	22

Tensile Testing

Tensile specimens were prepared according to ASTM D638 [7] and were cut from molded panels using a diamond blade band saw. Results are shown in Table 6.

Table 6. Dry as Molded Tensile Properties

Zytel® Grade	Sample Direction	Tensile Strength (MPa)			Tensile Modulus (GPa)			Strain at Break (%)		
		Mean	σ	COV (%)	Mean	σ	COV (%)	Mean	σ	COV (%)
70G30HSLR BK099	0°	160	22.5	14	8.9	0.6	6	2.4	0.5	19
	90°	71	10.9	15	5.6	0.4	7	1.5	0.3	21
75LG40HSL BK031	0°	200	11.9	6	11.7	0.5	4	2.0	0.1	3
	90°	83	12.5	15	6.7	0.4	6	1.4	0.3	18
75LG50HSL BK031	0°	222	17.8	8	15.5	1.4	9	1.8	0.2	10
	90°	107	13.4	13	9.8	1.2	12	1.4	0.2	11
HTN51LG50HSL BK083	0°	208	12.3	6	17.6	1.8	10	1.4	0.1	11
	90°	45	10.6	24	9.3	1.4	15	0.5	0.2	28

This may suggest polymer degradation and that the heat stabilization packages designed for injection molding compounds are not quite sufficient for compression molding.

Based upon the above, this particular processing equipment and methodology appear suitable for continued development of direct compounded, polyamide based materials in lieu of a complete D-LFT processing cell.

Conclusions

Processing trials were performed using off-the-shelf, injection molding compounds to establish the baseline processing characteristics and subsequent mechanical performance of these materials in an extrusion-compression molding process. A summary of the findings is highlighted in the list below.

- Charge handling was not an issue suggesting that injection molding grade material viscosities are also sufficient for direct compounding extrusion-compression molding.
- Mechanical performance of the extrusion-compression molded materials were slightly lower than datasheet properties for the same materials processed via injection molding
    1. In general terms, the tensile modulus was approximately 10% lower, the ultimate tensile strength was reduced by 15-20% and notched Izod impact was 25-30% lower
    2. The reduction in mechanical performance could be attributed to net-shape molding of the injection molded specimens versus excising samples from flat panels via machining
    3. Additional investigation is required to ascertain the reduction in mechanical performance of the extrusion-compression specimens relative to injection molded datasheet properties from this particular trial
- Dry as molded impact and tensile mechanical data is largely equivalent but reduced relative to injection molded datasheet values

References

1. ASTM Standard D256, 2006ae1, “Standard Test Methods for Determining the Izod Pendulum Impact Resistance of Plastics,” ASTM International, West Conshohocken, PA, 2006, DOI 10.1520/D0256-06A, www.astm.org.
2. ASTM Standard D638, 2008, “Standard Test Method for Tensile Properties of Plastics,” ASTM International, West Conshohocken, PA, 2008, DOI 10.1520/D0638-08, www.astm.org.

E. Natural Fiber Composite Retting, Preform Manufacture and Molding (Project 18988/Agreement 16313)

Principal Investigator: Kevin Simmons
Pacific Northwest National Laboratory (PNNL)
P.O. Box 999, Richland, WA 99354
(509) 375-3651; e-mail kevin.simmons@pnl.gov

Contributors: Dan Howe, Sachin Laddha, Leonard S. Fifield (PNNL)

Industry Consultants: Dan Houston (Ford) and Libby Berger (General Motors)

Technology Area Development Manager: Dr. Carol Schutte
(202) 287-5371; e-mail:carol.schutte@ee.doe.gov

Field Technical Monitor: Mark T. Smith
(509) 375-4478; e-mail: mark.smith@pnl.gov

Contractor: Pacific Northwest National Laboratory
Contract No.: DE-AC05-76RL01830

Objective

- To develop, build and demonstrate an economical, lab-scale, automated fiber retting process and apparatus suitable to bast-based fibers, including hemp, kenaf and flax.
- To develop and demonstrate a thermoset polymer preform compression molding process and produce panels to develop a mechanical and thermal natural fiber polymer composite database.

Approach, including industrial partner/collaborator and path to technology transfer and commercialization

- Explore existing and new fiber preparation approaches, including decortication techniques, high-speed fiber separation, steam explosion, chemical treatment and modified extrusion methods.
- Develop the fundamental understanding of bast fiber structure that will provide direction for fiber separation.
- Conduct several lab-scale process trials of fiber preparation-retting processes enabling the development of the most appropriate process and instrumentation.
- Develop and construct a non-aqueous natural fiber preforming process capable of integrating surface modification and hybrid fiber and preform geometries.
- Explore alternative material forms, including sheet-molding compounds from natural fiber and hybrid reinforcements.
- Conduct full mechanical, thermal and environmental characterization of manufactured panels.
- Interacting with commercial companies: Materials Innovations Technology, Ashland Chemical, Bast Fibre, LLC and BioTech Mills.

Metrics, Milestones, and Accomplishments

- Milestone (Completed September 2009) - Finalize design and demonstrate non-aqueous fiber preform manufacturing process and apparatus:

  1. Natural fiber sheet molding compounds (SMCs) are inherently difficult to flow in mold cavities. The preform manufacturing technique has utilized the carding process to make sheets of natural fiber material that are impregnated with vinylester or unsaturated polyester resins in sheet molding compound formulations. The sheets are then laid up and formed using soft (silicone tools) or elastic film material that is utilized as a release film. We have preformed a 127 mm by 127 mm box shape with a 25 mm radius feature in the bottom. These preforms are then molded for net shape test parts.

- Milestone (Completed December 2008)-The milestone to design, develop, and manufacture a prototype automated fiber retting apparatus to prepare fiber strands for polymer processing:

  1. The project designed a leaf stripper, designed and built a lab decorticator, purchased a fiber chopper, and designed and prototyped an air laid preforming system for molding panels for testing. The project utilized both off the shelf and custom built equipment to prototype the defibrillation of the fibers that will be used for molding and testing mechanical properties.

  2. Completed fiber analysis lab apparatus, developed fiber analysis procedure and conducted fiber analysis on major natural fiber varieties.

  3. Procured several pieces of hardware assembled into the mechanical fiber preparation line, including fiber cutting apparatus, extruder modification, decorticator and Wiley Mill.

  4. Conducted fundamental research on ionic liquid delignification, super-critical delignification, alkaline and thermal treatment delignification of natural fibers.

  5. Explored several natural fiber non-aqueous preform manufacture strategies and currently exploring two further with mock-up. The process was down selected and best practice put into use.

  6. Completed panel tool and have produced sheet molding compound (SMC) panels from the tool.

  7. Established technical relationships with U.S. kenaf farms, Kengro, Inc., and Bio Tech Mills, Inc.

  8. Developed relationships with resin suppliers (including AOC, Reichhold and Ashland Chemical) and processing companies (including Bio Tech Mills, Inc., Bast Fibers LLC, Material Innovation Technology, TimTek, Inc. and Canadian hemp supplier Stemergy, Inc.).

Future Direction

- Determine the most appropriate method to integrate fiber surface modification technology into the preform manufacture process.
- Interface with resin suppliers concerning SMC formulations for producing panels.
- Develop natural fiber SMC and hybrid-fiber architectures.
- Develop a method to make large parts/performs with natural fiber composites.

Introduction

The objective of this project is to develop a capability in the area of natural fiber retting, preform and composite manufacture to enable the large-scale insertion of natural fiber reinforcement into the automotive industry. The benefits of natural fiber reinforced composites are well known and include lightweighting, energy savings, cost reduction, carbon capture, recycling and the environmental benefits from using renewable resources. However, several technical milestones must be met before engineering, manufacturing and commercial sectors will embrace natural fiber as a viable replacement for glass fiber reinforcement. The PNNL work addresses three critical barriers restricting natural fiber usage in automotive manufacture: (1) development of an inexpensive, rapid, environmentally friendly mechanical process to remove natural fibers from plant stalks, (2) development of a rapid cost-effective method to create natural fiber preforms suitable for infusion of a thermoset polymer matrix, and (3) development of a natural fiber polymer composite molding process adaptable to hybrid fiber composites and ester, soy and urethane resins.

Retting is a fiber preparation process that traditionally has involved separating fibers via soaking fibers in water and partially rotting the fiber binders. Four methods of accomplishing this process include: dew retting, water retting, water retting combined with heat and chemical retting. Preparation should ideally prepare a fiber to be surface modified to promote bonding and adhesion and provide both dimensional stability and mechanical property enhancements. Surface modification of natural fibers can be employed to optimize properties of the fiber-matrix interface and can be integrated within the fiber preform manufacturing process. In this way a processed preform may be stored for long periods of time prior to composite manufacture without loss of mechanical properties from excessive moisture uptake and compromised composite fiber/resin interface.

Fiber Preparation

In the beginning of FY09 several hundred pounds of contractually grown kenaf was received from the Washington State University Irrigated Agriculture Research Extension Center (WSU-IAREC) in Prosser, Washington. Fiber was also purchased from KenGro of Mississippi.

PNNL personnel researched and developed the following processes and apparatus in an effort to develop a novel, mechanical-based fiber preparation process.

Decortication

In FY08, PNNL procured a lab-scale roll laminator and adapted it to perform the decortication process. The roll laminator modification was completed and it was used in FY09 to decorticate the Prosser kenaf crop harvested in the last quarter of FY08. Nearly 100 pounds of Prosser kenaf were mechanically decorticated

Two sets of rollers in series, used with various pressure settings based on previous data, were used to evaluate core removal effectiveness. The first roller set had two matching V-shaped designs that meshed with the lower rollers. The design of the first set of rollers was such that it pulled the core into the machine while the pressure helped split the stalk open. This set the stage for the second set of smooth rollers which helped shear the compressible core from the outer bast fiber.

A design of experiments was conducted according to the Taguchi Method of Orthogonal arrays. Six different factors were considered and two levels to form an L8 orthogonal array as shown in Table 1. The effect of all these parameters was studied on the performance of the decorticator. The performance is based on the efficiency of the decorticator to separate the core and the fiber with minimum labor handling.

Table 1. Factors and levels for Orthogonal arra

Factors	Levels	
	Low 1	High 2
Speed of feed (revolutions per minute (RPM) (A)	2	9
Angle of Insertion of stalks (B)	0°	45°
Direction of feed of stalk (C)	forward	forward & backward
Pressure of rollers on stalk (pounds/ sq. in.) (D)	20	60
Diameter of stalk (cm) (E)	1.00-1.75	1.76-2.50
Smash stalk With dead blow (F)	pre-broke stalks	unbroken stalks

The efficiency of the decorticator was defined based on the amount of core completely separated after processing. The signal to noise (SN) ratio was calculated as per the following equation: $SN_i = 10 \log (Y_i^2/S_i^2)$

Where, $(Y_i) = 1/N_i \sum_{u=0}^{N_i} y_i,u \; (S_i)^2 = 1/(N_i - 1) \sum_{u=0}^{N_i} (y_i,u - Y_i)$

i=Experiment number, u=Trial number and N_i=Number of trials for experiment i.

The different signal to noise (SN) ratio for the L8 orthogonal array were summarized sand then ranked in Table 2 for the response of all the factors. This table was created by calculating an average SN value for each factor.

Table 2. Response table of all the factors and ranking

Level	A	B	C	D	E	F
SN	105	124	146.1	104.2	165	146
Rank	4	6	2	5	1	3

According to the Taguchi method, the diameter of the stalk followed by direction of feed are the significant factors towards the efficiency of the decorticator. Having the diameter of stalk as 1.76-2.50 cm, direction of feed of 450 and pre-broke stalks would give the efficiency of the decorticator up to 97%.

Retting

We define fiber as a unit bundle of fibrils. An ultimate fibril refers to the smallest morphological unit of cellulose which makes up the fibril as shown in Figure 1a & 1b. The lignin and hemicellulose are the waxy coating and fibril binding materials, respectively, that give the plant fibers their composite strength. These components lead to resin compatibility, moisture uptake and composite processing challenges. The more crystalline cellulose portion gives the fiber its strength.

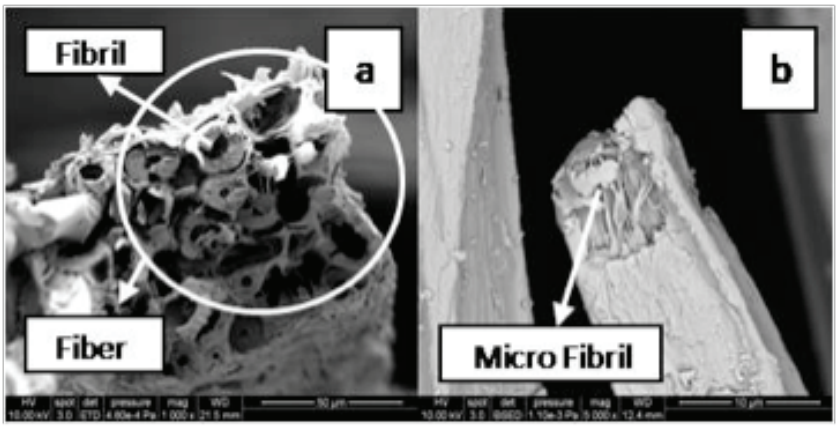

Figure 1. Fibers and fibrils for kenaf.

Ionic Liquid Delignification

After determining that ionic liquids (IL) can disperse pure lignin, their usefulness with natural fibers was examined. Milled samples of kenaf were reacted with the Hunig's-butanol IL with a stoichiometric amount of water at two different temperatures and two different times. The results of these experiments, suggest that the limiting factor in these reactions is the water available as an acid generating catalyst.

The next experiment reacted 50 mm fiber bundles with the IL's at different temperatures with different agitation methods, namely a stir bar and external agitation of the beaker (hand stirred). These fibers were then analyzed via x-ray diffraction (XRD) and scanning electron microscopy (SEM). The XRD results indicate the removal of amorphous compounds such as lignin and hemicellulose with increasing crystalline cellulose peak size at $2\theta = 22°$. Both of the 70°C runs showed the highest level of crystallinity which increased from 35% to 55.8%. Agitation methods did not show a trend in either direction for crystallinity values.

SEM imaging of the fibers showed that IL processing is effective in removing the waxes, resins, and coatings present on unretted fibers. All processed fibers showed significantly smoother fiber surfaces after processing. The images are shown in Figure 2.

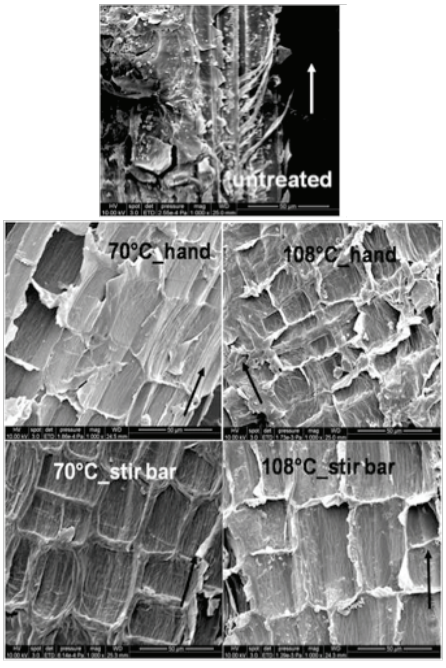

Figure 2. FE-SEM images of fiber surfaces before and post processing with ionic liquid. Smoother surfaces correspond to removal of waxes, resins, water soluble compounds, and extracellular lignin.

Breaking tenacity tests of the IL processed kenaf fibers showed that for all samples the tenacity decreased with processing, but the decrease was greatest in the mechanically agitated samples. This suggests there is an element of chemical weakening induced by removal of the lignin and hemicelluloses holding fibers together and that mechanical defect can be imparted through rough agitation. The tenacity testing throughout the project was done in accordance with American Society for Testing Materials (ASTM) 1294.

The results of the ionic liquid testing indicate that this is a strong candidate as a processing technology, but further optimization must be done. Factors to be optimized include the IL liquor to fiber ratio, water addition amount, water addition rate, processing temperature, time, and agitation method.

Ethanolysis of Kenaf Lignin

Supercritical fluids, solvents controlled at temperatures and pressures above their critical point, can have liquid-like densities and solvation characteristics while exhibiting vapor-like diffusivities. Reactants and solvents in the supercritical phase may effectively access a wide range of the micro and macro pores in a porous material to deposit chemical functionality or to extract material. The tunability of supercritical solvent characteristics by temperature or pressure adjustment can enable ease of separation of dissolved species from reactant solutions. These promising functions of supercritical fluids have the potential to extract components (such as lignin from biomass) selectively to simplify clean up of lignin processing solutions and facilitate recycling of reaction solvents.

Batch-type reactions of decorticated kenaf bast fibers and milled kenaf fiber flour with pure ethyl alcohol (ethanol) were carried out using a stainless steel tubular pressure reactor. The temperatures of the reactor and residence time of the reaction were both controlled through immersion and removal of the reactor from a heated sand bath. Reactions were carried out at 270ºC, above the critical point of ethanol, for periods up to 30 minutes. Crystallinity of the treated samples, as determined by x-ray diffraction, is a measure of the removal of the amorphous, non-cellulose components. It was observed that percent crystallinity of treated samples increased with reaction time. Fiber bundles were observed to separate into distinct fibrils following treatment as observed by SEM (Figure 3). This is consistent with removal of the lignin and hemicelluloses connecting fibrils in the untreated plant.

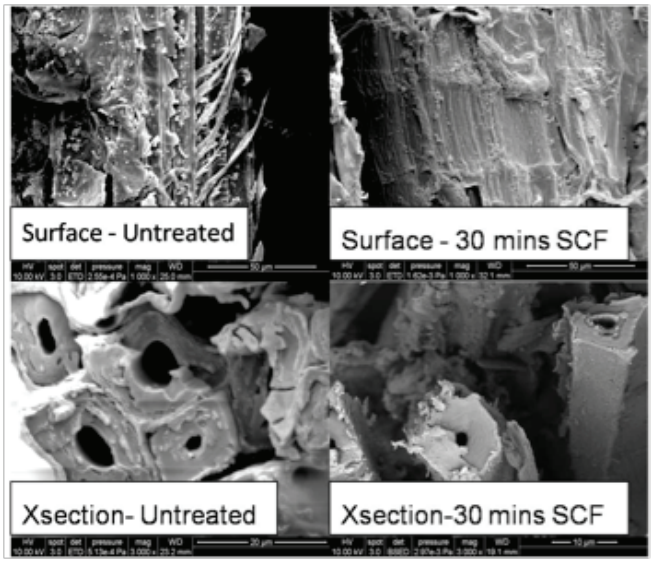

Figure 3. SEM images of untreated fibers and fibers treated with Supercritical ethanol for 30 minutes.

Motivated by the potential of supercritical fluids as processing solvents and the observation of selective lignin removal from woody biomass using supercritical alcohols by Shiro Saka's group at Kyoto University, we have pursued ethanol as a supercritical reactant/solvent for lignin removal from kenaf fibers.

Compared with the untreated kenaf fibers, super critical fluid treated fibers have a lower moisture-loss temperature peak, which illustrates that less water is bound to the surface even with higher surface area. The corresponding mass loss in Thermo-gravimetric Analysis (TGA) also decreased due to the increased crystallinity. The higher ordered crystallites offered better moisture resistance and thermal stability. Increased smoothness of the treated fiber surface was accomplished by the removal of wax, oil and other surface impurities present in the untreated fiber. As the non-cellulosic components such as hemicellulose, pectin and lignin were removed from the external surface of the fiber cell wall by treatment, the inside fibrils or short length crystallites were exposed. Similar surface morphology changes were revealed for the fibers treated with sodium hydroxide described below.

Thermal Treatment

A 24 factorial design of experiments was conducted to study the effects of temperature, pressure and time on the delignification of the kenaf fibers treated under nitrogen and in air.

XRD analysis confirmed the removal of amorphous lignin and hemicellulose structural components for treatment at 175°C for 6 hours in air. The fibers treated at this temperature showed an increase in crystallinity to 70%, twice that of untreated fiber at 35%, and had larger cellulose crystallite size.

Sodium Hydroxide (NaOH) delignification and characterization

In this study, treatment time of alkaline modification was studied at a sodium hydroxide (NaOH) concentration of 5%. The technique is the most common technique used for delignifying bast fibers. All alkali treated kenaf fiber specimens showed an initial endothermic peak between 50 and 150°C and an exothermic peak in the 325°C range in the Differential Scanning Calorimeter (DSC). The corresponding TGA inflection of untreated fibers showed a 3.1 wt% mass loss, which is attributed to the evaporation of absorbed water and volatile impurities, such as wax and water-soluble substances.

The endothermic peak shifted to higher temperatures after alkali treatment and the corresponding mass loss decreased to 2.36%, 2.23% and 2.19% for NaOH treatment for 1 h, 4 h and 16 h, respectively. This suggested removal of volatile impurities and improvement of surface hydrophobicity. The mass loss peak shoulder decreased with the alkaline treatment time until it disappeared for the 16 hour alkali-treated fibers, suggesting the significant removal of hemi-cellulose and pectin.

A similar phenomenon occurred to the super critical fluid treated kenaf fibers where the inflection around 283°C was absent, starting from a 5 minute treatment of ethanol. The evidence of an increased portion of cellulose in the alkali treated fiber over untreated fiber could be seen from TGA, as the onset temperature of weight loss for treated fibers was shifted to the higher temperatures. The reason for the decreased decomposition temperature of cellulose in the super critical fluid case is due to the increased crystallinity as seen in the XRD data Table 3.

Table 3. XRD Crystallinity comparison of alkaline and SCF treated fibers

Fiber samples	Crystallinity (%)	Crystallite size (ang.)
untreated	34.495	16.45
NaOH-1hr	39.412	16.69
NaOH-4hr	49.124	10.8
NaOH-16hr	58.515	16.41
NF-5min	31.54	15.86
NF-10min	45.683	17.51
NF-30min	75.24	23.98

Alkali treatment is often used to increase the surface roughness by disrupting the hydrogen bonds in the interconnected structure of fibers. For kenaf fiber composites, the resultant rough surface benefits mechanical interlocking between fiber and matrix. The exposed cellulose offers an increasing number of possible reaction sites. The cross-section micrographs of alkali treated fibers showed a slight separation of the fibrils, which revealed that some of the cementing materials has been removed (Figure 4). It does not seem to be as effective as the treatment by super critical fluid in removing the cementing materials from kenaf fibers.

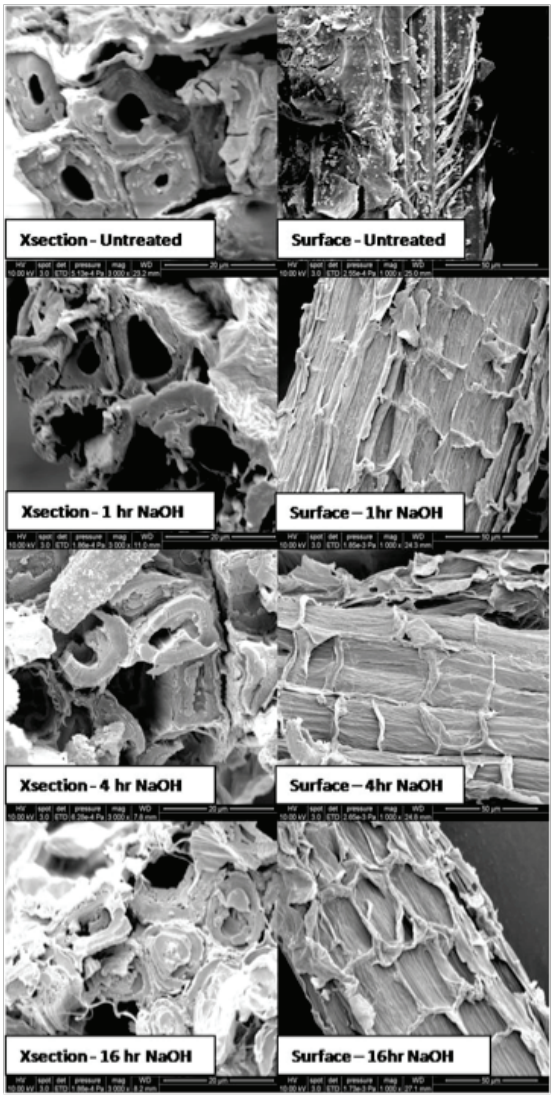

XRD confirmed the removal of amorphous structural components for both treatments, supercritical ethanol treated fibers showed higher crystallinity and larger crystallite size as well as increased spacing, while NaOH has no significant effects on the size and spacing. The ethanol treated fibers had an increase in crystallinity of nearly two times than the untreated material.

Figure 4. SEM images for NaOH treated Prosser kenaf for different time duration.

Both alkali and super critical fluid treatments are effective in removing lignin, pectin and hemicellulose; super critical fluid treated fibers showed the highest onset decomposition temperature of cellulose, indicating its efficiency in removing the non-cellulosic portion and effect of higher thermal stability. Alkaline processing directly influences cellulosic fibril degree of polymerization and the extraction of pectin, lignin and hemicellulosic components.

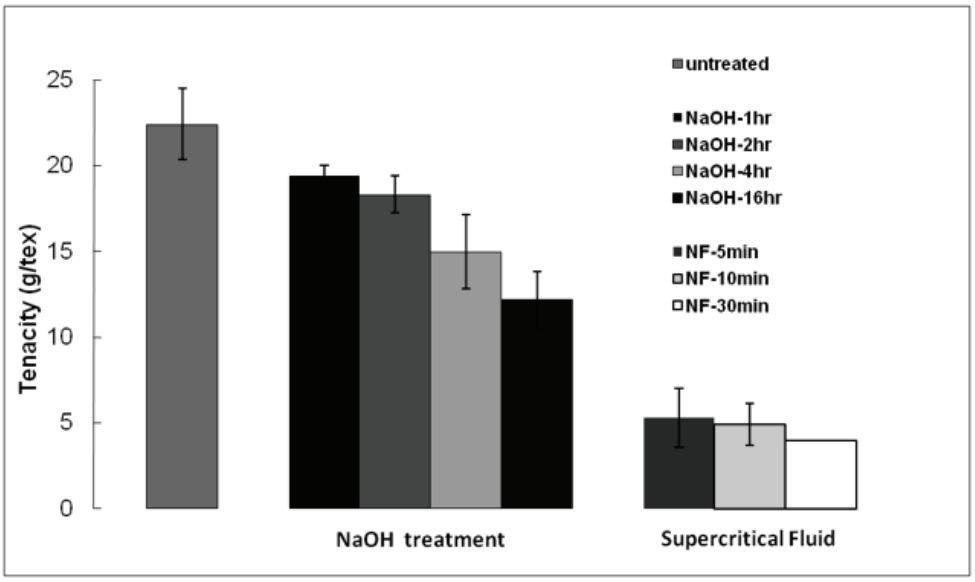

Figure 5. Influence of chemical treatments and treatment durations on the tenacity of kenaf fibers.

Most of the pectin and part of the lignin is removed during the chemical treatment, and delignification was found to increase the fineness but decreases the strength of the natural fibers. This is consistent with our study on the mechanical property of kenaf fibers. Kenaf fibers treated with alkaline solution and super critical fluid showed reduced tenacity, compared with the untreated fibers, and the decrease is more pronounced with longer treatment duration (Figure 5).

Notice that the fibers treated with super critical fluid demonstrated extremely low tenacity. Considering the complete separation of fibrils as seen in the fiber cross-section morphology, the reason could be attributed to the failure of stress transfer between fibrils under load due to the complete removal of cementing materials. In fact, the 30 minutes-super critical fluid treated fibers were too weak to repeat the testing. The fracture morphology in Figure 6 offers a good explanation of the reduced mechanical properties of the chemically treated kenaf fiber. The fracture surface of untreated fibers in Figure 6a is clean and smooth, indicating sufficient bonding among the fibrils in side of fiber unit. Alkaline treated fibers show rough surface after fracture, obvious fibril pull-out can be seen from Figure 6b.

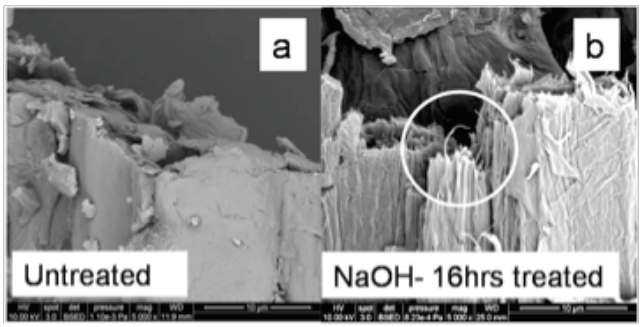

Figure 6. Fracture morphology studies.

As for the super critical fluid treated fibers, the separated fibrils are the entity that is subjected to the load, ultimate fibrils pull-out can be seen due to the abundant extraction of cementing materials. Treated fiber tenacity was reduced by impairing the stress transfer due to the loss of cementing materials. Fracture surfaces showed fibrils pull-out.

Preform Processing and Composite Manufacture

The goal of this task is to develop a preforming process to produce natural fiber reinforced preforms of a variety of geometries without an aqueous solution.

Figure 7a shows the 11 layers of kenaf fiber sheets which were used to manufacture one panel of kenaf fiber with 50 vol% fiber density shown in Figure 7b. The resin was applied to each of these layers to ensure uniform fiber to resin ratio throughout the panel. Panels produced from sheet molding compounds (SMCs) using this technique have been made with glass and kenaf fibers.

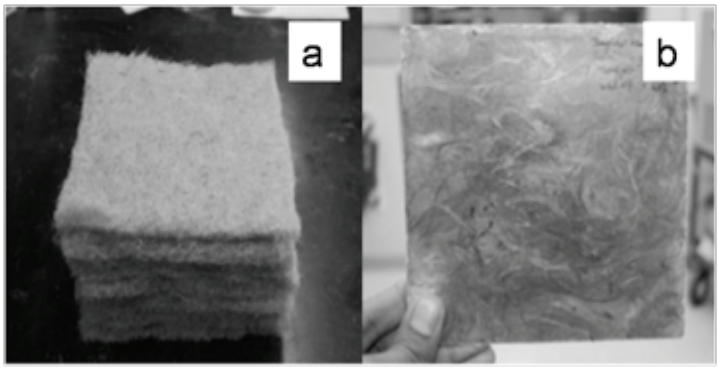

Figure 7. 50 Vol% SMC of Bangladesh kenaf fibers.

Initially, two different types of fiber laminating techniques were studied – hand lay-up and carded kenaf sheets. Panels were molded with 50 vol% kenaf at 275 °C for 20 minutes under pressure. Figure 8a and 8b give the difference in the fiber density across the panel with hand laying and carding techniques. It was found that the carding technique reduced the fiber density variation in the panel significantly. Hence, carded fiber sheets were used to manufacture the panels for mechanical property comparison.

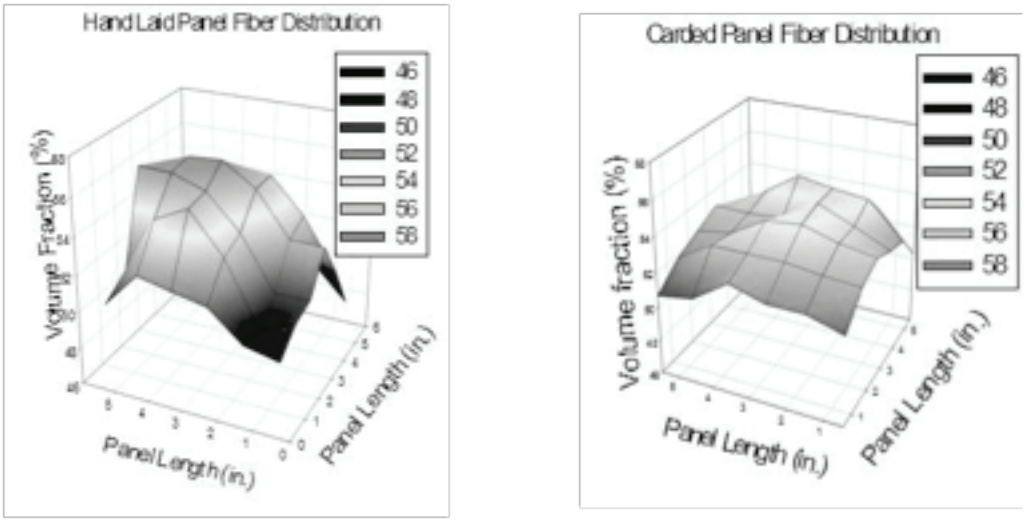

Figure 8. 3D plots of volume fraction as a function of panel length and breadth; a) hand laid, b) carded sheet.

After trying different methods, the kenaf fiber preforms were produced and are shown in Figure 9. A method was developed to impregnate the resin on the fibers and then mold the preform under the appropriate pressure at 275ºC to cure. The preform contains 50 vol% fibers with no fillers.

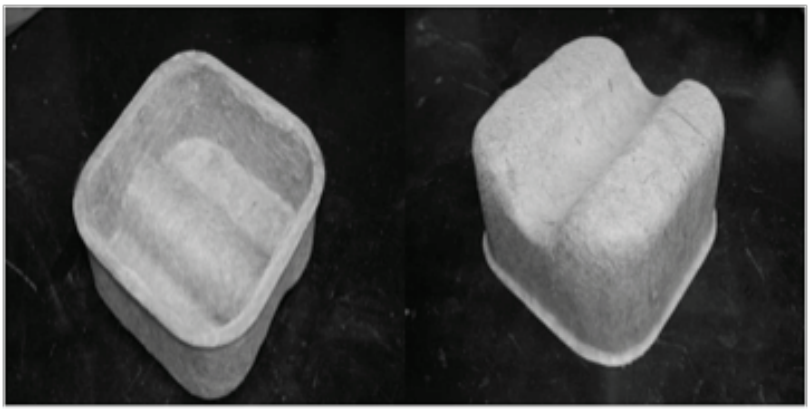

Figure 9. Preform of curved pieces with complex fillets

Mechanical Property Test of Composite

The compression molded panels were characterized for flexural and tensile properties using 50% RH conditioned samples and 24 hours water soaked samples. The test was done in accordance with the standard ASTM methods. (1)(2)

It was found that the flexural modulus of 50 vol% untreated kenaf composite conditioned at 50%RH was 10-12 giga-Pascal (GPa) compared to the equivalent glass composite which was 18-19 GPa. Tensile modulus, Tensile strength and Flexural strength showed a similar trend as the modulus. An interesting observation is the values of specific modulus (modulus per unit mass of specimen) which are shown in Figure 10. It shows that the specific modulus of kenaf composite is around 90% of the value of glass composite without any surface modifications.

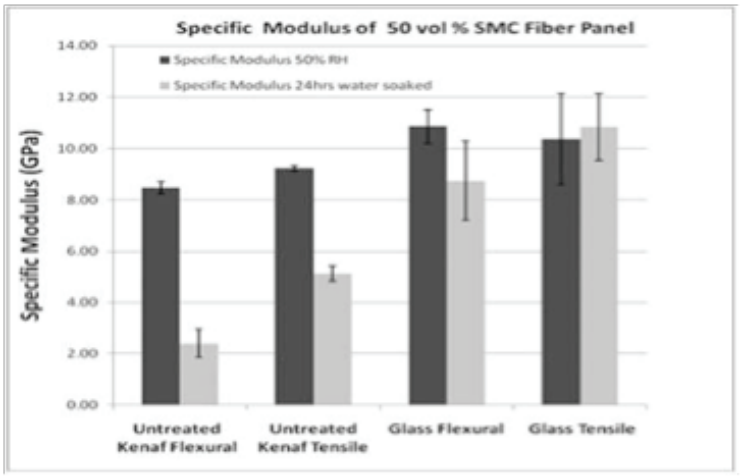

Figure 10. Specific Tensile Modulus of 50vol% SMC panels.

Conclusions

Natural fiber composites are experiencing increased application in automotive components due to weight savings, cost savings and environmental considerations. Continued extension of this trend to structural and semi-structural as well as external vehicle applications with resultant additional improvement in weight savings will require the development of natural fiber composites with improved processing, mechanical properties and durability in use.

Several promising retting techniques were explored and new understandings were gained on how to implement them in scaled processes. Ethanolysis demonstrated nearly a two fold increase in crystallinity which demonstrates its effectiveness in removing extractives in a very short period of time. Ionic liquids have also shown selectivity to lignin and a tailoring capability to target specific chemistries for removal.

PNNL developed a fiber processing technique utilizing materials and input from natural fiber suppliers including Biotech Mills, Bast Fibers, LLC and Tier 2 automotive resin suppliers including Ashland Specialty Chemicals.

Presentations/Publications/Patents

1. "Natural Fiber Composites in Transportation Applications: Market Opportunities and Technical Challenges" by JD Holbery. International Wood Composites Symposium 2009 Technical Workshop on Natural Fibers; Seattle, WA March 30, 2009
2. "Resin/Fiber Compatibility in Natural Fiber Reinforced Automotive Composites" by LS Fifield, C Huang and KL Simmons. 10th International Conference on Wood & Biofiber Plastic Composites; Madison, WI May 11, 2009
3. "Natural Fiber Composites in Transportation Applications – Fiber Preparation, Surface Modification, and Preform Manufacturing Synergy" by KL Simmons, LS Fifield, SG Laddha, DT Howe, and C Huang. 10th International Conference on Wood & Biofiber Plastic Composites; Madison, WI May 11, 2009
4. "Method of Cellulose Fiber Extraction"; KL Simmons, JD Holbery, DT Howe, LS Fifield. PNNL Invention Disclosure 16492-E

References

1. ASTM D 790 – 07 "Standard Test Methods for Flexural Properties of Unreinforced and Reinforced Plastics and Electrical Insulating Materials."
2. ASTM D 638 – 08 "Standard Test Method for Tensile Properties of Plastics"

F. Natural Fiber Composites for Structural Component Design in the Southern Regional Center for Lightweight Innovative Designs

Principal Investigator: Sheldon Q. Shi, Assistant Professor
Forest Products Department, Mississippi State University, Franklin Center, Rm. 222
100 Blackjack Road; Starkville, MS 39759
Phone: (662) 325-3110; e-mail: sshi@cfr.msstate.edu

Participants: M. Qatu, K. Liang, S. Lee, D. Ward, D. Nicolas, D. Zhang, J. Shi, I. Fulton, and W. Che

Technology Area Development Manager: Dr. Carol Schutte
(202) 287-5371; e-mail:carol.schutte@ee.doe.gov

Field Project Officer: Magda A. Rivera
(304) 285-1359; email: magda.rivera@netl.doe.gov

Contractor: Mississippi State University
Contract No.: DE-FC-26-06NT427

Objectives

- Develop fabrication and design methodologies of natural fibers (i.e., kenaf bast) for automotive structural component applications.

Approaches

- Natural fiber retting: Develop natural fiber retting technologies and recommend solutions aimed at improving the fiber quality and reducing the cost.
- Natural fiber treatment: Use nanotechnology and/or chemical modification on the natural fibers to enhance the compatibility and interfacial bonding between the fibers and polymer matrices.
- Composite fabrication and testing: Develop and optimize the natural fiber sheet molding compound (SMC) fabrication techniques to obtain the best performance.
- Composite modeling: Conduct micromechanical material modeling and simulation to provide guidance for the composite fabrication and to elucidate the functions of the deposited nanophase on the fiber surface for the natural fiber composites.

Industrial partner/collaborator and path to technology transfer and commercialization

- Kengro Incorporation, MS: Material supplies and technology transfer to scale up the developed fiber retting/treatment technologies.
- Ashland Chemicals, OH: Material supplies.
- Meridian Automotive System, IN: Materials supplies and natural fiber SMC product development.

Milestone, Metrics and Accomplishments

- An all chemical process was developed to obtain cellulose nanowhiskers (CNW) (Chapter 3).
- A continuing effort is ongoing to generate fibers from the developed chemical retting and inorganic nanoparticle impregnation (INI) processes (see 2008 annual report) for natural fiber SMC fabrication.
- A concept was proven on a novel nanophase treatment technique of natural fibers for the fabrication of functional natural fiber nanocomposite products (Invention Disclosure).
- A concept was proven on a novel technique for the conversion of celluloses into carbon fibers (Invention Disclosure).
- An initial attempt was made using the short mechanically retted kenaf fibers as reinforcements for the unsaturated polyester composites. The commercial mechanically retted fibers, after further grinding and screening to obtain short fibers with a relatively uniform fiber size, were mixed with polyvinyl acetate (PVA) to form into fiber mats. The unsaturated polyester resin was applied onto the mats and then laminated into composite panels. With this procedure, composites with high natural fiber content (over 60%) could be achieved. However, the disadvantages of this method are twofold: 1) an extra procedure is needed to obtain the acceptable fiber quality by grinding and screening; and 2) the commercial SMC additive, $CaCO_3$, was not incorporated into the processing, which would cause other performance concerns for the resultant natural fiber SMC products. In addition, a high natural fiber loading would result in high water absorption (WA) of the panels (the detailed data is not included in this report).
- Attempts have been made to investigate the mechanical properties for the natural fiber SMC products. The modulus of elasticity (MOE) for the natural fiber SMC could be obtained up to 15 GPa at a certain natural fiber SMC formulation with a fiber loading of about 60%. The WA tends to be a concern for the natural fiber SMC products. However, with a formulation of 25% natural fiber content and 30% $CaCO_3$ at a certain fabrication procedure, a composite with a 24-hour WA of less than 1.5% could be obtained (the detailed data is not included in this report).
- A study was conducted on combining natural fiber and fiberglass for the laminated SMC process (Chapter 1).
- An investigation was conducted on using soybean oil additive into the resin formulation for the performance improvement of natural fiber SMC products (Chapter 2).
- A study was initiated on applying molecular dynamics (MD) simulations to estimate the strength of the cellulose and the effect of nanophase and voids at the cellulosic fiber – polymer matrix interface on the interfacial bonding performance of the natural fiber polypropylene (PP) composites (Chapter 4).

Future Direction

- Continue to acquire funding and to work with industry to scale up the developed natural fiber technologies including the rapid weak chemical retting and inorganic nanoparticle impregnation (INI) through the previous effort.
- Look into other retting options, such as thermomechanical processing and bio-retting processing.
- Refine the all chemical process to obtain cellulose nanowhiskers.

- Obtain the single fiber tensile strength properties for different agricultural stems.
- Continue to explore the potentials on the innovative functional natural fiber based composite products with the disclosed nanophase treatment techniques.
- Finalize a few natural fiber SMC formulations for composite fabrication.
- Conduct detailed product evaluation including 1) durability (effect of moisture, temperature and UV), 2) mechanical performance, such as impact, shear, etc. 3) other product performance criteria, such as acoustic, thermal, etc.
- Continue to conduct MD simulations on cellulose structures and the natural fiber composites.

Introduction

Laminated sheet molding compound (LSMC) process was developed and applied to the fabrication of natural fiber based composite. By combining natural fiber and glass fiber into polymer matrix, the resulting hybrid kenaf/glass fiber SMC presented reasonable mechanical properties with a reduced density. Using soybean oil additive into the resin formulation as a sizing agent of natural fiber SMC products was investigated. The mechanical properties, flexural and tensile properties, were increased when 5 and 10 wt% maleinated acrylated epoxidized soybean oil (MAESO) were incorporated. An all chemical process to obtain cellulose nanowisker (CNW) was developed. A fiber yield of 10.4% from the raw kenaf bast fiber was obtained for the CNW, and 36.7% for the micro cellulose fiber. CNW-PVA composites presented a higher tensile strength and elongation compared to the pure PVA composites with a 46.2% improvement when 9% CNW was incorporated. A study on applying molecular dynamic (MD) simulation to the cellulosic fiber – polymer matrix interaction of fiber reinforced composites was initiated.

Natural/Glass Fiber Hybrid Sheet Molding Compounds

Objective: To evaluate the effect of the combining the natural fiber and glass fiber on the physical and mechanical properties of SMC from the lamination process.

Methods: Mechanically retted kenaf fibers in a mat were obtained from Kengro Incorporation, MS. The unsaturated polyester AROPOL Q 6585 resin was supplied by Ashland Chemicals. The unsaturated polyester fiberglass sheets with $CaCO_3$ were provided by Meridian Automotive Systems with 25 wt% fiberglass and 30 wt% $CaCO_3$. The unsaturated polyester fiberglass sheet was laminated with the kenaf fiber mat. The laminates were pressed at room temperature for three minutes. The resulting unsaturated polyester kenaf/glass fiber hybrid sheet was aged at 35°C for two days, and then cured at 150°C and 100 psi for 20 minutes. Four panel types (Table 1) were fabricated. The densities, 24-hour water absorption (WA), flexural and tensile properties of the composites were measured based on ASTM D1622-03, ISO 62, ASTM D 790, and ASTM D 638 standards, respectively.

Table 1. Natural/glass fiber hybrid sheet molding compound compositions.

Panel	1	2	3	4
Kenaf fiber, wt%	0	17	22	45
Glass fiber, wt%	25	21	20	14
$CaCO_3$, wt%	30	25	24	16
Resin mixture, wt%	45	37	34	25

Results and Discussion: Figure 1 shows the densities and 24-hour WA of the unsaturated polyester SMC. Panel 1 (without kenaf fiber) showed the highest density (1.98 g/cm3). As the kenaf fiber content increased, the density of the hybrid SMC decreased. The density of the

hybrid composite decreased by 27 % after 45 wt% of kenaf fiber was incorporated into the composites. The WA of the composites was increased as the kenaf fiber was incorporated into furnish, from 0.4 % (0% kenaf fiber content) to 10.4% (45 wt% of kenaf fiber content), thanks to the hydrophilic nature of the natural cellulosic fiber. However, it should be noted that the panel with 45% kenaf fiber content contained less amount of $CaCO_3$ (16% vs. 25 – 30%) that would attribute to the high WA for the composites. Because of the unique characteristics of the natural fibers, the process of incorporating the $CaCO_3$ into the SMC can be difficult to control. In addition, the natural fibers used in this study were commercial mechanically retted kenaf bast fibers, which had a lower fiber quality compared to those retted from the developed chemical process (higher cellulose content).

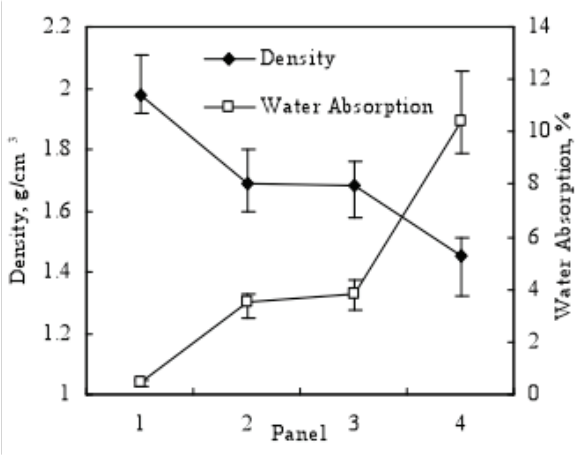

Figure 1. Density and water absorption of four SMC panels.

Ongoing research aims at developing an appropriate methodology to incorporate different ingredients for the natural fiber SMC formulation using the chemically retted kenaf bast fibers. The flexural modulus and strength of the composites (Figure 2) decreased as the kenaf fiber content increased. For Panels 2 and 3, the flexural moduli were above 8 GPa, and the flexural strength was around 100 MPa. Panel 2 had 17 wt% kenaf fiber, 21 wt% glass fiber, and 37 wt% resin mixture. Panel 3 had 22 wt% kenaf fiber, 20 wt% glass fiber, and 34 wt% resin mixture. Compared to Panel 1 (25 wt% glass fiber and 45 wt% resin mixture), less glass fiber and polymer resin were used in both Panels 2 and 3. The flexural modulus of Panel 4 (45 wt% of kenaf fiber, 14 wt% of glass fiber, and 25 wt% of resin mixture) was around 7 GPa and the flexural strength was around 60 MPa. The tensile moduli (above 8 GPa) were obtained for the four different panel types (Figure 3). Interestingly, the tensile strength of the SMC decreased as the kenaf fiber content increased. When 45 wt% of kenaf fiber was incorporated into the composites, the tensile modulus and strength were reduced by 12% and 37%, respectively.

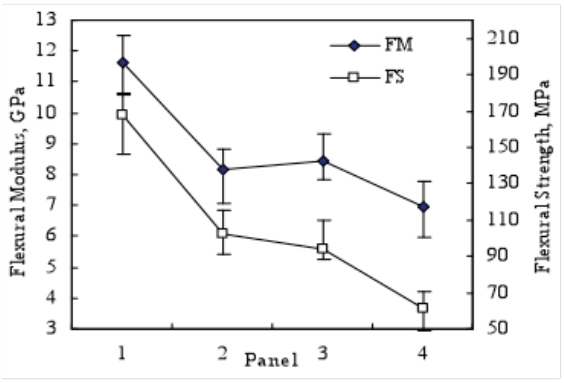

Figure 2. Flexural modulus and strength of four SMC panels

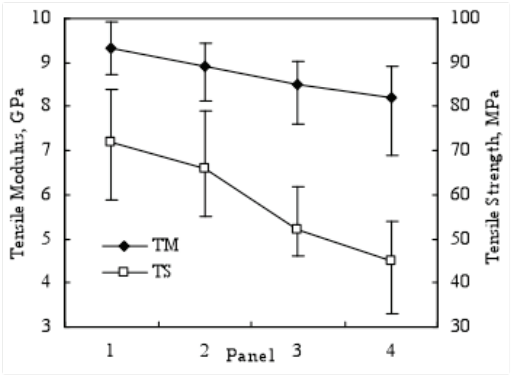

Figure 3. Tensile modulus and strength of four SMC panels.

Resins from Soybean Oil-based Additives for Natural Fiber Sheet Molding Compound (SMC) Composites: Synthesis and Characterization

Objectives: To obtain a suitable sizing agent from soybean oil to improve the compatibility between natural fiber and the SMC molding resin. Soybean oil is an excellent annually renewable natural resource. Figure 4 shows the chemical structure of maleinated acrylated epoxidized soybean oil (MAESO). Acrylate functional groups, acid groups and more unsaturation groups are added to soybean oil triglyceride molecules, which can be used as a sizing agent to provide strong bonding between the natural fiber and the SMC resin matrix. The double bonds of MAESO can react with styrene and get into the unsaturated polyester and styrene crosslink network. The hydroxyl groups of MAESO and nature fiber can react and bond with each other.

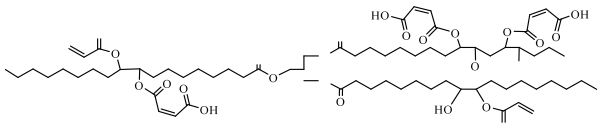

Figure 4. Chemical structure of MAESO.

Methods: The details on the kenaf fibers and unsaturated polyester used in this study were described in the previous chapter. MAESO (Figure 4) was synthesized by reacting acrylated epoxidized soybean oil (AESO) with the maleic anhydride (MA). For the natural fiber SMC fabrication, the kenaf fiber was controlled at 38 wt%. Five panel types (Table 2) were fabricated. The resulting composites were cured at a temperature of 100 ºC and a pressure of 100 psi for two hours and post-cured at 150 ºC for two hours.

Table 2. LSMC compositions.

Panel	1	2	3	4	5
AROPOL Q 6585 resin	60.5	57.6	54.5	48.5	42.4
MAESO	0	2	4	8	12.1
Styrene	0	1	2	4	6
Catalyst (TBP)	1.3	1.3	1.3	1.3	1.3
Inhibitor (BHT)	0.1	0.1	0.1	0.1	0.1
Kenaf Fiber	38	38	38	38	38

Results and Discussion: The densities of the composites (Figure 5) with MAESO were higher than those without. As the MAESO content increased, the density of the composites increased. Several functional groups should be presented in the MAESO molecule after the chemical modification, such as acrylate, cyclic anhydrides, carboxylic acid, and unsaturated functional groups. The resulting MAESO monomer was copolymerized with styrene and incorporated into the unsaturated polyester and styrene crosslink network to form rigid polymers. The multifunctional groups in MAESO react with the hydroxyl groups of natural fibers to form hydrogen bond. These should induce more efficient and compact polymer and natural fiber network that would increase the densities of the composites with MAESO. All of the composites with the MAESO had a lower 24-hour water absorption (WA) property (Figure 5) than those without.

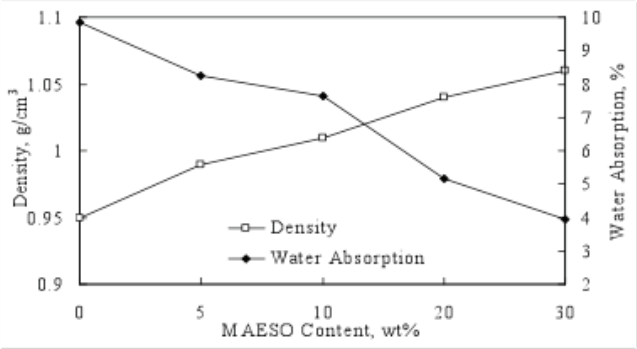

Figure 5. Density and 24-hour water absorption of composites as a function of MAESO content.

The multifunctional groups in MAESO monomers rendered many reactive sites by forming the hydrogen bond with the hydroxyl groups of natural fibers. Therefore, by adding MAESO, the hydroxyl groups of natural fibers were locked so that less hydroxyl groups would be available to attract the water molecules. The flexural strength of the composite (Figure 6) increased when 5 to 10 wt% of MAESO was incorporated but decreased when 20 to 30 wt% of MAESO was incorporated. The flexural modulus of the composite increased at 5 wt% of MAESO but decreased by adding more MAESO. Both are shown in Figure 7. The scanning electron microscope (SEM) micrographs of the composites with 0, 10, and 30 wt% MAESO are shown in Figure 8. Fiber pullout is clearly visible in the fracture surfaces of the SEM micrographs of the composite without MAESO. A good adhesion was not realized inside this composite. However, the fracture surface of the composites with 10 and 30 wt% MAESO did display some of the simultaneous fracture behavior between the polymer matrix and fibers. This was a sign of improved affinity between fiber surface and polymer matrix by adding MAESO into the polymer matrix. The number of fiber pull-outs was less in the specimen with 30 wt% MAESO than that in the specimen with 10 wt% MAESO. Apparently, when more MAESO molecules are present in a composite, more reactive sites are available for the polymer matrix to lock with the hydroxyl groups of the natural fiber resulting in stronger interfacial bonding between the polymer matrix and natural fibers.

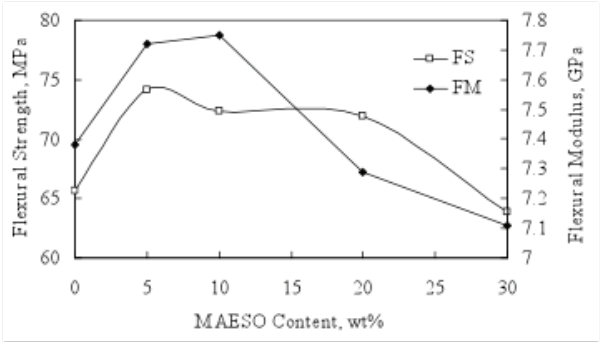

Figure 6. Flexural strength and modulus of composites as a function of MAESO content

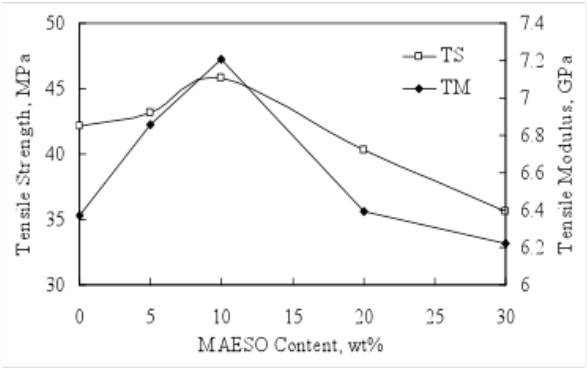

Figure 7. Tensile strength and modulus of composites as a function of MAESO content.

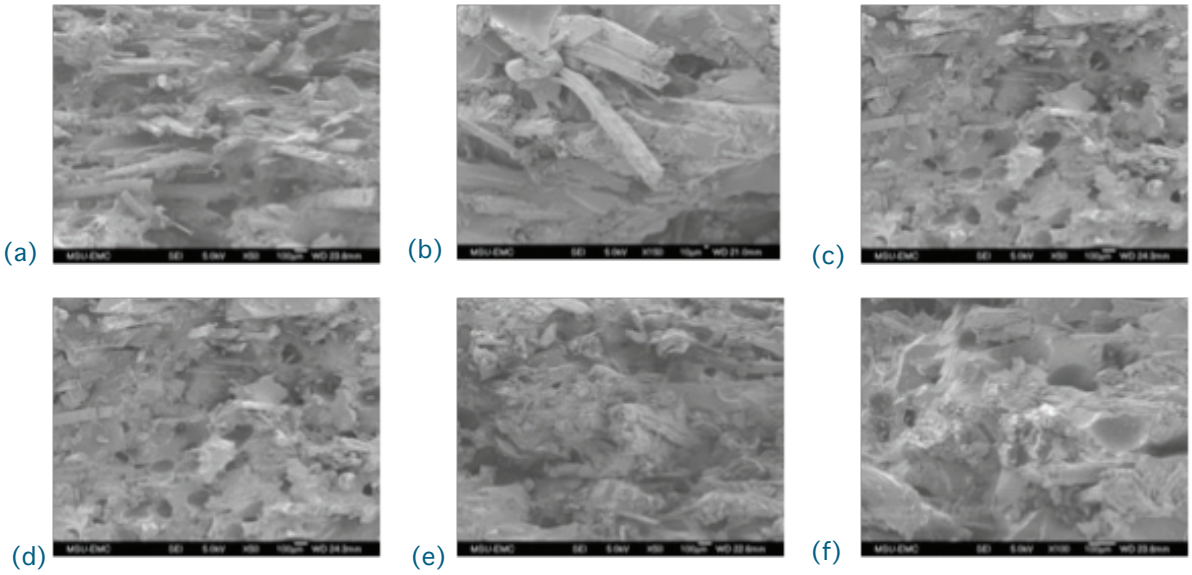

Figure 8: SEM micrographs of fractural surface of composites for (a, b) sample without MAESO, (c, d) sample with 10 wt% MAESO, (e, f) sample with 30 wt% MAESO.

Preparation of Cellulose Nanowhiskers from Kenaf Bast Fiber for Polymer Composites.

Objectives: It was reported (Zadorecki and Michell (1989)) that the elastic moduli of solid wood, single pulp fiber, microfibrils, and crystallites were 10 GPa, 40 GPa, 70 GPa, and 250 GPa, respectively, which indicated that stiffness of the fibers could be improved significantly by breaking down the cellulosic fiber into smaller sizes. Much research has been conducted on high crystalline cellulose fibers, e.g., microfibrils, nanowhiskers, or nanofibers in the recent years (Henriksson et al. (2007); Sui et al. (2008)). Cellulosic nanofibers and microfibers had been applied to reinforce some polymers, such as polyurethane and polylactide (Iwatake (2008)). Cellulose nanowhiskers (CNW) had also been applied in polyvinyl alcohol (PVA) (Tang and Liu (2008)). The objective is to prepare cellulose nanowhiskers from kenaf bast fibers by chemical processes and fabricate polymer composites reinforced with the CNW.

Methods: The preparation process of CNW and composites from raw kenaf bast fiber is shown in Figure 9. The raw fibers underwent alkaline retting, bleaching, and acid hydrolysis. CNW and microfibers were obtained after acid hydrolysis and separated by centrifugation. Polyvinyl alcohol (PVA, MW=100,000) powder was dissolved in distilled water and mixed with the CNW suspension. Sonication was used to mix the solution for five minutes. PVA films with or without CNW were formed by a film casting method. The CNW contents in composites were controlled at 1%, 3%, 6% and 9%.

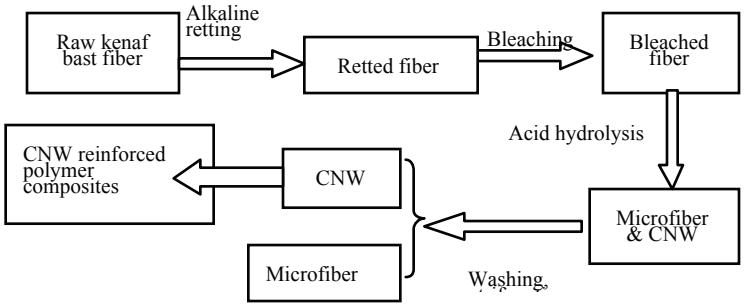

Figure 9. CNW preparation and the composite fabrication

Results and Discussion: The fiber production (Table 3) was calculated based on the oven-dry weight as the percentages to the original weight of raw kenaf bast fiber. The microfiber lengths (Figure 10) ranged from 10 to 100 μm and the diameters were around 10 μm. The lengths and diameters of the obtained CNW (Figure 11) were in the range of 100 to 500 nm, and 10 to 50 nm, respectively. Therefore, the aspect ratio of the CNW was calculated as 10 to 50. The FT-IR spectra (Figure 12) provide the chemical functional groups of the fibers. The peak between 3,000 cm^{-1} to 3,500 cm^{-1} indicates the presence of the hydroxyl groups (-OH). The peaks at 2,896.6 cm^{-1}, 1,718.3 cm^{-1}, 1,307.5cm^{-1} and 1,020 cm^{-1} represent the C-H, C=O, C-O, and C-C stretching, respectively. The peak at 1,648.8 cm^{-1} (C=C stretching) of untreated kenaf bast fibers disappeared in all of the treated fibers. The crystallinities of the fibers (Table 4) at each treatment stage were measured by X-ray diffraction (XRD) and were calculated by the Segal method based on the X-ray diffraction spectra (Figure 13). The tensile strength of the composites (Table 5) increased as the CNW content increased from 0 to 9%. The tensile strength of the PVA composites was increased by 46.2% when 9% CNW was incorporated. The elongations (Table 5) at the ultimate load of the CNW-PVA composites were higher than that of the control indicating that CNW resulted in a better ductility.

Table 3. Fiber production at different fiber processing stages

Fibers	Retted fiber	Bleached fiber	Micro fiber	CNW
Production	44.6%	41.4%	26.3%	10.4%

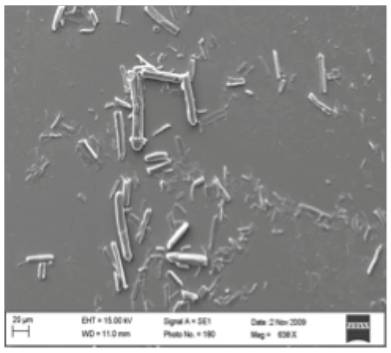

Figure 10: SEM image of microfibers.

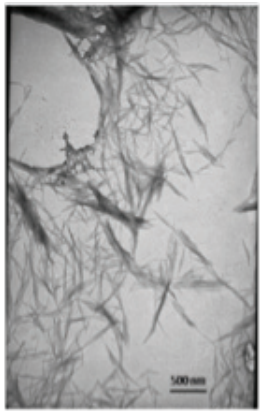

Figure 11: TEM image of CNW.

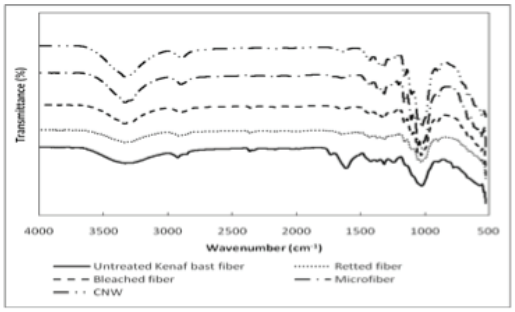

Figure 12: FT-IR spectra of fibers.

Table 4. Crystallinity of treated fibers at different stages

Fibers	Raw fiber	Retted fiber	Bleached fiber	Micro -fiber	CNW
Crystallinity	49.9%	63.8%	68.9%	83.5%	83.9%

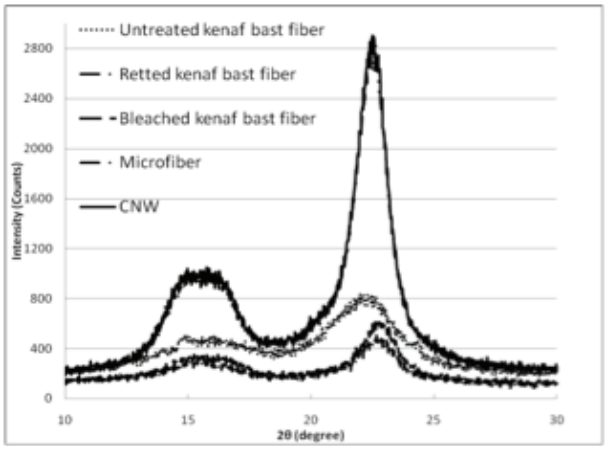

Figure 13: X-ray diffraction spectrums of treated fibers.

Table 5. Ultimate tensile strength and elongation of CNW-PVA composites

	Ultimate tensile strength (MPa)		Elongation at break (%)	
	Mean	SD	Mean	SD
Pure PVA	26.33	1.53	342.00	83.02
PVA+1%CNW	29.67	2.08	361.67	57.95
PVA+3%CNW	32.67	4.16	367.33	63.79
PVA+6%CNW	36.33	3.51	414.67	44.66
PVA+9%CNW	38.50	4.95	393.00	46.67

Molecular Dynamic Modeling of Nanophase Cellulose - Polypropylene Composites

Objectives: The objective of this research was to use a molecular dynamics (MD) approach to study the cellulosic fiber – polymer matrix interaction of fiber reinforced composites. The purpose of these simulations is to establish the interfacial properties for eventual use in larger length scale simulations.

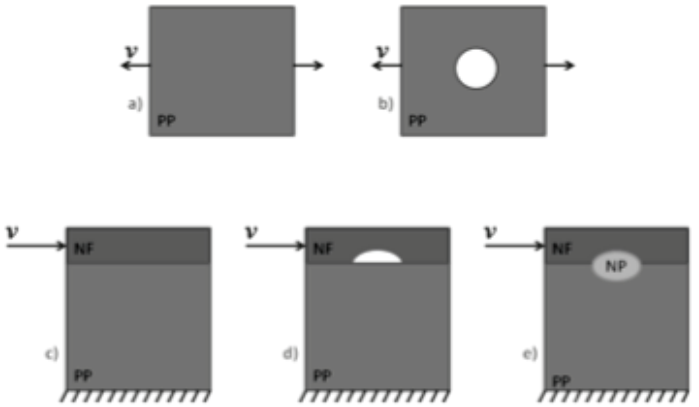

Figure 14: Schematic of simulations for fiber-matrix interface: a) uniaxial loading of the matrix bulk polypropylene (PP), b) uniaxial loading of the matrix PP with a void, c) sliding of clean nanofiber (NF) on the PP matrix, d) sliding of NF with a void along the PP matrix, and e) sliding of NF with embedded nanoparticle (NP) along PP matrix, the sliding during the presence of a nanoparticle on the fibers surface.

Methods: The schematic of simulations to study the fiber-matrix interface is described in Figure 14. The simulations include a five-step process. First the properties of the matrix need to be understood to remove the matrix properties from the interface properties. Figure 14a and b show uniaxial loading of a polypropylene (PP) matrix with and without a void. The next three simulations, Figure 14c-d, represent the nanofiber (NF) - matrix interactions. Figure 14c shows the sliding of a defect free NF across a defect free PP matrix. Figure 14d represents the sliding of a NF with a void along the PP matrix. Figure 14 e represents the sliding of nanoparticle (NP) at the fiber-polymer interface. The sliding simulations are performed by applying a velocity to the NF while holding the bottom of the PP matrix fixed inducing a shear stress at the interface. The simulations use two different suites of software to model the simulations LAMMPS and Accelrys Materials Studio. Additionally, within the two suites of software, apply two different potentials to the interatomic interactions the Dreiding and the Compass potentials, respectively.

Results and Discussion: The chemical structure of cellulose and polypropylene are shown in Figures 15 and 16, respectively. These structures provide the basis for the MD simulations. We started by examining the glass transition temperature (T_g) using LAMMPS for a simulation consisting of 20 chains of 1,000 monomers per chain with fully periodic boundary conditions. Figure 17 shows the results of this simulation that yields a T_g=315 K. This temperature was a little high relative to the experimental value (275K) but was reasonable for our purposes. The first mechanical examination focused on the glassy regime just below T_g at 250K. Initial simulations of PP under uniaxial loading at 250K with a strain rate of 10^9/s gave the stress-strain response shown in Figure 17. Figure 17 also shows the deformation during the uniaxial straining of the PP. The stress initial increased linearly, reached a peak at 1% true strain followed by softening. At 60% strain the simulation began to show large voids and chain alignment associated with localized damage.

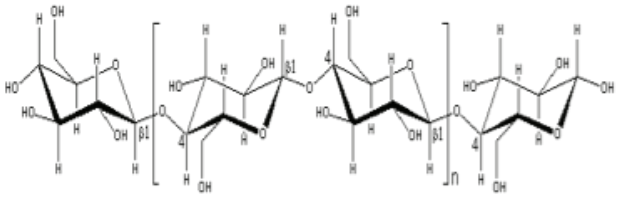

Figure 15: Chemical structure of cellulose.

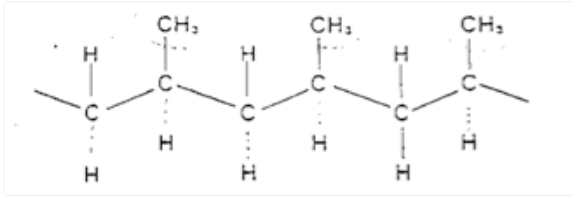

Figure 16: Chemical structure of polypropylene (PP).

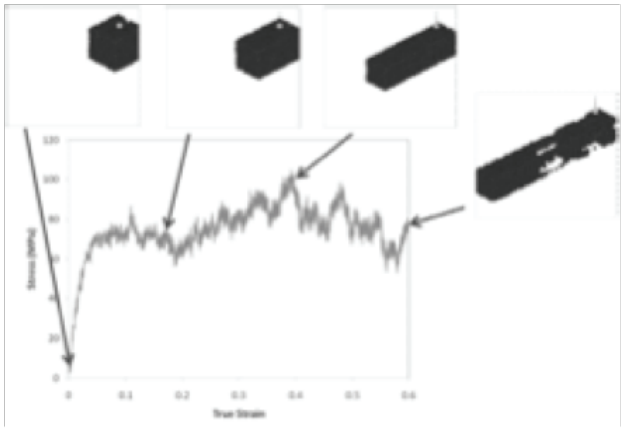

Figure 17: Stress-strain response for a simulation of bulk polypropylene (PP) and images of the simulation during the deformation.

Conclusions

Kenaf/glass fiber sheet molding compounds with different weight percentage of kenaf and glass fiber were fabricated. The density of the hybrid SMC decreased as the kenaf fiber content increased. The water absorption of the composites increased as the kenaf fibers were incorporated into the glass fiber polymer matrix. The flexural modulus and strength and tensile strength of the SMC decreased as the kenaf fiber content increased thanks to the hygroscopic characteristics of the natural fibers. The decrease may also be caused by the reduced resin content for the SMC panels. The tensile modulus of the SMC was not affected by the incorporation of the kenaf fibers. The modified soybean oil molecules, MAESO, provided more functional groups and, thus, had more crosslink sites. This resulted in an increased density and a reduced water uptake for the composites with MAESO compared to those of the controls. The mechanical properties, flexural and tensile properties (except for the flexural strength) increased when 5 to 10 wt% MAESO was incorporated but decreased when the MAESO content increased to 20 and 30 wt%. SEM pictures showed a better interfacial compatibility at the interface between the surface of kenaf fibers and polymer matrix in the composites with MAESO. Cellulose nanowhiskers were successfully processed through an all chemical procedure. The CNW has a diameter ranging from 10 to 50 nm and a length of 100 to 500 nm. The crystallinity of the fibers increased at each stage of the chemical process and decreased amorphous regions of cellulose molecular chain. A high crystallinity (83.9%) was obtained for the CNW. A fiber production of 10.4% CNW from the raw cellulosic fiber was obtained. CNW-PVA composites presented a higher tensile strength and elongation compared to the pure PVA composites with a 46.2% improvement when 9% CNW was incorporated.

References

1. M. Henriksson, G. Henriksson, L.A. Berglund, T. Lindstrom. 2007. Eur Polym J 43:3434-41
2. Iwatake, M. Nogi, H. Yano. 2008. Compos Sci Technol 68: 2103-06.
3. X. Sui, J. Yuan, W. Yuan, M. Zhou. 2008. Chem Lett 37(1):114-115.
4. Tang, Liu H. 2008. Composites: Part A 39:1638-43.
5. P. Zadorecki, A.J. Michell. 1989. Polym Compos 10(2):69 -77.

G. Evaluation of Composite Natural Fiber-Resin Compatibility

Principal Investigators: Leonard S. Fifield and Kevin L. Simmons
Pacific Northwest National Laboratory (PNNL)
P.O. Box 999; Richland, Washington 99352
(509) 375-6424; e-mail: leonard.fifield@pnl.gov

Rick Battiste
Oak Ridge National Laboratory (ORNL)
P.O. Box 2008; Oak Ridge, Tennessee 37831
(865) 574-0736; e-mail: battisterl@ornl.gov

Technology Area Development Manager: Dr. Carol Schutte
(202) 287-5371; e-mail:carol.schutte@ee.doe.gov

Field Technical Manager: Mark T. Smith
(509) 375-4478; e-mail: mark.smith@pnl.gov
Industry Consultants: Dan Houston (Ford Motor Company), Libby Berger (General Motors)

Contractor: Pacific Northwest National Laboratory
Contract No.: DE-AC05-76RL01830

Objective

- Develop and evaluate fiber treatment methods to enable compression-molded, natural fiber-reinforced composites to retain high mechanical performance after exposure to moisture.

Approach, including industrial partner/collaborator, and path to technology transfer and commercialization

- Partner with domestic and international fiber suppliers, including Biotech Mills, Inc. and Bast Fibers LLC, to evaluate natural fiber sources.
- Treat fibers and evaluate effects of treatments on fiber mechanical, moisture uptake, and wetting properties in collaboration with team members from Oregon State University and Washington State University.
- Partner with Tier 2 automotive resin suppliers, including Ashland Specialty Chemical (Ashland) and with Pacific Northwest National Laboratory (PNNL) Project 18988/Agreement 16313 to develop processes for natural fiber composite formatting, pre-forming, and compression molding of treated fibers.
- Mold non-woven, natural fiber-reinforced composite test panels with controlled fiber fractions.
- Using target performance metrics supplied by Dan Houston of Ford Motor Company (Ford), evaluate, in collaboration with the Oak Ridge National Laboratory (ORNL) team, composite performance after conditioning at standard relative humidity and complete immersion.
- Determine path to implementation of fiber treatment technologies in conjunction with Tier 1 suppliers, such as Continental Structural Plastics (CSP), with the guidance of Libby Berger of General Motors (GM) and Dan Houston of Ford.

Milestones, Metrics and Accomplishments

- Milestone 1–Complete initial performance evaluations of selected natural fiber surface treatments (completed August 2009).

    1. The results of selected natural fiber treatments on fiber moisture uptake, fiber bundle tenacity, and fiber bundle contact angle were determined to facilitate an increased understanding of the fiber structure/performance relationship relevant to improved incorporation of fibers in reinforced composites. In addition, the effects of treatments on fiber structure and fiber chemical content were investigated using a series of imaging, thermal, chemical, and spectroscopic techniques.

- Milestone 2–Evaluate the applicability of low molecular weight agents, such as those used for paper sizing, for the treatment of natural fibers for polymer reinforcement (completed September 2009).

    1. Two common paper-sizing treatments, alkyl ketene dimer (AKD) and alkenyl succinic anhydride (ASA) were applied to kenaf fiber with guidance from Georgia-Pacific. The effect of the sizing treatments on fiber moisture uptake and fiber mechanical properties was evaluated. The molding behavior, moisture uptake, and mechanical behavior of composite panels made using the sizing-treated fibers also were examined.

- Milestone 3–Determine bridging strategies for chemically incorporating natural fibers into the cured resin matrix (completed August 2009).

    1. Single- and dual-component approaches were explored for kenaf and hemp fiber treatment prior to molding into unsaturated polyester composites. Treatments were successful in reducing moisture uptake of the composites and increasing both tensile and flexural properties relative to those of the untreated fiber composites.

- Major fiber metric for fiber treatment:

    1. Percent weight gain of fibers relative to untreated fibers and glass fibers (percent improvement over control).

- Major composite metrics for fiber treatment:

    1. Percent weight gain of treated fiber composites relative to that of untreated fiber composite and Ford-supplied target values (percent improvement over control).

    2. Tensile and flexural strength and stiffness performance of wet- and dry-treated fiber composite relative to that of wet- and dry-untreated fiber composite and glass-fiber composite (percent improvement over control).

- Selected kenaf as the natural fiber of primary focus based on kenaf fiber stiffness, strength, and availability. Characterized as-received kenaf fiber forms (retted and unretted), microscopic surface structure, moisture uptake, wetting behavior, thermal stability, crystallinity, and chemical content.

- Explored fiber treatment methods, including thermal, wet chemical, and resin additive.

- Characterized treated fibers to determine mechanical and wetting performance relative to that of untreated fiber.

- Selected standard composite panel fabrication method to use for comparing fiber treatments and evaluating effects of treatments on composite performance.

- Selected list of key standard tests for composite evaluation, including moisture uptake, tensile, and flexural performance with input from ORNL and Dan Houston of Ford.

- Fabricated series of baseline panels using untreated kenaf fiber and glass fiber.

Future Direction

- Continue selection and evaluation of fiber treatment methods with emphasis on retention of composite mechanical properties with exposure to moisture. Key criteria for treatment method selection will be the cost and ability of the method to be scaled to high fiber volumes.
- Investigate composite failure modes to guide optimization of the fiber/resin interface.
- Extend promising treatment methods to the fabrication of larger composite panels for more extensive testing such as for impact performance and coefficient of linear thermal expansion.
- Partner with fiber suppliers, such as Biotech Mills, and Tier 1 automotive suppliers, potentially including CSP, (with guidance from GM and Ford) to transition developed technology into demonstration components appropriate for development of natural fiber semi-structural original equipment manufacturer (OEM) specifications.

Introduction

Cellulose-based plant fibers, herein referred to as natural fibers (NFs), are increasingly used to replace glass fibers in automotive composites [1]. The primary drivers for this trend are weight and cost savings. In addition, NFs represent a bio-based and renewable resource. Most natural fiber composite (NFC) vehicle components consist of fiber-filled thermoplastics, such as polypropylene, and find application in non-structural interior parts. Use of NFCs in structural and semi-structural exterior automotive parts likely will involve thermoset composites and will require environmentally durable performance. The mechanical robustness of these parts must persist at the temperature and moisture extremes encountered by the vehicle during its operational lifetime.

As with glass and carbon-reinforced polymer composites, it is the fiber that provides strength and stiffness in an NFC. The mechanical performance of the composite is based both on the inherent properties of the fiber and on the fiber/resin interface. It is the interface that determines mechanical load transfer to the fiber from the matrix. The fiber/resin interface likely is a major influence on both moisture uptake of the fiber and the effect of that uptake on the composite mechanical properties.

Fibers

Many types of plant-based NFs have been used for structural composites since antiquity, but bast fibers and leaf fibers present particularly promising selections for use in modern stiffness-dominated automotive composites [2]. In nature, these types of plants have relatively long fiber lengths used to provide structural rigidity to tall stems and long, heavy leaves. Species of plants producing bast fibers include: jute, ramie, hemp, flax, and kenaf. Leaf fibers of outstanding mechanical properties include pineapple, sisal, banana, and palm. Current efforts are focused on kenaf fibers since they exhibit relatively high strength and stiffness properties and are readily available. Kenaf may be a preferable long-term solution for use in automotive composites since it grows rapidly, has a large capacity for carbon uptake, remediates the soil, and has the potential to be grown in large scale in the United States (US). However, it is believed the processing, forming, treating, and molding techniques developed for kenaf may be transferred for use with fibers from many plant species. The broad selection of potential fiber species that may be geographically convenient to the composite manufacturing site is another advantage of NF use in automotive component manufacturing.

Kenaf bast fiber is obtained for use in NFCs by separation from the leaves, core, and bark of the plant through a process known as decortication. The fibers themselves are separated into more discreet bundles through a process known as retting, in which materials, including pectin and lignin, are removed from cellulosic fibers. Pacific Northwest National Laboratory (PNNL) has partnered with domestic and international fiber suppliers, including Biotech Mills, Inc., and Bast Fibers, LLC, to receive retted fibers in specified 1-inch (in.) and 2-in. lengths. The parallel PNNL project is working with fiber growers and suppliers to develop mechanical retting processes to incorporate with fiber treatment, fiber formatting, and fiber molding, in an integrated process [3]. Currently, integrated processes have been developed in formatting and molding of kenaf fibers. Example kenaf fibers are shown in Figure 1.

Figure 1. Chopped Kenaf Fiber Bundles (in inches)

The moisture uptake and mechanical properties of a NFC are a function of the physical, chemical, and mechanical properties of the fiber used. The microscopic structure and structural changes of kenaf fibers were investigated using scanning electron microscopy as in Figure 2 [4].

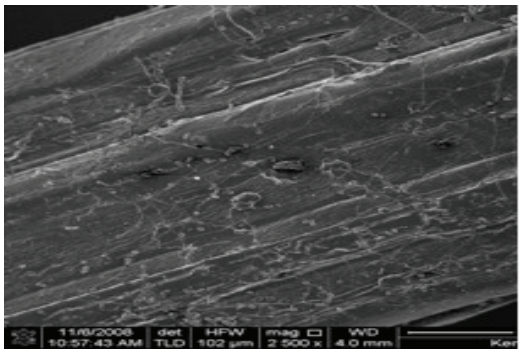

Figure 2. Scanning Electron Micrograph of Kenaf Fiber Surface

Certain thermal and chemical treatments are seen to exfoliate fiber bundle components, likely through removal of lignin and hemicellulose material between the fibers, as in Figure 3. Such fiber separation increases surface area and resin interface. Surface coating treatments have altered roughness of the kenaf fiber bundles, potentially influencing the fiber/resin interface.

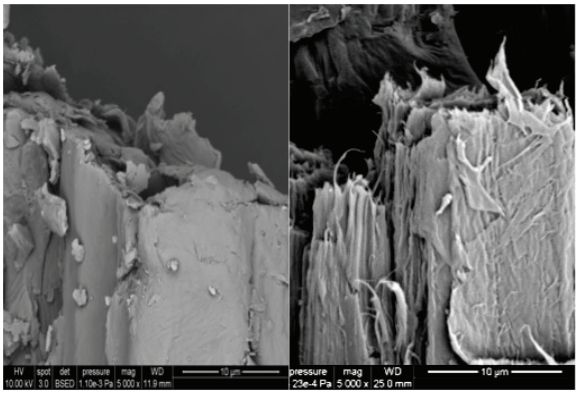

Figure 3. Scanning Electron Micrographs of Untreated (left) and Alkali Treated (right) Kenaf Fiber Fracture Surfaces Showing Increase Fibril Exposure with Treatment

Plant fibers have three primary constituents: cellulose, hemicelluloses, and lignin. These are natural polymeric materials composed of glucose, hexose and pentose, and propyl phenolic monomers, respectively [5]. The plant's architecture is designed to draw transport moisture from the roots to the rest of the plant. The components are consequently very good at moisture uptake —not a generally compatible feature for use in moisture-stable automotive composites. The hydrophilic nature of NFs is due to their porous structure that facilitates capillary action and the hydrophilic chemical groups of the lignocellulosic monomers. For instance, hydroxyl groups on cellulose and hemicellulose chains contribute to the double-digit gain in weight percent of water that fibers experience at intermediate levels of relative humidity. Directed chemical action on these hydroxyl groups can serve the dual purpose of attenuating moisture uptake and facilitating cross-linking, or otherwise favorable interface, with the resin matrix. Wet end chemistry—used to control moisture uptake in the paper industry—is being explored in addition to other currently available industrial scale chemistries to tune and control the fiber/resin interface. Information has been obtained regarding the chemical content of unmodified and modified fibers using various spectroscopic methods, including x-ray photoelectron, solid state nuclear magnetic resonance, and Fourier transform infrared spectroscopy.

Tenacity, a concept from the textile industry, is used to measure mechanical performance of kenaf fiber bundles from different sources and with different treatments. It is defined as the maximum specific stress with extension and is given in units of grams/tex, where tex is the mass in grams of 1000 meters of the fiber. In this way, strength performance can be compared without tedious determination of irregular fiber bundle cross-sections. The crystalline cellulose portion within NFs is the principal source of mechanical stiffness in the fibers. X-ray diffraction (XRD) has been used to investigate the effects of thermo-chemical treatments on fiber crystallinity. Figure 4 shows the effect of alkali treatment duration on both the tenacity of kenaf fiber bundles and on the crystallinity of the material.

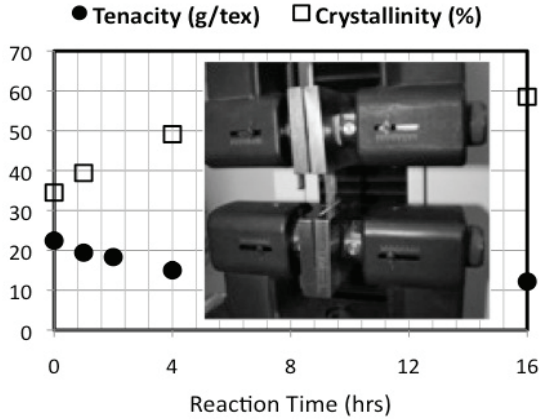

Figure 4. Tenacity and Crystallinity of Kenaf Fiber Bundles as a Function of Alkali Reaction Time (The inset shows a kenaf fiber bundle in the tenacity test fixture.)

Figure 4 shows tenacity decreases with removal of non-crystalline material in the fiber bundles. Lignin and hemicelluloses are almost completely amorphous. Separation of bundles into fibers through removal of the amorphous connective components may decrease bundle integrity while increasing surface area and interface in the composite. This disconnect between fiber mechanical properties and composite mechanical properties, which are expected to increase with surface area and fiber crystallinity, has led to the conclusion that composite properties, rather than fiber bundle properties, must be the primary metrics for evaluation of the fiber/resin interface. The surface-energy-related wetting behavior of treated fibers was measured using the tensiometer-determined contact angle of both packed cell versions of fibers and fiber bundles rather than labor-intensive measurement of individual fibers. For example, alkyl ketene dimer (AKD) treatment of kenaf fibers was seen to increase fiber wetting in the styrene resin solvent as shown in Figure 5.

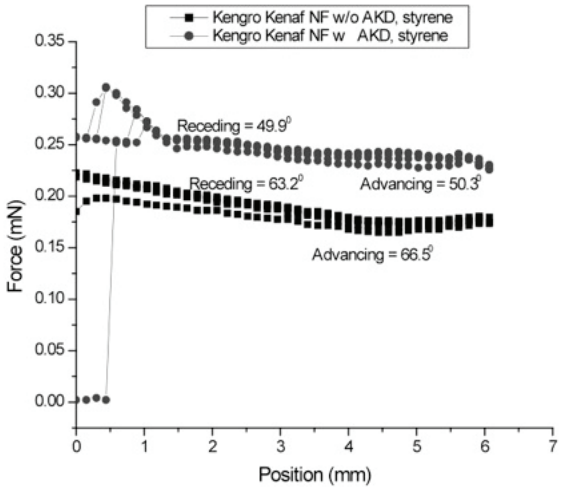

Figure 5. Tensiometer Plot Showing Force Versus Depth of Kenaf Bundles Immersed into Styrene (Advancing and receding contact angles are indicated for each step.)

Oil absorption behavior also was determined and moisture uptake of baseline and treated fibers measured according to ASTM standard [6]. It is reasonable that fiber mechanical and wetting properties influence and inform NFC properties. However, the complex interplay between resin matrix, molding process, and fiber requires that the actual properties of molded composites be used to compare treatment methods.

A potential limiting factor for the use of NF in certain composite-molding processes and vehicle applications is the relatively low thermal stability of plant fibers compared to glass and carbon fibers. The effect of fiber treatment on thermal degradation onset using thermal analysis was investigated using a laboratory mill to grind fibers into a fine powder. Thermal stability enhancement, however, has been determined to be of lower priority than moisture uptake and retention of mechanical properties upon exposure to moisture for application of NFs in thermosets. Vinyl ester thermoset can be processed at lower temperatures than thermoplastic polypropylene.

Transition of fiber treatment technology to Tier 1 automotive suppliers will require an understanding of the most efficient and effective methods for treatment application. In the next year of this project, the relative effectiveness of wet chemical application of a fiber treatment, spray application of the treatment, and use of the treatment as a resin additive will be investigated.

Composites

Most NFCs in vehicles are injection molded and consist of a NF fiber-filled thermoplastic. NF-reinforced thermosets present the opportunity for parts requiring higher mechanical properties,

such as external underbody panels. Compression molding of NFCs can help to meet required molding times for high volume applications.

As part of this work, Oregon State University Assistant Professor Kaichang Li and colleagues [7] have investigated the effect of a series of chemical treatments on moisture uptake behavior of hemp and kenaf fiber (shown in Figure 6). The property chemical treatments developed at Oregon State University are designated as Treatment I, II, III and IV, respectively. The effects of fiber treatment on the mechanical properties of hemp-filled and kenaf-filled, compression-molded, unsaturated polyester composites also were determined. As shown in Figure 7 and Figure 8, both the tensile strength and the flexural properties of modulus of rupture (MOR) and modulus of extension (MOE) of the treated kenaf fibers significantly increase relative to those of the untreated fibers. Results of hemp fiber treatments were similar (not shown).

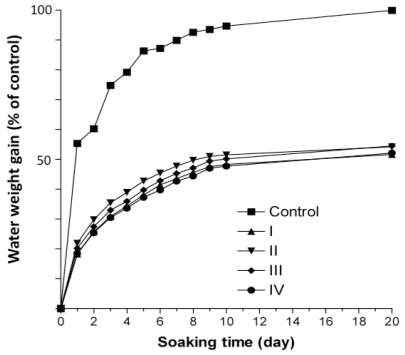

Figure 6. Moisture Uptake Comparison of Treated Kenaf Fibers

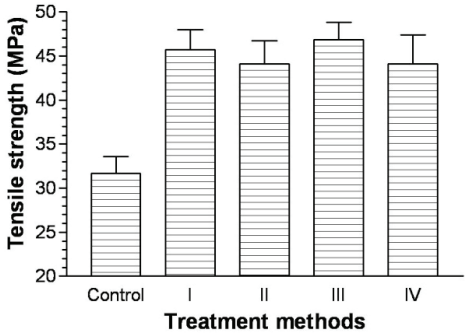

Figure 7. Tensile Strength Comparison of Compression-molded Kenaf Fiber in Unsaturated Polyester

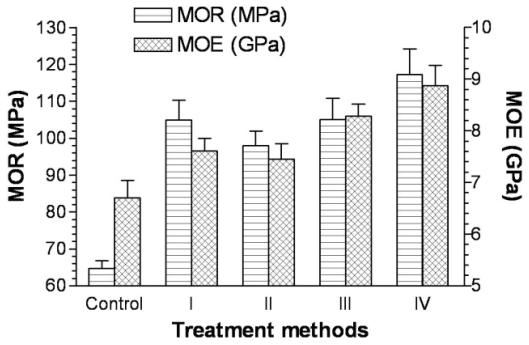

Figure 8. Flexural Property Comparison of Treated Kenaf in Compression-molded Unsaturated Polyester

In combination with the parallel PNNL project [3] and Tier 2 automotive resin supplier, Ashland, a standard fiber formatting and compression molding method was established to use for evaluation of fiber treatments on moisture stability and on the fiber/resin interface. Based on

input from Dan Houston (Ford), the work is focusing on using a vinyl ester resin system with low levels of inorganic filler. This is based on the anticipation that compression-molded thermoset NFCs will not find initial application in Class-A surface finish components. Six-inch square panels of one-eighth in. thickness are molded with selected volume fraction fiber loadings. NFCs are compared with glass fiber composites of equivalent fiber volume fraction to evaluate composite density, moisture uptake, and mechanical properties.

Benefiting from extensive ORNL experience in composites testing , PNNL partnered with ORNL to select a testing scheme for the mechanical property evaluation of composite specimens based on ASTM standard methods [8]. Initial screening and evaluation of NFCs made from fibers with different treatment methods measured the tensile and flexural performance of five specimens from each panel representing each condition. As illustrated in Figure 9, composite specimens are preconditioned at either dry (50% relative humidity at 25 degrees Celsius [°C] for 48 hours) or wet (immersed in water at 25 °C for 24 hours) conditions prior to testing (based on specification input from Ford's Mr. Houston).

Future work will investigate the effects of both fiber length and fiber volume loading on composite performance. Extension of this work will involve molding of larger panels and additional application-critical testing, such as impact performance, coefficient of linear thermal expansion, and dynamic mechanical analysis. Transition of developed technology to implementation with the automotive industry will involve molding and testing of complex shapes in conjunction with Tier 1 suppliers under consultation with Ms. Berger (GM) and Mr. Houston (Ford).

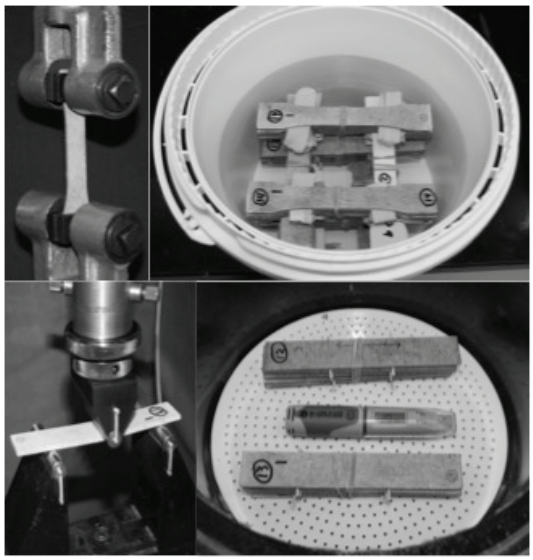

Figure 9. Tensile Specimens (top) and Flexural specimens (bottom) are Conditioned at "Wet" (immersed, upper right) and "Dry" (50% relative humidity, lower right) Conditions Prior to Testing

Conclusions

Natural fibers are experiencing increased application in automotive composites due to weight savings, cost savings, and environmental considerations relative to the glass fibers. Continued extension of this trend to structural and semi-structural, as well as external vehicle applications, with resultant additional improvement in weight savings will require the development of NFCs with improved mechanical properties and durability.

A challenge in comparing the NFC performance values reported in the literature with each other or current work is the wide variety of fiber types, fiber loadings, degree of fiber treatments, resins, fiber formatting methods, molding methods, and testing methods used. PNNL has developed a standard

fiber preparation and compression-molding process using materials and input from natural fiber suppliers (including Biotech Mills and Bast Fibers) and Tier 2 automotive resin suppliers (including Ashland). PNNL uses this method of NFC fabrication as the standard platform by which to reproducibly evaluate fiber treatments according to the performance requirements guidance of GM and Ford. In this way, merits of previously demonstrated and novel fiber treatment methods can be directly compared to inform both the potential of compression-molded NFCs for use in extended vehicle component applications and the transition of fiber use from the laboratory to pilot scale testing and application by Tier 1 automotive suppliers such as Continental Structural Plastics (CSP).

Presentations/Publications/Patents

Holbery JD. 2009. "Natural Fiber Composites in Transportation Applications: Market Opportunities and Technical Challenges." March 30, 2009, Seattle, Washington. 43rd International Wood Composites Symposium 2009 Technical Workshop on Natural Fibers.

Fifield LS, C Huang, and KL Simmons. 2009. "Resin/Fiber Compatibility in Natural Fiber Reinforced Automotive Composites." May 11, 2009, Madison, Wisconsin. 10th International Conference on Wood & Biofiber Plastic Composites.

Simmons KL, LS Fifield, SG Laddha, DT Howe, and C Huang. 2009. "Natural Fiber Composites in Transportation Applications – Fiber Preparation, Surface Modification, and Preform Manufacturing Synergy." May 11, 2009, Madison, Wisconsin. 10th International Conference on Wood & Biofiber Plastic Composites.

Simmons KL, JD Holbery, DT Howe, and LS Fifield. "Method of Cellulose Fiber Extraction." PNNL Invention Disclosure 16492-E.

Holbery JD, C Huang, and LS Fifield. "Chemical Agents to Facilitate Incorporation of Natural Fibers in Automotive Composites." PNNL Invention Disclosure 16493-E.

References

Holbery JD and D Houston. 2007. "Natural-fiber-reinforced polymer composites in automotive applications." JOM Journal of the Minerals, Metals and Materials Society 58(11):80-86.

Pickering KL, ed. 2008. Properties and performance of natural-fibre composites. CRC/Woodhead Publishing, Cambridge, England.

Simmons K. DOE Office of Vehicle Technologies Lightweighting Materials Project 18988/Agreement 16313.

A portion of this work was performed in collaboration with PhD student Feng Chen of Jinwen Zhang group at Washington State University, Pullman, Washington.

Wallenberger FT and N Weston, eds. 2004. Natural Fibers, Plastics and Composites. Kluwer Academic Publishers, Norwell, Massachusetts.

ASTM D1348-94. 2008. Standard Test Methods for Moisture in Cellulose. American Society for Testing and Materials, Philadelphia.

Li K, X Ren, and R Qiu. Department of Wood Science & Engineering, Corvallis, Oregon.

ASTM D 790–07. 2007. Standard Test Methods for Flexural Properties of Unreinforced and Reinforced Plastics and Electrical Insulating Materials; ASTM D638–08. 2008. Standard Test Method for Tensile Properties of Plastics. American Society for Testing and Materials, Philadelphia.

H. Predictive Technology Development & Composite Crash Energy Management

Principal Investigator: Khaled W. Shahwan, PhD
Chrysler Group LLC
Chrysler Technology Center
800 Chrysler Drive (CIMS: 483-05-10)
Auburn Hills, Michigan 48326
Tel: (248) 576-5609; Email: kws8@chrysler.com

Technology Area Development Manager: Dr. Carol Schutte
(202) 287-5371; e-mail:carol.schutte@ee.doe.gov

Contractor: U.S. Automotive Materials Partnership (Cooperative Agreement) for the Automotive Composites Consortium Energy Management Working Group
Contract No.: DE-FC26-02OR22910 through the DOE National Energy Technology Laboratory

Objective

- Develop, verify, and validate efficient, robust, and physics-based modeling and analysis tools for predicting (not just simulating) damage initiation, progression, energy absorption, and overall crush behavior of composite components in lightweight vehicle structures using micromechanical, phenomenological, or hybrid computational approaches.
- Develop design, testing, modeling and analysis guidelines for advanced lightweight automotive composites for safety and crashworthiness applications in vehicle development.

Approach

- Conduct extensive experimental tests to characterize the quasi-static and dynamic properties of selected structural composite materials and micro-architectures, including damage modes and progression mechanisms. The tests will identify and measure material properties as well as coupled material-structural properties, and expose the various damage morphologies and modes.
- Develop advanced models based on phenomenological and micro-mechanical approaches to predict the material and structural response during the full regimes of behavior including ascending branch, peak strength, post-peak and softening, and plateau characteristics of the stress-strain and force-displacement for coupons, sub-components and full structural components.
- Verify and validate the computational tools by predicting quasi-static and dynamic behavior of experimental tests at the coupon and structural levels. Further validation by predicting structural crash performance of lightweight automotive composites.

Milestones, Metrics and Accomplishments

Much has been accomplished towards qualitatively and quantitatively understanding the fundamental physics governing the nonlinear mechanical behavior and damage progressions in multi-phase materials and composites. The exposition of the new phenomena underlying such physics continues to warrant further investigations especially since this project's overall goals and objectives demand validated computational-modeling tools that are robust, physics-based, and truly-predictive.

For metals—and metallic-based structures—which can be modeled using simpler material models, the mechanisms responsible for damage initiation, progression and energy absorption are relatively more understood, have been maturing over many decades, and are much fewer in number (e.g., plasticity, crack tip fracture), culminating in predictive tools that correlate reasonably well with tests. However, for more complex multi-phase materials such as composites, developing material models for damage prediction has been posing quite a formidable challenge for the computational modeling communities. This can be attributed mainly to the fact that there are a much larger number of competing mechanical phenomena responsible for damage initiation, progression and energy absorption modes. Further, such phenomena can manifest themselves in a verity of ways (e.g., matrix plasticity, micro-cracking, tow splitting, fiber debonding, fiber/tow kinking and buckling, macro-cracking, delamination, etc.). To complicate matters further, such damage modes can sometimes co-exist as well as change dominance depending on several factors such as the speed of the phenomena, and size of the damage with respect to the overall size of the structure, to mention a few.

Modeling and robustly predicting the physics of damage initiation and progression in multi-phase solids (such as composites) remains one of the most formidable problems in mechanics to date. However, lots of progress has been made with the aid of modern modeling tools and advanced numerical techniques. Albeit pseudo-predictive and useful, many of the well-known commercial Computer-Aided Engineering (CAE) modeling tools still rely on empirical techniques in their crush simulations of composite structures. In order to move away from empirically-dominated approaches a multitude of experimental-characterization and computational-modeling projects have been devised to identify and quantify the primary damage mechanisms and their direct effects on the dominant regimes of mechanical response and modes of damage-initiation and progression.

This project (ACC100) has played a major role in accomplishing that and leading such advancements. Examples are:

- Exposed, via extensive testing and modeling, that the employment of modeling techniques which contain mostly physically-defined and measurable quantities (i.e., non-phenomenological) is possible and achievable in order to predict the post-peak and softening behavior of such materials.
- Exposed, via extensive testing and modeling, that for robustly predictive applications the reliance on abstract mathematical concepts and techniques to quantify damage initiation and progression in composites may not be necessary and is insufficient, and can be useful only in a very limited number of situations.
- Exposed, via extensive modeling that the smallest repeating Representative Unit Cell (RUC) (employed for objective modeling purposes) does not necessarily imply that such an RUC will also be the smallest repeating material region necessary to describe and model damage initiation and progression. And that the minimum number of RUCs needed to accurately predict the damage zone and its subsequent progression may not always be known a priori and can depend on a host of factors [Ref. 1 & 2].
- Exposed that modeling damage initiation and progression in textile composites necessitates the inclusion of some measures for local/global imperfections. Both, the pre-peak and post-peak response of RUCs are a function of the degree and shape of pre-existing imperfections.
- Developed test-validated modeling techniques to study size effects in braided textile composites. Experimental tests have confirmed and quantified size effects on the strength in such quasi-brittle composites, and showed that nominal strength can sometimes depend on the relative size of specimen with respect to the size of existing damage as well as the local scale of constituents. This is of great importance especially for selecting the size of laboratory test specimen, as well as the corresponding mesh size of finite-elements in modeling.
- Exposed that the local properties of constituent materials within a cured composite can sometimes differ from their presumed bulk (neat) properties measured after curing but prior

to mixing with reinforcement (fibers, textile). Hence, for certain mechanical modeling purposes it may be very important to know the in-situ (post-cure) properties. And that obtaining such knowledge can be part of the overall modeling approach and analysis process especially since they can depend on cure-time, cure-temperature, and location within the composite material (i.e., in resin-rich zones, within a fiber-tow, near a tow, etc.)

- Verified, via extensive experimental testing and modeling, that post-peak softening in quasi-brittle textiles cannot be considered a constitutive property especially in homogenization techniques (as is commonly done), and that the coupled local material-structural behavior plays a major role in characterizing such softening and overall response envelope. This is very important for distinguishing between what is a material property and what is not.
- Completed a study aimed at using multiscale modeling and numerical analysis techniques to model and simulate damage evolution during quasi-static and dynamic crush of braided carbon structural tubes. The development of Multiscale Design System (MDS) software was funded as part of this project. This MDS tool is hybrid in nature requiring some pre-existing experimental data in order to calibrate some of the empirical parameters used to characterize some material properties.
- A state-of-the-art Modeling Database (MDB) is being developed. Unlike material-property databases in which material properties are just simply searched for and extracted, this MDB is used to select from the various advanced modeling approaches developed. Depending on the particular application, this tool has been customized for utilization within some of the most widely used commercial CAE tools in the industry. The MDB contains advanced modeling techniques and algorithms that are state-of-the-art.
- Carbon composites, especially braided textiles which exhibit mass density of about 1400 kg/m^3 [~ 80% lighter than common structural steels], have been characterized as viable materials for automotive structural applications. Their low densities as well as other characteristics such as specific structural stiffness, strength, and energy absorption, are well-suited to meet many of the contemporary lightweighting challenges. The following specific accomplishments are aimed towards achieving that:

Future Direction

- Complete the MDB development. This will serve as a central point for all predictive crashworthiness analyses for lightweight automotive composites.
- Investigate ways to minimize (or even mitigate) size effects in such quasi-brittle textile composites. Having characterized and quantified such important and inherent size effects within braided carbon textiles further investigations would provide important insights on how to minimize such effects at the early material/architecture design/selection stages so that predictive tools, computational modeling and laboratory testing can be further simplified and streamlined.
- Material properties' changes with service/environmental factors (e.g., fatigue, high-frequency high-amplitude pulses/vibrations, moisture, and large thermal fluctuations, etc.) and their influence on energy absorption, and mechanical response during a component's life-cycle. This could be focused on characterizing the in-situ properties of in-service structural components and studying which factors influence (and to what degree) the mechanical response and energy absorption capacity of lightweight carbon textile composites for automotive applications.
- Develop a demonstration project in which all completed accomplishments will be utilized to show the viability of carbon fiber-reinforced composites as a primary structural material for automotive subassembly (e.g., front-end), as well as the viability and validity of the modeling and predictive tools developed thus far.

Introduction

The purpose of the Predictive Technology Development and Crash Energy Management Program is to develop and demonstrate the technologies required to apply production-feasible composites in primary-structural automotive crash and energy management applications. Specific projects within the program are intended to understand the mechanisms of polymer composite crash, develop analytical tools for use in design, and build a knowledge base for the products' applications. These projects relate to materials, processes, and design configurations that are useful in realistic applications. Engineering methods will be developed which can be used at several different steps in the design process, accordingly, the projects are diverse and span several disciplines in mechanics and composites in order to develop a strong fundamental understanding of such complex lightweight materials.

Multiscale Modeling of Triaxially Braided Tubes

This multiscale formulation involved the development of a reduced-order multiscale model in which the fiber-matrix interface was modeled using a traction-separation law where the value of fracture toughness in modes I, II and III measured in quasi-static tests were used. The interface strength values were assumed to be identical to those of the matrix strength in the corresponding direction. These values were taken from the prior tests. It is instructive to comment on the computational complexity of the reduced-order multiscale model with interface debonding which consists of 46 state variables. The state variables include six eigenstrain components times four phase partitions (24 total), three components of eigenseparations per each of the three interface partitions (9 total), one phase damage state variable for each phase partition (4 total), and three interface damage state variable for each of the three interface partitions (9 total). In addition, in-situ inelastic phase properties of matrix and tows have been recalibrated to the coupon test data from the transverse tension, longitudinal tension, and longitudinal compression – all conducted on the 45° braided composite architecture(Figure 1).

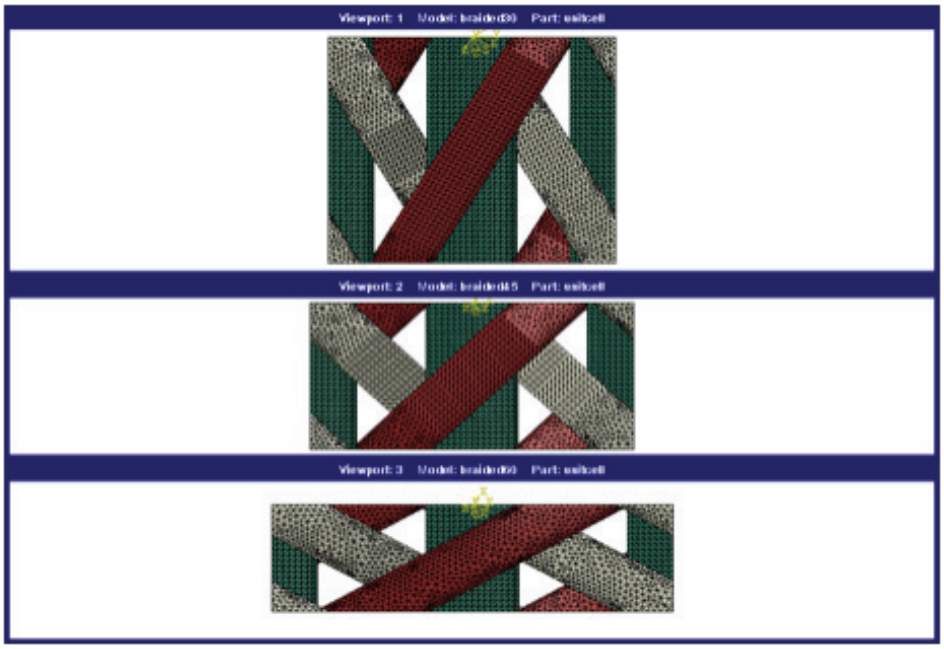

Figure 1. Representative Unit Cell (RUC) finite element models for 30º (top figure), 45º (middle) and 60º (bottom) braided textiles.

Using the above Representative Unit Cell (RUC) in finite element models for simulating the ¼ tube model, a comparison was made to the experimental results. Recall that RUC is the smallest repeating geometric unit which can be used to model the entire braid architecture (axial tows,

bias tows, and matrix, where tows are bundles of fibers containing for example 12000, 24000, or 50000 fiber filaments). Figures 2 and 3 compare the test data to the simulation results of the reduced-order multiscale model. It is important to note that the analysis proceeds by first calibrating the composite material properties (constituents) for the 45° braided architecture by using optimization techniques and coupon data obtained from experimental tests on the 45° braids. The calculated properties are estimated once and assumed to be the same for all other braided architectures, namely the 30° and 60° braids.

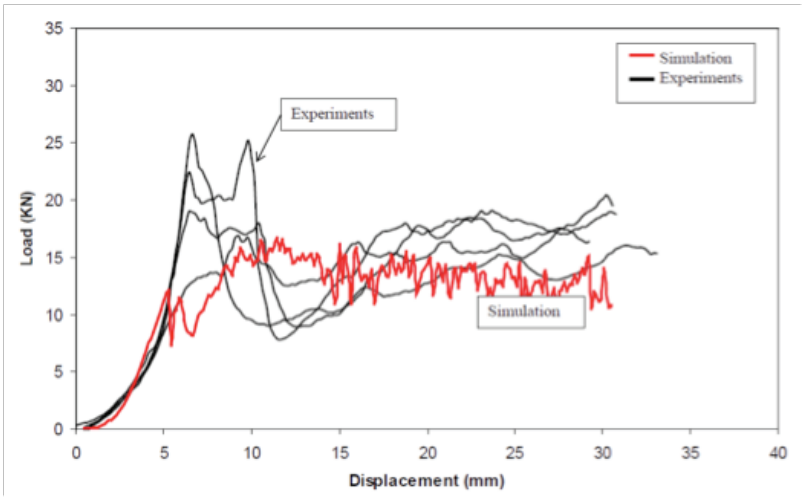

Figure 2. Simulations vs. tests for 30° carbon braided circular tube (quarter model).

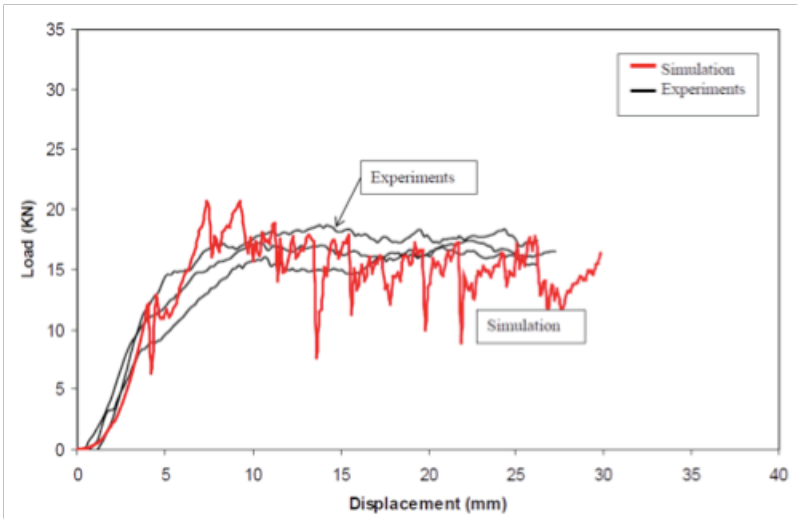

Figure 3. Simulations vs. tests for 60° carbon braided circular tube (quarter model).

The study also investigated the effects of incorporating interface debonding (damage) on the overall structural response, and the simulations did not show any remarkable improvement to the results. It is suspected that the main reason for this unremarkable improvement is due to the fact that phase properties were calibrated based on the coupon tests of 45° braid architecture rendering the local in-situ properties for other angles to be independent from braid angle. Additional analyses were performed in which comparisons were made to uniaxial coupon compression tests in the longitudinal (axial tow) direction. Preliminary results that the reduced-order multiscale modeling approach showed some agreement in trends, but still does not fully predict the pre-peak, peak, and post-peak responses reasonably well to within acceptable levels.

Size Effects on Strength in Textile Composites

This project is focused on developing a qualitative and quantitative understanding of the important topic of meso- to macro-size effects in automotive structures made of quasi-brittle textile composite materials. Such an understanding plays a role in the accurate modeling and characterization of structural crashworthiness and energy absorption in components made of lightweight quasi-brittle materials (such as textile composites). Obtaining an understanding and useful insights of size effects, along with verifiable experimental evidence and clarification of the implications of the size effects for finite element (computational) modeling of structures made of two-dimensional triaxially-braided composites (2DTBC), is the major goal of the project.

It is important at this point to clarify what is meant by "size" and what are the "effects". "Size" refers to the size of specimen/structural dimensions relative to the size of the damage zone and/or micro-structure. "Effects" refer to those effects on damage characteristics, nominal strength, and post-peak regime in materials exhibiting such strength–size dependence.

This project is motivated by the following fundamental question: What is the relationship between the measurements of energy released and dissipated (i.e., fracture properties and material nonlinearities) carried out in the laboratory at the coupon level of a 2DTBC, and their manifestations at the structural level in a real crash setting of a structure made of the same 2DTBC. I.e., do the measured overall material/structural properties change when different size specimens are tested. It is important to note that the primary interest in this topic (relating specimen size effects on measured material properties) does not stem from the well-known statistical distribution of micro-flaws in a material (e.g., Weibull theory), but rather from an energetic consideration driven by the relatively recent findings that quasi-brittle materials exhibit size effects because their fracture process-zone is not negligible (in size) compared with the overall structural dimensions and the size of local scales.

The work is focused on designing, manufacturing, testing and modeling different-size structural plaques using one matrix/resin system and three carbon fiber-braid architectures (+/-30°, +/-4 5°, and +/-60°). Various sizes of plaques were made encompassing a certain numbers of Representative Unit Cell (RUC) as determined by the project's plan (Figure 4). Each plaque made was multi-layer (up to 8 layers), each having axial tows as well as braider tows exhibiting one the above angles. The main objective is to provide insights and guidelines on how best to model and test such materials in order to accurately model their true behavior under static and dynamic loads. It is worth noting that such a topic has not been extensively studied for such types of materials.

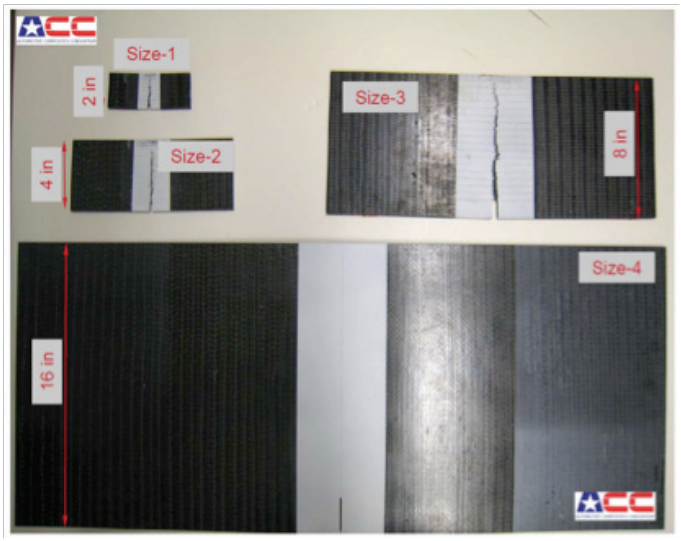

Figure 4. Four different structural sizes were selected in order to study size effects on carbon composites' nominal strength. The sizes range from a small 2-inch coupon to a 16-inch deep plaque. All have the same thickness.

Tests have been carried out on small samples and larger ones representing multiple RUCs. Based on the experimental data and observations, such braided carbon-fiber textiles seem to exhibit strong and rapidly evolving size effects. I.e., as one tests and compares the response of one RUC vs. multiple RUCs, the emergence of size effects becomes apparent and changes rapidly as larger-size plaques are tested.

Figure 5 shows the evolution of the deformation zone (strain field contours obtained using advanced optical techniques) near and around the initial crack (bottom mid-point of the specimen) in a 30° carbon braided textile. Figure 6 shows similar plots but for a 45° carbon braided textile specimen. Additional tests were performed on 60° braids. It is observed that for the same specimen size the deformation zone in the 30° braids is more pronounced and evolves more rapidly occupying a larger zone (as viewed optically) than in the 45° and 60° braids.

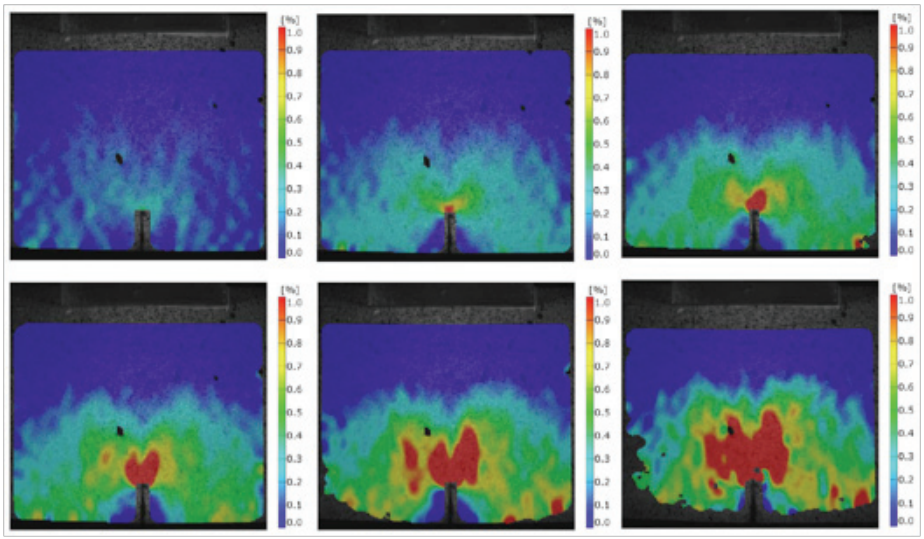

Figure 5. Evolution of the deformation zone (strain field contours) near and around the initial crack (bottom mid-point of the specimen) in a 30° carbon braided textile.

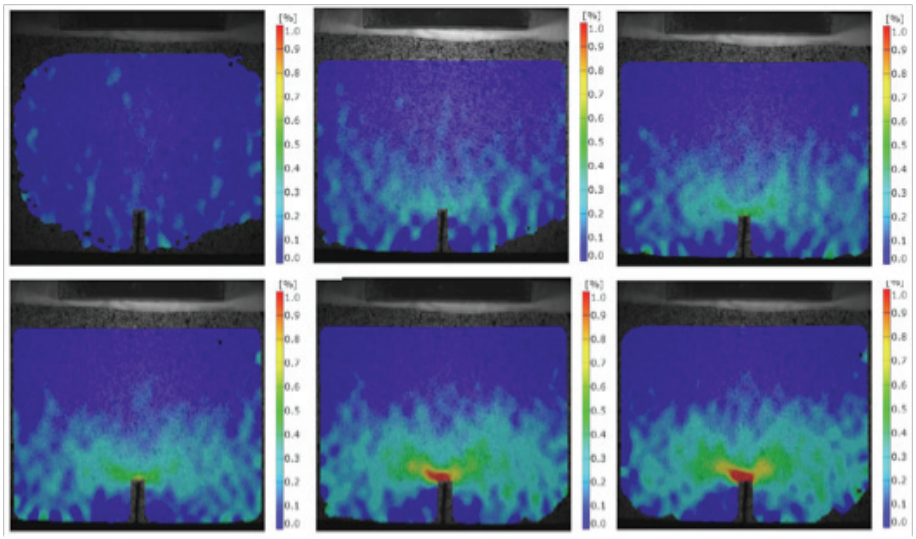

Figure 6. Evolution of the deformation zone (strain field contours) near and around the initial crack (bottom mid-point of the specimen) in a 45° carbon braided textile.

Figure 7 shows the strong size-effects that are present in such quasi-brittle textiles. The figure presents the log of normalized strength ($\sigma N/\sigma o$) vs. log of normalized specimen size (shown as log D/D_o)—presenting effects of size on the nominal strength using log format is common in the literature. This implies that the measured strength characteristics depend not only on the

material properties but also on the size of the specimen being tested. Such dependence poses special challenges to modeling and response prediction. Ongoing work is focusing on developing an enhanced version of the Microplane models used for modeling and analyzing damage and fracture in various types of inhomogeneous materials.

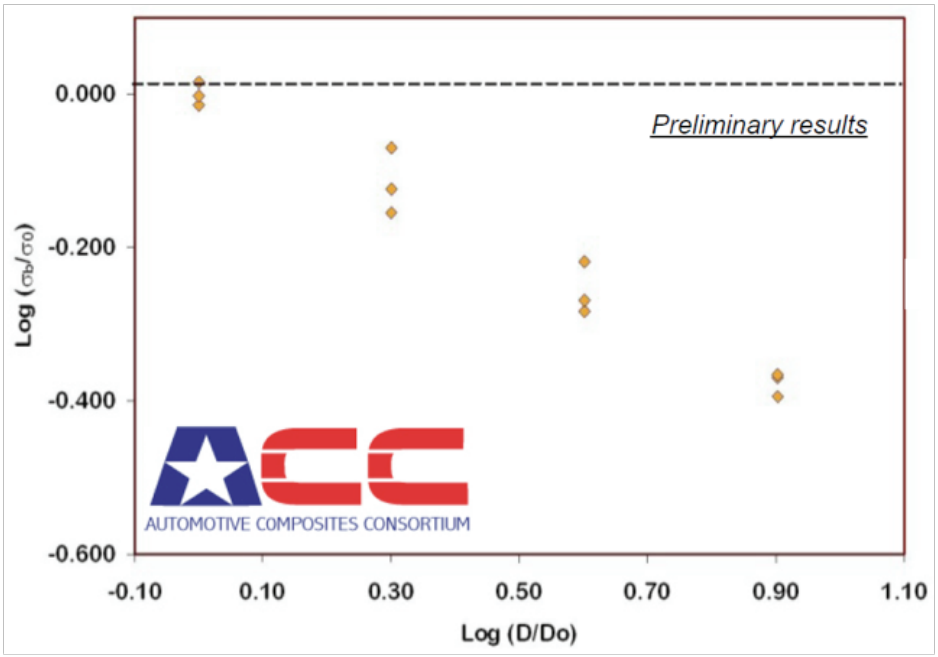

Figure 7. Experimental tests showing how the normalized structural strength [log(σN/σo)] changes with specimen size [log(D/D_o)] for 30° braided-carbon fiber specimen. The trend is similar for other braid angles.

In order to predict the above experimental observations an extensive parallel program has been developing state-of-the-art modeling methodologies to model the complex physics of such materials. Several approaches were investigated including the Microplane modeling technique. In this technique the stress-strain relationships at a material point are mapped onto a mathematical sphere with infinite tangent surfaces, and then simplified by selecting a finite number of surfaces. This number of surfaces dictates the number of coupled structural-material parameters the model requires to model damage initiation and growth for the specific application and degree of accuracy. It is important to note that the majority of these parameters are physical and can be measured or estimated based on a limited numbers of experimental tests.

Figure 8 shows two different levels of finite element model-representations used to model the different sizes of braided specimens. One level uses highly-detailed 3D finite elements model for all the constituents with an RUC (Figure 8, top). The modeling includes the matrix, as well as the actual axial-tow and bias-tow shapes (final cured shapes—i.e., does not use idealized cross-sectional geometry like prismatic-circular). These actual geometries are obtained using cross-sectional imaging/scanning methods. The other level uses a much coarser mesh of the RUC (Figure 8, bottom). Here, each RUC is made up of a fewer number of 3D elements, and irregular (rugged) boundary/edges. The coarse RUC model is very efficient but requires more approximations especially for modeling the damage of the resin-rich regions between the tows. However, the fine mode (Figure 8, top) requires very few approximations but is very large in size requiring intensive computational resources. It is worth noting that efforts are underway to increase the computational efficiency of such detailed models by using advanced model-reduction techniques in order to render them more efficient and less resource-intensive.

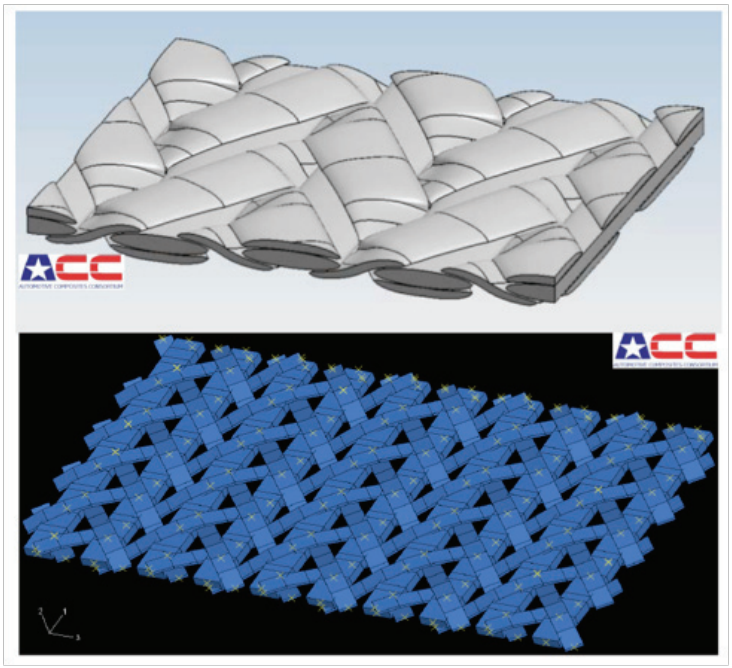

Figure 8. Two different modeling approaches to model different size of braided specimens. The top figure shows a very detailed 4 RUC specimen (2x2). The model use 3D finite element for the matrix, and for representing the actual axial-tow and bias-tow shapes. The bottom figure includes a much coarser model of a full plaque made up of 25 RUCs (5x5). Each RUC is made up of 3D elements and irregular (rugged) boundary/edges. Only axial and braider tows are shown for clarity.

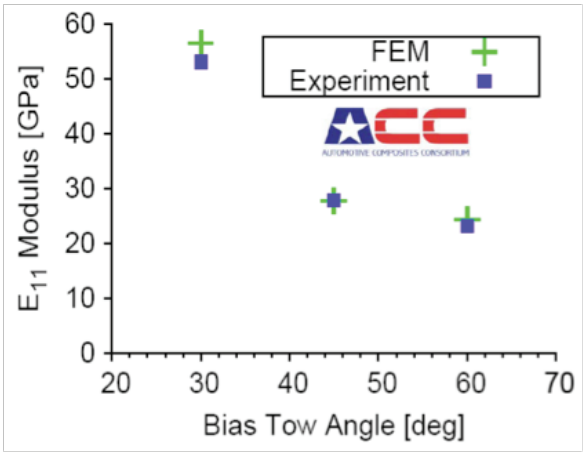

Figure 9. Examples on the computational (FEM) validations for all three braid angles (30°, 45° and 60°)

The developed models were verified and validated on a wide range of problems. Figure 9 shows examples for some of the preliminary validations with tests. The figure shows mean values for E_{11} (elastic modulus along the axial-tow direction) for all three braid angles (30°, 45° and 60°). Note that unlike nominal strength measurements (to be shown), E_{11} values for the same braid architecture do not change with the size of the specimen.

The developed models were then employed to predict the nominal strength for each specimen tested in order to study its capability in predicting the evolution of strength with size. Figure 10 shows the fitted computational predictions for nominal strength [Log(σ_N)] which, as the specimen size [Log(D)] increases, asymptotes the Linear Elastic Fracture Mechanics (LEFM) line (dashed) which has a slope of -½. The figure also shows the experimental tests data (circles). Note that as the presented specimen size and strength are normalized quantities.

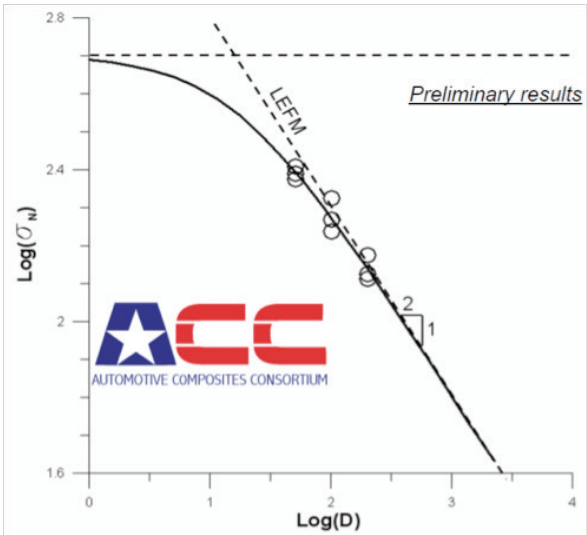

Figure 10. Experimental tests and fitted numerical predictions (solid line) showing the change of the log of normalized strength (σN) vs. change in specimen size (shown as log D) for 30° braided specimen.

Figure 11 shows plots of load vs. displacement for different specimen sizes for 30° braids. The computational values show acceptable correlation when predicting the pre-peak and peak loads for the larger specimen. However, as the specimen size gets smaller such predictions become less correlated with tests. Current work is being carried out in order to address the causes of such differences. Note that peak-load values will depend on the size of the specimen because larger specimens require higher loads to reach their strength limits. This should not be confused with size-effects on nominal strength which is commonly assumed to be specimen-size independent—an assumption which may be erroneous especially for some quasi-brittle materials.

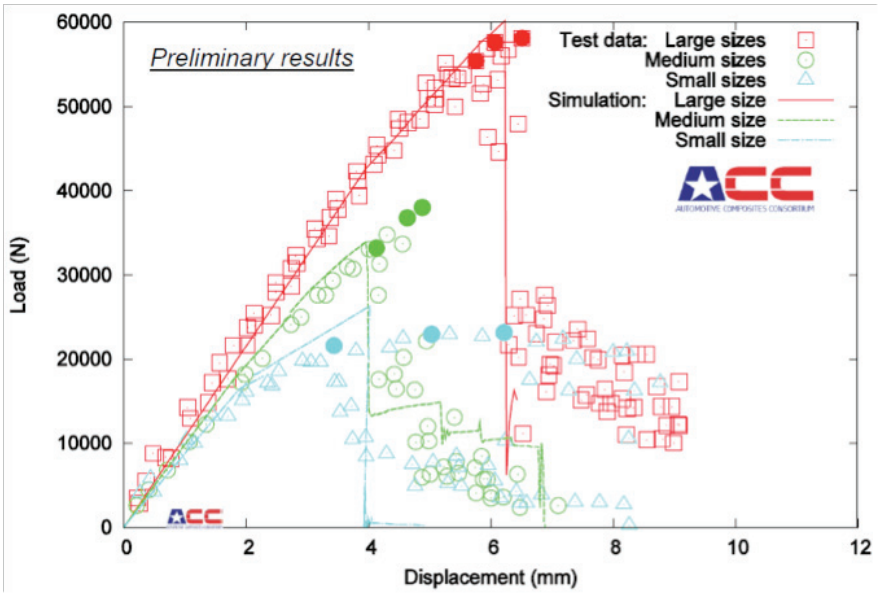

Figure 11. Experimental tests (symbols) and fitted numerical predictions (solid lines) showing specimen Load (N) vs. Displacement for 30° braids. Test data for different specimen sizes are presented as: large=red squares, medium=green circles, small=blue triangles)

Modeling of the Manufacturing Process Induced Effects (MPIE) on the Matrix Properties of Textile Composites ("In-Situ Properties Predictions")

During the manufacturing process of textile reinforced composites (TRC) the material properties of a polymer resin (matrix) do change over the curing cycle. Resin's liquid-to-solid transition is accompanied by volume change, coupled with mismatches in thermal coefficients between fibers and resin (and applied mechanical stresses) may result in inhomogeneous curing of TRC structural specimen. Such spatial variations could result in built-in local residual stresses and potentially pre-existing micro cracks. Such local field-variations within the cured material are a result of the physics of curing in materials with complex microstructure, which can result in differences between the presumed material properties (usually virgin/neat properties) and the actual in-situ material properties. The actual response of a structural component made of TRC may be accurately predicted by using well-characterized in-situ material properties not the virgin/neat properties which are sometime the presumed input to analysis codes.

It is of value to know and assess such differences in properties in order to objectively know when they can be considered to have primary influence on the predictive models' accuracy and validity. This project is aimed at developing the knowledge needed and the tools necessary to make such assessments within an objective framework based on engineering mechanics. It is the primary objective of this project to develop qualitative and quantitative methodologies (and modeling tools) to better understand and predict the in-situ properties within a fully-cured structural component made of TRC.

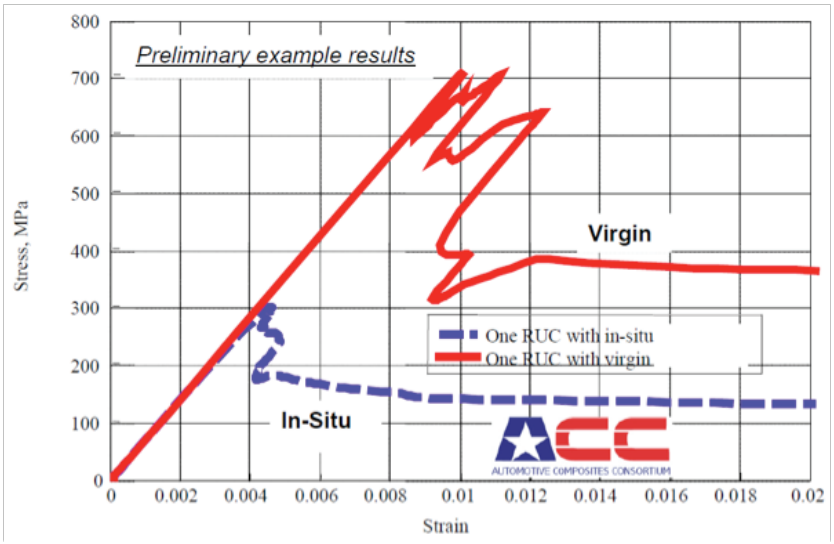

Figure 12. The responses of one RUC using the finite-element model for a triaxially-braided carbon-composite material specimen. The shown difference is a demonstrative example on the use of in-situ properties vs. their neat/virgin counterparts.

Figure 12 shows a simple demonstrative example of the difference in response of one Representative Unit Cell (RUC) model of a tri-axially-braided carbon-composite material specimen. The figure demonstrates the effects of using virgin/neat matrix properties (solid red curve) vs. their in-situ counterparts (dashed blue curve) on the model's response of one RUC. [Note: it is important to recall that the response of one RUC represents only the response of that small region of material and may not represent the nonlinear response of the larger region—i.e., specimen, structure, etc.].

It is of prime importance to realize the relevance of this project to the overall goals and objectives of the ACC 100 which are aimed at characterizing and modeling energy absorption and crashworthiness of composite structures. Because of the many dependent and independent phenomena governing the energy absorption mechanisms in composites, especially textile

composites, it is very important to develop models that are robust and predictive. Doing so requires knowing which aspects of the model are physical (physics-based), which are computational (numerical-based), and which are user-driven (input data-based). Although it is sometimes a nontrivial task to discriminate between the three especially when one is dealing with highly nonlinear mechanical problems, it is prudent that one minimizes "inaccuracies" in the latter (input data) in order to improve prediction accuracy and robustness. One way to accomplish that is by knowing a priori the properties which are actually in-situ not what those which are presumed to be in-situ—a fine but important distinction.

TRC materials are quasi-brittle systems whose energy-dissipation characteristics are dominated by micro-cracks which are controlled by local geometry and in-situ properties. A need exists to develop a robust computational predictive tool which uses as input stress-relaxation, evolution of extent-of-cure, and thermal conductivity properties measured/calculated from simple mechanical tests without resorting to back-calculations using full nonlinear finite element analysis (FEA) simulations. Currently, for modeling purposes in-situ properties are typically back-calculated using several laboratory tests as well as elasto-plastic analytical theories (in conjunction with computer models). Although the current process has been verified and validated, and is based on well-established theories from mechanics of materials, it is not efficient especially during the preliminary development process.

This project involves three major aspects: a) spatial material characterization of cured matrix in resin-rich locations, adjacent to fibers within a tow, as well as in between fibers and tows; b) temporal and thermal evolution of constitutive properties (using state-of-the-art optical techniques) as functions of time, extent-of-cure, and imposed thermal conditions at the boundaries; and c) development and validation of predictive tools that model the manufacturing and curing processes including mechanical and thermal stresses, visco-elasticity, and visco-plasticity.

More specifically, resin-filled cylinders will be subjected to temperature variations based on manufacturer curing profile. Time and radial variation of temperature, extent of cure, strains and stresses will be measured and calculated. The cured resin will be removed and subjected to additional mechanical tests. The above detailed procedure will be repeated but with a fiber tow (simulating TRC) placed concentrically in the cylinder prior to curing and repeated tests. A complete set of experimental and modeling results are deliverables including: nano-indentation characterization (Figure 13); characterization using optical techniques such as Brillouin Light Scattering (BLS) and Raman Light Scattering (RLS) (Figures 14 and 15); and a Finite Element Modeling procedure capable of simulating the MPIE (no resin fluid-flow simulations). The effects of process cure parameters and their effects on matrix cracking modeled through the thermomechanical FE code is also a deliverable (no modeling of individual micro-cracks).

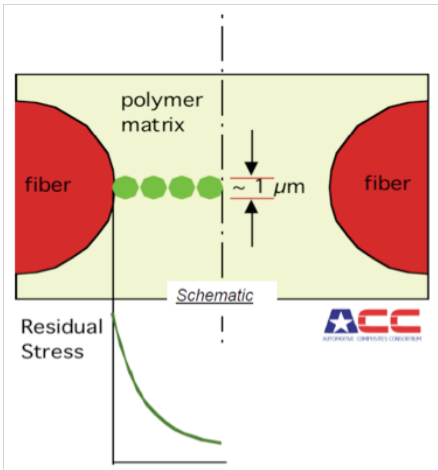

Figure 13. Schematic showing examples of locations (four small green circles) where nano-indentation may be used to extract values for the modulus distribution near and away from the fiber (larger red semi-circles) as well as within resin-rich regions.

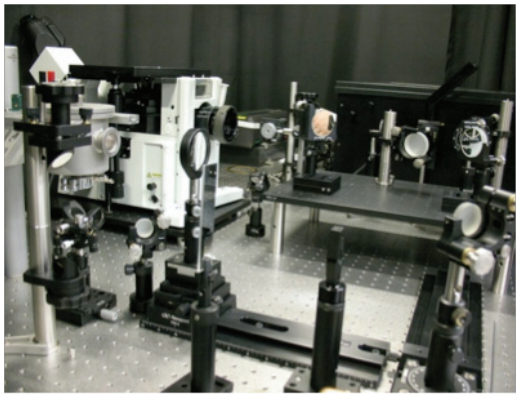

Figure 14. Experimental setups for the Brillouin Light Scattering (BLS) and Raman Light Scattering (RLS) experimental optical techniques.

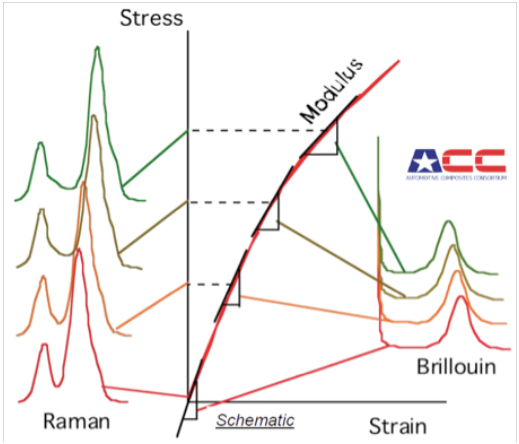

Figure 15. Schematic showing the basic idea of using BLS and RLS as optical techniques to measure the mechanical properties of a material.

Figure 16 shows some preliminary results from laboratory tests designed to measure elastic modulus of an Epon resin sample while it is curing (i.e., degree-of-cure) plotted vs. curing time at different imposed boundary temperatures. The tests used state-of-the-art optical techniques to measure the modulus.

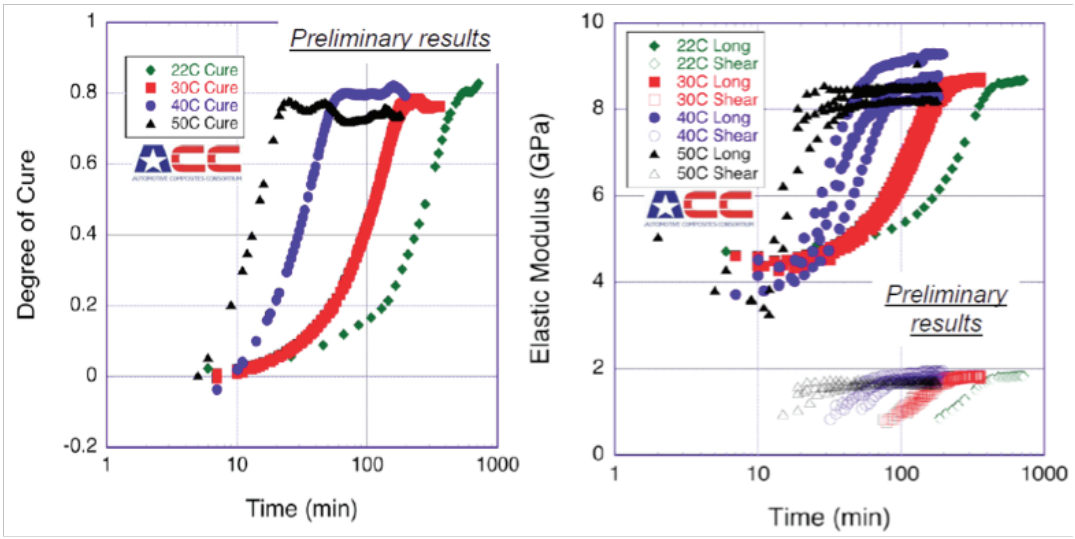

Figure 16. Plots of resin's degree-of-cure (left figure) and elastic modulus (right figure) vs. time at different boundary temperatures. Note that the curves in the lower region of the right figure represent shear modulus data, while the upper curves represent the longitudinal (extensional) modulus.

One of the main planned outcomes of this multi-year project is the development of a predictive tool which can be incorporated into any existing composite material-damage model. Such a tool will remove the need for carrying out parallel (and additional) tests as well as extensive nonlinear FEA (as currently is the practice) in order to "back-out" the actual in-situ material properties which influence the structural response and local damage characteristics.

Another important contribution of the project is to expose the main factors contributing to such in-situ properties and their evolution during the manufacturing and curing process. For example, using nano-indentation (Figure 13) it was found that not only matrix properties vary with time (while curing) and with location (i.e., how close to a fiber/tow) but also that because of the very nature of chemical curing, the apparent fiber properties within a tow differ depending on the type of resin (Figures 17). Here, the somewhat expected preliminary results highlight the importance of understanding the time history, the manufacturing process, and spatial variation of material properties within a cured structural component.

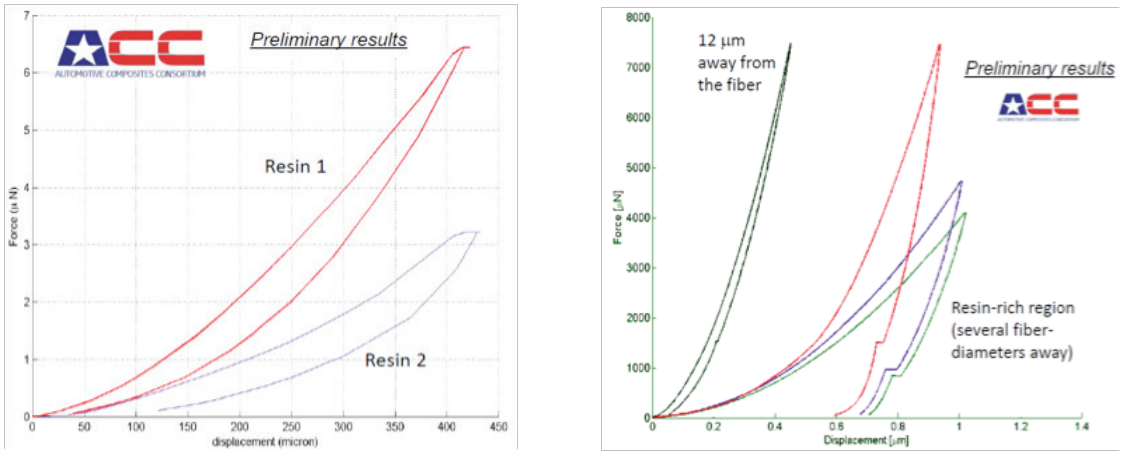

Figure 17. Preliminary laboratory test measurements show the results of using nano-indentation to measure the transverse force-displacement (F-D) response. The figure on the left shows the F-D response using two carbon fibers each embedded in different (cured) resins. The figure on the right shows the F-D response of cured matrix as a function of the distance away from the edge of a single carbon fiber embedded in the cured matrix.

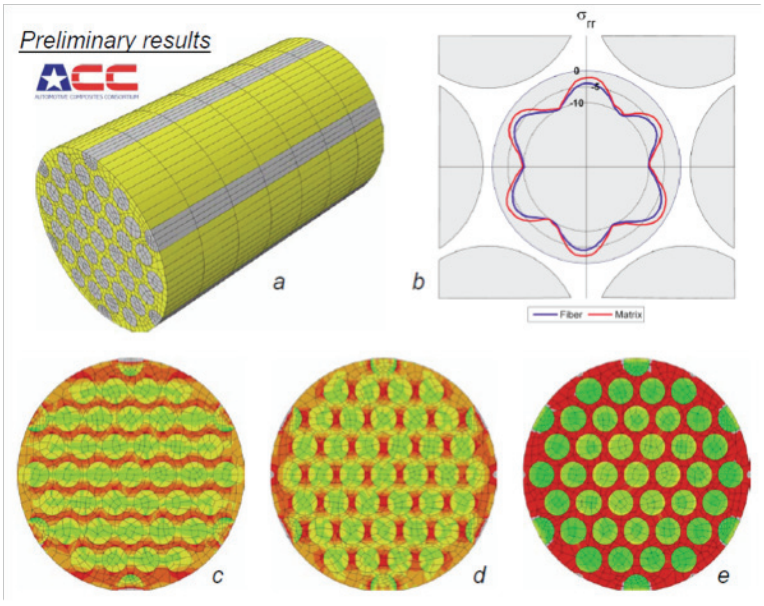

Figure 18. Preliminary FE analyses simulating the residual stresses in a cured tow containing carbon fibers and matrix. (a) 3D nonlinear model of tow segment; (b) radial stress variation within a fiber; and stresses components in the lateral/horizontal direction (c), transverse/vertical direction (d), and axial direction (into the page) (e).

Detailed 3D Finite Element (FE) modeling were carried out in order to better understand the residual stress distributions within a cured tow segment which contains fibers and matrix. Figure 18 shows the radial as well as three Cartesian components of stresses around the fibers (within a tow) in the three principal directions. Such detailed micro-models are not expected to be part of any larger models for structural components to be analyzed for their global mechanical response and energy absorption. However, these detailed model, albeit computationally resource-intensive, are important in understanding the physics of curing and its effects on the final mechanical properties within various locations. Once the final (cured) mechanical properties obtained computationally (at the end of curing process) are validated via the nano-indentation experimental tests, the global mechanical models can be extended towards modeling the energy absorption of a specimen under static and dynamic loads. The above are one of the critical steps which the project is currently completing. One of the next steps will be to extend the thermo-mechanical matrix-curing model to include a bi-material interface which is manifested as internal (fiber edge) and external boundary constraints within the visco-plastic formulation.

Publications/Presentations

1. Song S, A M Waas, K W Shahwan, O Faruque, and X Xiao (2009), Effects of Matrix Microcracking on the Response of 2D Braided Textile Composites subjected to Compression Loads, Journal of Composite Materials, (published online 8/19/2009; paper in print).

2. Song S, A Waas, K Shahwan, O Faruque, and X Xiao (2009), Compression Response, Strength and Post-Peak Response of an Axial Fiber Reinforced Tow, International Journal of Mechanical Sciences, 51, pp. 491–499.

3. Caner, F, Z Bazant, C Hoover, A Waas, and K Shahwan, Microplane Model for Fracturing of Triaxially Braided Fiber-Polymer Composites, ASME Journal of Engineering Materials and Technology, paper in review.

I. Development of Standard Test Methods for Crashworthiness of Composites

Co-Principal Investigator: J. Michael Starbuck
Oak Ridge National Laboratory
P.O. Box 200; Oak Ridge, TN 37831-8048
(865) 576-3633; e-mail: starbuckjm@ornl.gov

Co-Principal Investigator: Daniel O. Adams
University of Utah
Department of Mechanical Engineering
50 S. Central Campus Drive; Room 2110 MEB; Salt Lake City, UT 84112-9208
(801) 585-9807; e-mail: adams@mech.utah.edu

Team Member:
Graham Barnes - Engenuity Limited
Contractor: Oak Ridge National Laboratory (ORNL)
Contract No.: DE-AC05-00OR22725

Technology Area Development Manager: Dr. Carol Schutte
(202) 287-5371; e-mail: carol.schutte@ee.doe.gov

Field Technical Manager: C. David Warren
Oak Ridge National Laboratory
P.O. Box 2008, Oak Ridge, TN 37831-6065
(865) 574-9693; e-mail: warrencd@ornl.gov

Objective

- Develop both coupon-level and element-level standardized test methods for characterizing the Specific Energy Absorption (SEA) associated with the progressive crushing of composites.

Approach

- Develop flat-plate test specimen geometry for coupon-level testing.
- Develop square-tube test specimen geometry for element-level testing.
- Develop standards that are accepted by the composites community that will facilitate material selection and improve new product developments for composite automotive structural components.

Accomplishments

- Initiated procurement requirements for University of Utah subcontract.
- Identified potential candidate material systems for baseline Year 1 testing.

Future Direction

- Conduct baseline material tests.
- Develop a draft standard for coupon-level testing.
- Develop a draft standard for element-level testing.

Introduction

Progressive crush is an important mechanism by which the kinetic energy of an automobile is dissipated in a collision to protect the safety of occupants. Unfortunately, the mechanism governing the progressive crush response of composite materials proposed for automotive applications are not well understood. Additionally, many of these materials are known to exhibit responses that are sensitive to rate of loading. Understanding the influence of loading rate, fiber and matrix materials, and laminate design on the energy absorption during dynamic crush loading is critically important for crashworthiness design. Additionally, from a structural standpoint, the deformation (or strain) rate is generally not unique from either a spatial or temporal standpoint. Consequently, it is important to quantify the behavior of materials at various strain rates.

When investigating dynamic deformation of materials, the critical parameter is the material strain rate and not the velocity of deformation. Strain rates may vary from the minimal values of 10^{-7}/sec produced in a creep test to greater than 10^{8}/sec in a nuclear detonation. In a broad sense, strain rates can be divided into two regimes: 1) above 10^{5}/sec where inertia forces due to shear and shock wave propagation are important, and 2) below 10^{5}/sec where inertia forces are negligible. Most of the testing for energy absorption of composite materials falls below the 10^{3}/sec. strain rate and is classified as a relatively low-rate dynamic test. For such testing high-rate servo-hydraulic test machines, pneumatic sleds, and drop towers are the most common loading methods used.

Several test methodologies have been utilized at both the coupon-level and element-level to characterize energy absorption in composite materials. However, there is no standard by which either type of test method may be executed. Further no existing standards consider the effect of different strain rates (or test velocity) and the corresponding test methods that are required for different rates. Thus, test data is generally not comparable from different material systems, laminates, and loading rates that have been produced by different laboratories. Current activities within the Composite Materials Handbook-17 subcommittee on crashworthiness are beginning to focus on this issue but only on a volunteer basis and by a limited number of committee members. Thus, it is important that properly designed and universally accepted test methods be developed for assessing and comparing energy absorption characteristics of candidate composite materials. These test method developments will be performed in conjunction with ASTM D 30 (American Society for Testing of Materials) Committee on Composites and CMH-17, the Composite Materials Handbook.

Status

The research program will build upon past and current projects involving the experimental characterization of composite crashworthiness. Primary issues to be addressed in test method development will include specimen size/shape/thickness, support conditions provided by the test fixture, the use of a trigger mechanism, the measurement methods for force/displacement/strain, and procedures used for obtaining the SEA. An idealized curve for SEA is shown in Figure 1. Additionally, the test methodologies should provide guidance for determining the transition from static to dynamic, e.g., test velocities or strain rates and what speed defines “dynamic”. I t is desirable to have the same test method and fixturing apply to both static and dynamic tests,

but this is not viewed as a requirement and may not be possible. Figure 2 shows a prototype coupon-level test fixture developed at the University of Utah. Additionally, a coordinated effort between ORNL and the University of Utah to develop both a coupon-level and element-level standardized test method will lead to a maximum degree of commonality between the two proposed test methods.

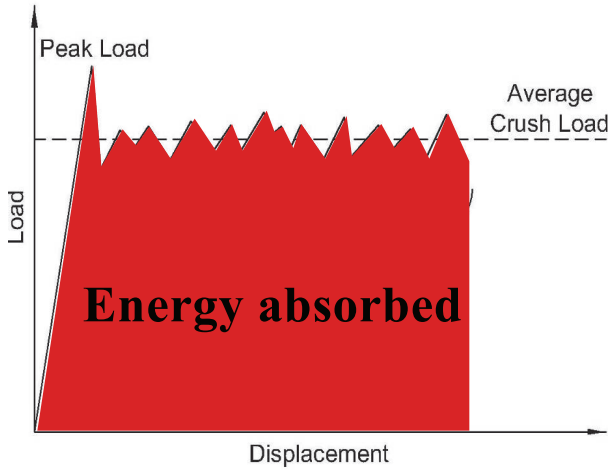

Figure 1. Idealized energy absorption curve.

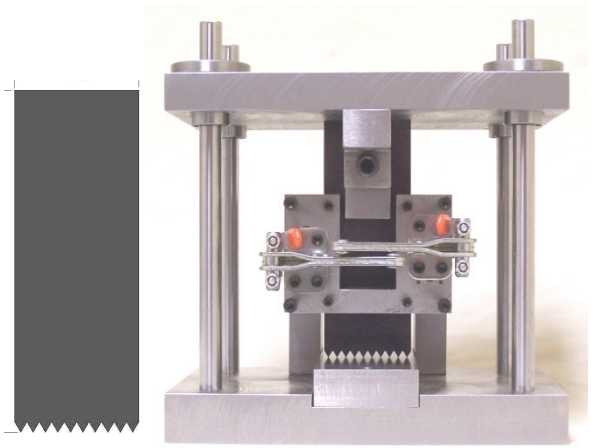

Figure 2. Prototype coupon-level fixture and test specimen.

For FY 2009, the project activities focused on developing the statement of work for the University of Utah subcontract. In addition to this, the Composite Materials Handbook (CMH) 17 meeting was attended and the process of selecting materials for the baseline tests was initiated. The involvement of CMH-17 members early in the project will be beneficial later on when a standardized test is proposed.

Conclusions

A coupled three-year research program, to be performed at the University of Utah and Oak Ridge National Laboratory, was initiated to develop standardized test methods for the dynamic crush testing of flat and tubular composite specimens. The development of a coupon-type test method for investigating the energy absorption associated with the crushing of composite laminates will be performed at the University of Utah. This low-cost coupon-level test method, featuring an end loaded flat specimen, is attractive for investigating failure modes and the associated energy

absorption associated with different materials, laminates, and loading rates. The development of a structural tube-type test for investigating the failure modes and energy absorption associated with composite structures will be a collaborative effort involving both Oak Ridge National Laboratory and the University of Utah. Although costlier than coupon-level testing, this element-level test produces measures of energy absorption that may be applied more directly to automotive applications. The proposed research program is divided into two distinct but dependent tasks that will be performed in parallel.

J. Engineering Property Prediction Tools for Tailored Polymer Composite Structures

Principal Investigators: Ba Nghiep Nguyen
Pacific Northwest National Laboratory
902 Battelle Blvd.; PO Box 999; Richland, Washington 99354
(509) 375-3634; e-mail: Ba.Nguyen@pnl.gov

Industry Consultants: Peter Foss - General Motors
Michael Wyzgoski and Gerry Trantina - American Chemistry Council

Industry Participants: American Chemistry Council, DOW Chemical, DuPont, SABIC, and Ticona
Cooperative Research and Development Agreement (CRADA): AutoDesk/Moldflow

Vlastimil Kunc - Oak Ridge National Laboratory
PO Box 2009; Oak Ridge, Tennessee 37831
(865) 574- 8010; e-mail: kuncv@ornl.gov

Technology Area Development Manager: Dr. Carol Schutte
(202) 287-5371; e-mail:carol.schutte@ee.doe.gov

Field Technical Manager: Mark T Smith
(509) 375-4478; e-mail:Mark.Smith@pnl.gov

Contractor: Pacific Northwest National Laboratory (PNNL), Oak Ridge National Laboratory (ORNL)
Contract Nos.: DE-AC05-76RL01830 (PNNL), DE-AC05-00OR22725 (ORNL)

Objective

- Develop predictive modeling tools for injection-molded long-fiber thermoplastic (LFT) composites.
- Enable the optimum design of lightweight automotive structural components using LFT composites.

Approach, including industrial partner/collaborator and path to technology transfer and commercialization

Phase II: Research and Development: Phase II aims at developing an integrated approach that links process to structural modeling, allowing the optimum design of LFT composite structures. This work includes:

- Develop process models for LFTs that allow simulations of LFT structures in order to predict flow-induced fiber orientation and other microstructural features, such as fiber length distribution.
- Develop and implement LFT constitutive models for structural finite element analyses that make use of the composite microstructure predicted by process modeling. These constitutive models will predict the composite thermoelastic properties and its nonlinear behaviors due to damage, fatigue, creep, and impact.
- Develop characterization methods for LFT materials.

- Injection-mold larger samples.
- Conduct experimental testing to determine the model parameters and to validate the process and constitutive models.

Project partners and collaborators

- University of Illinois at Urbana-Champaign (subcontract with PNNL) developed process models.
- Autodesk, Inc. (Cooperative Research and Development Agreement (CRADA) with PNNL) implemented process models in Autodesk Moldflow Insight.
- American Chemistry Council and its members provided the materials and played an advisory role.
- General Motor Corporation served in a consulting role.

Path to technology transfer and commercialization

- Dissemination of research results through significant publications, presentations, and workshops.
- Implementation of process models in Autodesk Moldflow Insight enables commercialization of these models.
- Creation of Eshelby-Mori-Tanaka Approaches for Nonlinear Analyses (EMTA-NLA) software and its implementation in ABAQUS via user-subroutines for structural analyses facilitate the future commercialization of this capability.

Milestones, Metrics and Accomplishments

Milestone 1:

Complete the development and implementation of a fiber length attrition model for injection-molded LFTs with associated testing, and complete the development and implementation in ABAQUS of a fatigue damage model for LFTs with associated testing (completed March 2009).

Milestone 2:

Complete the development and implementation in ABAQUS of an impact damage model for LFTs with associated testing (completed September 2009).

Accomplishments

- A new fiber length attrition model in the mold for LFTs was developed and implemented into the ORIENT processing code. The model can capture the experimental fiber length distribution profile.
- The fiber length attrition model has been implemented in Autodesk Moldflow Insight, which can now predict fiber length distributions in moded plaques.
- A fatigue damage model for LFTs was developed and implemented in ABAQUS via EMTA-NLA. Initial validation of the fatigue model was carried out using the data obtained for a glass-fiber/polyamide 6,6 (PA6,6). The predicted reduction of elastic moduli for this composite as a function of the number of cycles were in agreement with the experimental results.
- An impact damage model for LFTs was developed and implemented in ABAQUS via EMTA-NLA. First validation of the impact damage model was carried out using the data obtained for a glass-

fiber/PA6,6. The predicted damage accumulation and crack propagation patterns agreed with the experimental observations.

- Fiber length distribution was characterized along the flow length for glass/PA6,6 and glass/polypropylene (PP) samples.
- Fiber orientation and dispersion were characterized for glass/PP samples.
- Fatigue and creep data were generated for glass/PA6,6 and glass/PP samples in the flow and cross-flow directions.
- Multi-axial impact tests were performed for glass/PA6,6 samples.
- A set of tomography tests was performed on miniature test samples.

Future Direction

- Further validate the developed process and constitutive models for representative LFT materials for automotive applications.
- Define and injection-mold a complex LFT part.
- Validate the developed process and constitutive models for this complex LFT part.

Introduction

In FY 2009, efforts focused on completing the development of a fiber length attrition model for long-fiber thermoplastics (LFTs) and the developments and implementations in ABAQUS of a fatigue damage model and an impact damage model for these materials. Testing was performed to support model developments.

Experimental effort has focused on glass-fiber/polyamide 6,6 (PA 6,6) and glass-fiber/polypropylene (PP) plaques. Fiber length distributions (FLDs) were obtained along the flow length for two thicknesses and two fiber contents. These results were also compared to FLD from bucket shots. Tension-tension fatigue testing has been conducted for the dry glass-fiber/PA6,6 specimens to obtain the fatigue data (i.e., modulus reduction versus number of cycles). Tests were performed at various load levels; however, the peak stress of a cycle is between 30% and 50% of the ultimate tensile stress. Multi-axial impact tests were performed to support development of an impact model. A complete set of tests was designed for glass-fiber/PP samples. Microstructure and mechanical properties of material containing 30% of glass were characterized.

In contrast to fiber orientation modeling, before this project, no standard model was developed to predict the fiber length distribution in molded fiber composites. Pacific Northwest National Laboratory (PNNL) has worked through a subcontract with the University of Illinois at Urbana-Champaign for the development of a fiber length attrition model for injection-molded LFTs. Phelps and Tucker [1] developed a model that takes into account the micromechanics of fiber breakage in a fiber suspension. They relate fiber orientation to the hydrodynamic loading of a fiber. This orientation-dependent model for fiber loading is subsequently related to a classical buckling criterion to predict fiber breakage. Finally, the fiber breakage model is implemented into an expression for the conservation of the total fiber length to derive a rate equation for fiber length distribution.

A fatigue damage model for LFTs was developed using a mechanistic approach to damage, combining micromechanical modeling with a continuum damage mechanics description [2]. Matrix microcracking has been identified as the key mechanism responsible for fatigue damage. A modified Eshelby-Mori-Tanaka (EMT) approach is then used to compute the stiffness reduction of the

composite as a function of the microcrack volume fraction. Next, a continuum damage mechanics formulation is used to derive the constitutive relations and the damage evolution law. The fatigue model was implemented in ABAQUS via Eshelby-Mori-Tanaka Approaches for Nonlinear Analyses (EMTA-NLA) and has been validated for a glass-fiber/PA6,6 material.

An impact damage model for LFTs was developed that considers elastic fibers embedded in an elastic-plastic damage resin matrix. The impact damage model is an extension of the previously developed quasi-static damage model to predict damage under impact loading [3]. Therefore, a rate formulation is used to express the damage evolution as a function of the stress and strain quantities. This model was implemented in ABAQUS via EMTA-NLA and has been validated for a glass-fiber/PA6,6 material.

Modeling Fiber Length Attrition

Phelps and Tucker [1] have developed a fiber length attrition model to predict FLD in a mold cavity during injection molding. First, using a model by Dinh and Armstrong [4], an expression for the hydrodynamic force acting along the fiber axis is obtained. The condition for buckling that leads to fiber breakage compares this hydrodynamic force to the buckling force from classical Euler buckling theory. This condition states that a fiber of length l_i and orientation **p** will break if

$$\frac{F_i(\mathbf{p})}{F_{\text{crit}}} = \left[\frac{4\zeta\eta_m l_i^4}{\pi^3 E_f d_f^4}\right](-2\mathbf{D}:\mathbf{pp}) > 1 \tag{1}$$

Here, F_{crit} is the critical compressive force based on the Euler buckling theory; ζ, a dimensionless drag coefficient from the Dinh-Armstrong model; η_m, the resin viscosity, D, the rate of the deformation tensor; and E_f and d_f are the fiber elastic modulus and diameter, respectively.

Using this criterion in combination with typical orientation statistics of fibers, Phelps and Tucker express the probability that a fiber of length will break during a time increment Δt as $P_i\Delta t$, where P_i is given by:

$$P_i = C_B\dot{\gamma}\{1-\exp(1-\hat{\gamma})\} \tag{2}$$

C_B is a phenomenological coefficient that scales the breakage rate, and $\hat{\gamma}$ is the expression in square brackets in Equation (1).

The local FLD is represented by a set of values: N_i, i = 1 to n, that give the number of fibers of length $l_i = i\Delta l$. Typically, n = 130 bins is used in the length distribution. As fibers break, this distribution must satisfy a conservation equation of total fiber length.

$$\frac{\partial N_i}{\partial t} + \mathbf{v}\bullet\nabla N_i = -P_i N_i + \sum_k R_{ik} N_k \tag{3}$$

In this equation, R_{ik} is the rate of production of child fibers of length l_i by breaking parents of length l_k, and v is the fluid velocity. R_{ik} is determined by a combination of the parent breakage rate P_k and the assumption that breaking points are distributed along the parent fiber length in a Gaussian profile. Together with Equations (1)–(3), this provides a full set of equations to solve for the FLD.

This fiber length model has been combined with ORIENT, the injection mold filling research code used by the University of Illinois group, to make fiber length predictions for injection molded LFT parts. ORIENT provides local values of viscosity, velocity, and shear rate. Each node in the filling mesh has a length distribution (a set of N_i values). The FLD is carried along with the polymer as it fills the mold cavity and changes as the fibers break in response to the local shear rate. The measured FLD just inside the gate is used as an initial condition, and the model predicts the length distribution at all downstream locations.

Figure 1 shows measured and predicted FLDs for a glass-fiber/PP disk. The experimental length distribution is typical of samples with a significant amount of fiber length attrition: the majority of the fibers are less than 2 millimeters (mm) long, but some longer fibers remain. The predictions of this fiber length attrition model adequately capture the features of this data.

The change of average fiber length along the flow path is shown in Figure 2 for the same glass-fiber/PP molding. The plot shows number-average (L_n) and weight-average (L_w) fiber lengths as a function of distance from the injection point. Again, the model accurately predicts these changes.

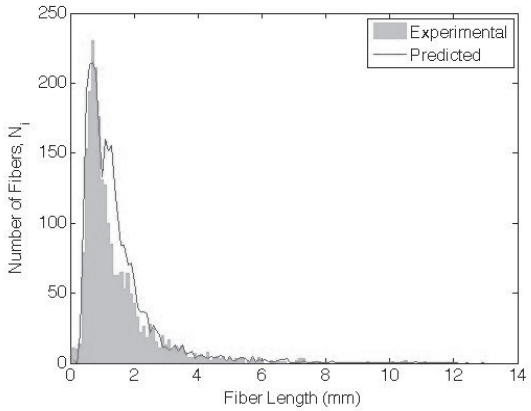

Figure 1. Measured Number of Fibers vs. Fiber Length for a Glass/PP Disk (compared to predictions of the fiber length model)

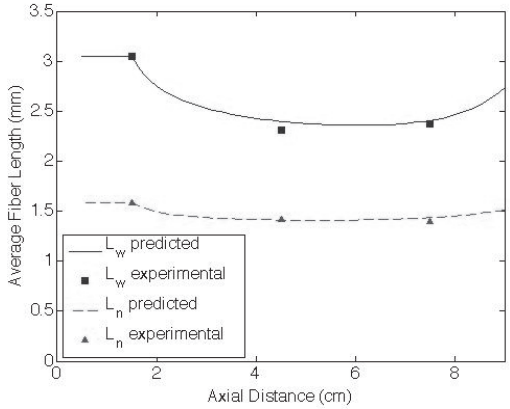

Figure 2. Predicted and Experimental Average Fiber Lengths for the Glass/PP Disk Shown in Figure 1

A Fatigue Damage Model for LFTs

A fatigue damage model was developed that accounts for matrix cracking as the responsible damage mechanism [5-6]. The development of this model requires the establishment of [2]: i) the stiffness reduction law, ii) the constitutive relations, and iii) a damage evolution law as a function of the governing variables such as the strains and cyclic loading parameters.

The stiffness reduction law is established assuming matrix microcracks as fiber-shape inclusions with zero stiffness. An EMT-type model is used in combination with techniques for averaging fiber orientation and length distributions to compute the stiffness of the as-formed composite. The experimental modulus reduction data are used to identify the evolution of the microcrack volume fraction versus the number of cycles. As fatigue damage due to cyclic loading often occurs at low stress levels, the elastic damageable behavior is assumed for the composite. By selecting the matrix microcrack volume fraction, D, as the damage variable, and the elastic deformation energy, Φ , as the thermodynamic potential, the constitutive relation and the damage evolution law are derived using a thermodynamic formulation:

$$\sigma_{ij} = \frac{\partial \phi}{\partial \varepsilon_{ij}} = \overline{C}_{ijkl}(D)\,\varepsilon_{kl} \tag{4}$$

$$dD = \frac{\frac{d\overline{C}_{ijkl}}{dD}\varepsilon_{ij}d\varepsilon_{kl}}{\frac{1}{2}\frac{d^2\overline{C}_{ijkl}}{dD^2}\varepsilon_{ij}\,\varepsilon_{kl} + \frac{\partial F_c}{\partial D}} + \frac{\frac{dF_c}{dN}dN}{\frac{1}{2}\frac{d^2\overline{C}_{ijkl}}{dD^2}\varepsilon_{ij}\,\varepsilon_{kl} + \frac{\partial F_c}{\partial D}} + \frac{\frac{dF_c}{d\sigma_{max}}d\sigma_{max}}{\frac{1}{2}\frac{d^2\overline{C}_{ijkl}}{dD^2}\varepsilon_{ij}\,\varepsilon_{kl} + \frac{\partial F_c}{\partial D}} \tag{5}$$

In this instance , ε_{ij} is the mechanical strain, and $\overline{C}_{ijkl}(D)$ is the composite stiffness tensor that is a function of D. F_c is the damage threshold function that obeys the damage criterion (Equation 6):

$$f = F(\varepsilon_{ij}, D) - F_c(D, N, \sigma_{max}, R, \omega) \le 0 \tag{6}$$

F_c is a function of the key cyclic loading parameters in addition to the damage variable. These parameters are the number of cycles *N*, the maximum stress within a cycle σ_{max}, the ratio of the minimum-to-maximum stresses R (= $\sigma_{max}/\sigma_{max}$), and the frequency . F_c can be identified using the quasi-static loading data for microcrack volume fraction versus applied stress and microcrack volume fraction versus number of cycles for given cyclic loading conditions. Damage can evolve according to Equation (5) until a critical state characterized by D = D_{cr}. D_{cr} represents the critical value of D at which the composite fails due to fatigue.

The fatigue damage model was implemented in ABAQUS via EMTA-NLA. It has been validated for the DuPont glass-fiber/PA6,6 material having 50% fiber weight fraction.

Figure 3 shows the predicted evolutions of the flow-direction modulus, E_{11}, with the number of cycles for different values of σ_{11}^{max}. The predictions for R = 0.1, $\omega = 3$ Hertz, and σ_{11}^{max}=0.3UTS, 0.4UTS, and 0.5UTS (where UTS is the ultimate tensile stress) agree with the experimental results also presented in Figure 3. Figure 4 presents the evolution of σ_{11}^{max} with the number of cycles to failure (S-N curve) for the studied material. The predictions also agree with the experimental data shown on the same figure.

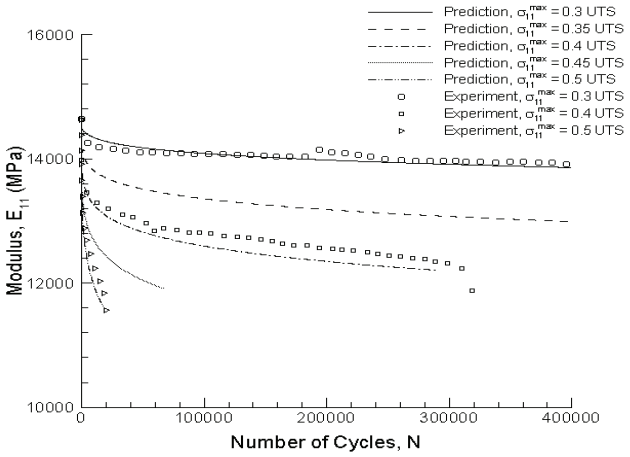

Figure 3. Flow-Direction Modulus E_{11} of 50% Weight Fraction of Glass-Fiber/PA6,6 vs. Number of Cycles for Different σ_{11}^{max}

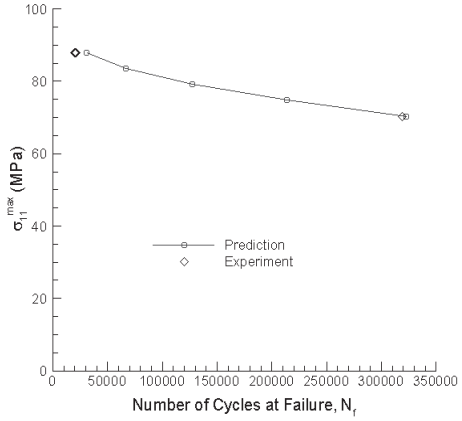

Figure 4. Evolution of σ_{11}^{max} with the Number of Cycles at Failure (S-N curve) for the Studied Glass-Fiber/PA6,6

An Impact Damage Model for LFTs

The Nguyen-Kunc elastic-plastic damage model developed last year for LFTs subjected quasi-static loading [7-8] has been extended to predict damage accumulations leading to failure of these materials under impact loading [3]. This model accounts for the elastic-plastic damage behavior of the matrix material described by the modified Ramberg-Osgood relation:

$$\bar{\varepsilon}_{\mathrm{m}} = \frac{\bar{\sigma}_{\mathrm{m}}}{E_{\mathrm{m}}(1-D)} + \frac{\sigma_0}{E_{\mathrm{m}}}\left(\frac{\bar{\sigma}_{\mathrm{m}}}{\sigma_0(1-D)}\right)^n \tag{7}$$

where $\bar{\varepsilon}_{\mathrm{m}}$, $\bar{\sigma}_{\mathrm{m}}$, E_{m}, σ_0, and n are the matrix equivalent strain, equivalent stress, elastic modulus, reference stress, and power-law exponent, respectively. D is the damage variable describing matrix cracking. Next, using the deformation theory of plasticity, an evolution law for D is sought in terms of stress and plastic strain quantities. To this end, the Lemaitre-Chaboche three-dimensional damage model in deformation for isotropic hardening materials is used [8]:

$$\dot{D} = \frac{D_{\mathrm{c}}}{\bar{\varepsilon}_{\mathrm{m}}^{\mathrm{R}} - \bar{\varepsilon}_{\mathrm{m}}^{\mathrm{D}}}\left[\frac{2}{3}(1+\nu_{\mathrm{m}}) + 3(1-2\nu_{\mathrm{m}})\left(\frac{\sigma_{\mathrm{m}}^{\mathrm{h}}}{\bar{\sigma}_{\mathrm{m}}}\right)^2\right]\dot{\bar{\varepsilon}}_{\mathrm{m}}^{\mathrm{p}} \tag{8}$$

D_c is the value of the damage variable at rupture and $\bar{\varepsilon}_m^D$ and $\bar{\varepsilon}_m^R$ are the matrix equivalent plastic strains at damage threshold and rupture, respectively. σ_m^h is the matrix hydrostatic stress, and V_m is matrix Poisson's ratio. $\dot{\bar{\varepsilon}}_m^p$ is the matrix equivalent plastic strain rate that captures the effect of impact loading on the deformation state. The composite stress/strain response is obtained using an incremental EMT procedure that provides the relationship between the overall effective stress ($(\Delta\tilde{\sigma}_{ij})$) and strain increments ($\Delta\varepsilon_{ij}$) for the composite:

$$\Delta\tilde{\sigma}_{ij} = \overline{H}_{ijkl}\Delta\varepsilon_{kl} \tag{9}$$

where the composite tangent stiffness tensor $\overline{H}_{ijkl}$ is affected by both plasticity and damage of the matrix material.

In the incremental EMT procedure, fiber/matrix debonding is captured by a parameter that controls fiber/matrix interfaces.

Damage evolves according to Equation (8) up to a critical state ($D=D_c$) at which total failure occurs. Total failure leading to initiation and propagation of a macroscopic crack is captured by a vanishing element technique.

The present model has been implemented in ABAQUS via the user-subroutines. These user subroutines are part of EMTA-NLA that is embedded in the subroutine VUMAT of ABAQUS for dynamic analysis using an explicit formulation.

Testing for glass-fiber/PA6,6 plaques subjected to impact loading was performed at Oak Ridge National Laboratory (ORNL). Figure 5 shows the damage analysis by EMTA-NLA/ABAQUS using this impact damage model for a tested plaque. A circular region of the plaque was analyzed with boundary conditions reflecting the actual fixture. A constant velocity of 254 mm per second (mm/sec) was prescribed to the impactor. Damage accumulation leads to crack initiation and propagation in the flow and cross-flow directions (Figure 6) as observed in the experiments (see Figure 12).

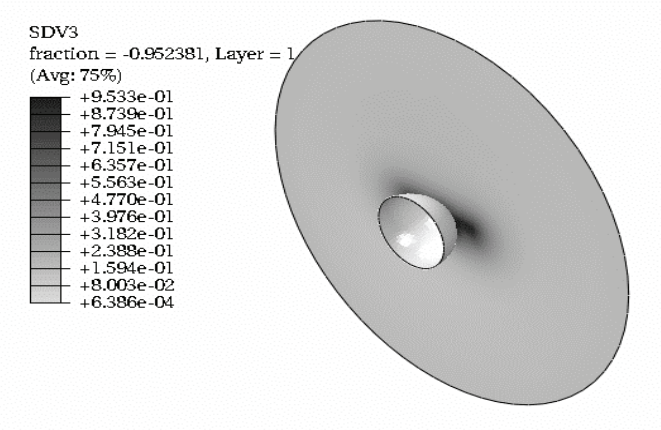

Figure 5. Predicted Damage Accumulation in a Glass-Fiber/PA6,6 Plaque After Impact

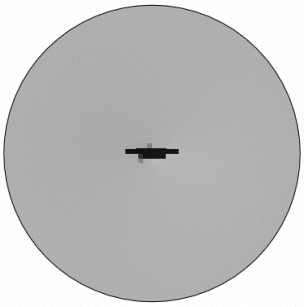

Figure 6. Predicted Crack Propagation Patterns During Impact Loading of the Glass-Fiber/PA6,6 Plaque

Fiber Length Distribution Measurement for Glass/PA6,6 Samples

Fiber attrition was examined in end-gated 305 mm square glass-fiber/PA6,6 plaques of 2.78 mm and 5.85 mm thickness. Fiber weight fractions of 34% and 50% were considered. Fiber weight fraction of 34% is equivalent to the fiber volume fraction of approximately 20% examined in previous molding trials and was obtained by blending 50% glass-fiber/PA6,6 pellets with the neat PA6,6 pellets.

Measurements were performed at three locations in the mold cavity along the centerline to compare fiber length distribution near the gate, at the middle of the plaque and at the end of the plaque. A previously developed procedure [10] was used to obtain average fiber length distributions. Figure 7 shows an example of measurements for 5.85-mm thick sample molded with 34% glass fiber weight fraction. It can be observed from the measurements that the FLD does not change significantly as a function of the spatial position in the mold. In fact, FLD does not change significantly as a function of fiber volume fraction or plaque thickness for these samples as illustrated in Figure 8. Figure 8 compares measurements performed at centers of plaques for previously indicated material and thickness combinations. Comparison for these measurements would indicate that samples molded with greater fiber volume fraction contain a greater amount of short fragments. While this observation is supported by a number of measurements and prior knowledge, inherent errors in measurement should be kept in mind before drawing conclusions from small differences in FLDs at the extreme short end of FLD measurements.

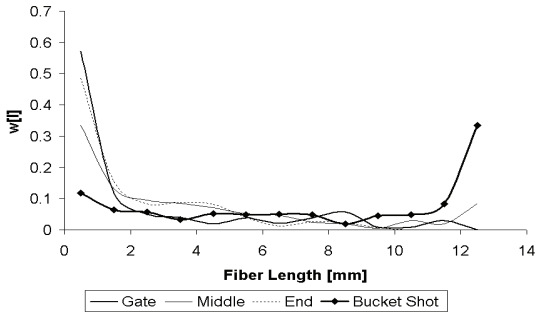

Figure 7. Fiber Length Distribution for 5.85 mm Thick Glass-Fiber/PA6,6 Samples with 34% Fiber Weight Fraction

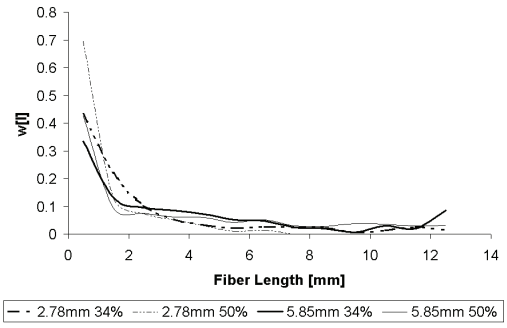

Figure 8. Fiber Length Distribution for 2.78-mm and 5.85-mm Thick Plaques Molded with 34% and 50% Weight Fraction Glass-Fiber/PA6,6 Measured at the Plaque Center

Figure 7 contains a measurement for a “bucket shot” for comparison with in-mold measurements. Bucket shot material is obtained by removing the mold from the injection molding machine and collecting material directly from the nozzle without introducing a restriction.

Creep and Fatigue Tests for Glass-Fiber/PA6,6 Samples

Previously reported quasi-static testing of glass-fiber/PA6,6 material was performed on 25.4-mm wide samples. The results were subsequently compared to a small set of quasi-static tests on 12.5-mm wide samples manufactured based on the D638 Type 1 specimen standard [11]. The differences in test results were insignificant. Samples 12.5-mm wide were used for all long-term tests to allow for greater number of replicates, as well as easier access to appropriate test equipment.

After cutting and routing specimens in the flow and cross-flow directions, the specimens were dried in a vacuum oven. Samples were then removed from vacuum and exposed to laboratory air several minutes before the start of each test.

Creep tests were conducted in a servo-hydraulic machine at 20%, 30%, and 40% of the ultimate tensile strength. Samples were loaded at a given load rate to the desired load level and held at this load level for 12 hours. Subsequently, the sample was ramped to zero load at a constant load rate and held at zero load for 12 hours.

Tension-tension (R=1) fatigue tests were performed at various load levels on previously described samples. In the flow direction and dry condition, 50% glass-fiber/PA6,6 specimens were loaded between 30% and 50% UTS. At 30% UTS, the specimens did not fail before reaching one million cycles, while short fatigue life was observed for samples loaded above 50% UTS. Tests were performed with 3 Hertz (Hz) frequency with periodic stiffness checks at 1 Hz frequency.

Changes in stiffness of samples indicating damage were monitored and recorded as a function of the number of cycles. Modulus reduction during fatigue tests performed at 50% UTS for 50% glass/PA6,6 samples in the flow direction is shown in Figure 9. Typical rapid stiffness degradation at the beginning of the loading followed by a plateau and brief degradation just prior to failure can be seen in the data. Environment control proved to be critical for longer-term tests as temperature changes may influence test results.

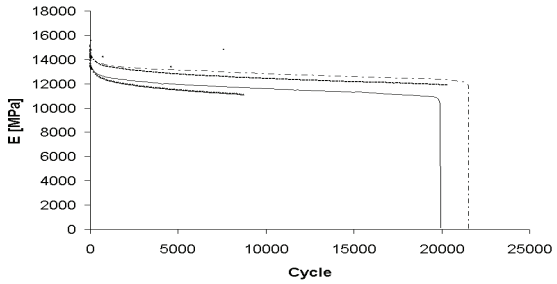

Figure 9. Reduction of the Flow Direction Modulus of 50% Weight Fraction of Glass-Fiber/PA6,6 Samples During Fatigue Tests Performed at 50% UTS

Multi-Axial Impact Tests

Multi-axial impact tests were performed on the glass-fiber/PA6,6 material. Specimens containing 40% of glass with thickness 2.78 mm and 5.85 mm were tested with impact occurring in the middle of a 152 mm by 152 mm specimen. Previous fiber orientation distribution, fiber length distribution, and mechanical property measurements were performed at the impact location. Samples were strain gauged in the flow and cross-flow directions. Tests were first performed in a smaller machine that achieved speeds of 0.25 meters per second (m/s). The test setup shown in Figure 10 was subsequently moved to the Testing Machine for Automotive Crashworthiness, and tests up to 5 m/s were performed.

Figure 11 shows typical failure of 2.78-mm thick plaque with fractures following flow and cross-flow directions.

Figure 10. Multi-Axial Test Setup with Impactor (visible at the bottom of the image and specimen in the circular opening of the fixture)

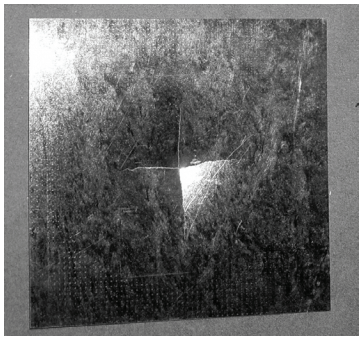

Figure 11. Typical Failure of 2.78 mm Thick Plaque in Multi-Axial Impact Test (fractures following flow and cross-flow directions)

Molding and Testing of Glass/PP Samples

A set of 310 mm by 270 mm plaques was molded with 30% glass-fiber/PP STAMAX material by SABIC-Europe. Mold type, molding conditions, instrumentation and material requirements, and test plans were considered in consultation with the steering committee members and all parties involved in the project. The complete plan is to mold two types of plaques at 2-mm, 3-mm, and 4-mm thickness with 20%, 30%, and 40% glass-fiber weight fraction. Two conditions for fill time and back pressure will be examined. Additionally, neat resin plaques, short shots, and bucket shots will be obtained during future molding.

Three replicate samples were X-rayed for each condition to establish general nature of fiber dispersion and fiber orientation. Samples molded with a low back pressure contained some incompletely dispersed bundles, and the flow pattern was clearly visible. Samples molded with high back pressure appear to be completely dispersed. These observations correspond to fiber length distribution measurements. Samples molded with low back pressure contain longer fibers. Figure 12 shows wider core region for samples molded with low back pressure.

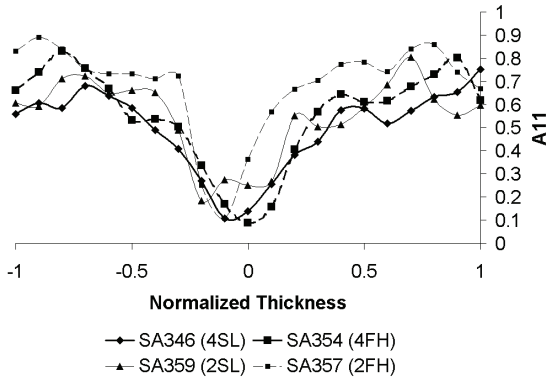

Figure 12. A11 Orientation Component for Glass-Fiber/PP plaques (Legend: 2,4–thickness in mm; S,F–slow or fast fill speed; L,H–low or high back pressure)

This is consistent with the fiber length measurement, as well as subsequent mechanical property measurement. Orientation was measured for three samples along the flow centerline for every plaque type.

Quasi-static stress/strain response was obtained for five replicates of each plaque type in flow and cross-flow directions. Samples molded with high back pressure were stronger and stiffer in the flow direction, while the stiffness and strength of samples molded with low back pressure were approximately equal in flow and cross-flow direction. This is consistent with fiber length and orientation observations. Creep and fatigue tests were also performed for model validation.

Conclusions

In FY 2009, activities included: i) the completion of the development of a fiber length attrition model for injection-molded LFTs; ii) development of the a fatigue damage model for LFTs and its implementation in ABAQUS; iii) development of an impact damage model for LFTs and its implementation in ABAQUS; iv) development of characterization methods for fatigue testing; v) characterization of creep and fatigue responses of glass-fiber/PA6,6 and glass-fiber/PP; vi) characterization of fiber length distribution along the flow length of glass/PA6,6 and glass-fiber/PP; and vii) characterization of impact responses of glass-fiber/PA6,6.

The fiber length attrition model accurately captures the fiber length distribution along the flow length of the studied glass-fiber/PP material. The fatigue damage model is able to predict the S-N and stiffness reduction data, which are valuable to the fatigue design of LFTs. The impact damage model correctly captures damage accumulation observed in experiments of glass-fiber/PA6,6 plaques.

Further work includes validations of these models for representative LFT materials and a complex LFT part.

References

1. Phelps JH and CL Tucker III. 2009. "Processing-Microstructure Modeling for Long-Fiber Thermoplastics." Internal Report submitted to PNNL.

2. Nguyen BN, V Kunc, and SK Bapanapalli. 2009. "Modeling Fatigue Damage in Long-Fiber Thermoplastics." In Proceedings of the 24th Annual Technical Conference of The American Society for Composites, eds. JW Gillespie and SV Hoa. DEStech Publications, Lancaster, Pennsylvania.

3. Bapanapalli SK, BN Nguyen, and V Kunc. 2009. "Modeling of Low Velocity Impact Damage in Injection-Molded Long Fiber Composites." In Proceedings of 24th Annual Technical Conference of The American Society for Composites, eds. JW Gillespie and SV Hoa. DEStech Publications, Lancaster, Pennsylvania.

4. Dinh SM and RC Armstrong. 1984. "A Rheological Equation of State for Semi-Concentrated Fiber Suspensions." Journal of Rheology 28(3):207-227.

5. Hitchen SA and SL Ogin. 1993. "Matrix Cracking and Modulus Reduction during the Fatigue of an Injection-Molded Glass/Nylon Composite." Composites Science and Technology 47:239-244.

6. Noda K, A Takahara, and T Kajiyama. 2001. "Fatigue Failure Mechanisms of Short Glass-Fiber Reinforced Nylon 66 Based on Nonlinear Dynamic Viscoelastic Measurement." Polymer 42:5803-5811.

7. Nguyen BN and V Kunc. 2009. "An Elastic-Plastic Damage Model for Long-Fiber Thermoplastics." International Journal of Damage Mechanics (published online).

8. Nguyen BN, V Kunc, SK Bapanapalli, JH Phelps, and CL Tucker III. 2009. "Damage Modeling of Injection-Molded Short- and Long-Fiber Thermoplastics." In Proceedings of the 9th Annual SPE Automotive Composites Conference & Exhibition, Society of Plastics Engineers.

9. Lemaitre J and JL Chaboche. 1985. "Mécanique des Matériaux Solides." Dunod, Paris.

10. Kunc V, B Frame, BN Nguyen, CL Tucker III, and G Velez-Garcia. 2007. "Fiber Length Distribution Measurement for Long Glass and Carbon Fiber Reinforce Injection Molded Thermoplastics." Proceedings of SPE-ACCE. [11] ASTM D638-03. 2003. Standard Test Method for Tensile Properties of Plastics. American Society for Testing and Materials, Philadelphia.

Presentations/Publications/Patents

1. Nguyen BN, V Kunc, JH Phelps, CL Tucker III, and SK Bapanapalli. 2009. "Prediction of the Elastic-Plastic Stress-Strain Response for Injection-Molded Long-Fiber Thermoplastics." Journal Composite Materials 34:217-246.
2. See Ref. 2
3. See Ref. 3
4. See Ref. 7
5. See Ref. 8

K. Simulating Molding Processes of Thermoplastics Reinforced with Long Fibers

Principal Investigator: Donald G. Baird
Virginia Polytechnic Institute and State University
Department of Chemical Engineering
Blacksburg, VA 24061
(540) 231-5998; email: dbaird@vt.edu

Co-Principal Investigator: Peter Wapperom
Virginia Polytechnic Institute and State University
Department of Mathematics
Blacksburg, VA 24061
(540) 231-7252 ; email: pwapperom@math.vt.edu

Participants: Kevin C. Ortman, PhD. student, email: kco3@vt.edu
Kevin J. Meyer, PhD. student, email: kjmeyer@vt.edu
Neeraj Agarwahl, MS student (completed degree 8/10/09)

Contractor: Virginia Polytechnic Institute and State University
Contract No.: DMI-052918

Objective

- Improve the accuracy of the simulation of long (flexible) fiber orientation in thermoplastics during molding processes by using theory that incorporates fiber flexibility in combination with state-of-the-art numerical techniques.
- Establish a method (independent of the molding process) for determining a unique set of material parameters that are based on the transient shear rheological behavior of the composite fluid.
- Evaluate the accuracy of the simulation technique by comparing numerical predictions of glass fiber orientation to that found in rheometrical flows and then in molded parts (produced using basic mold geometries).

Approach

- Develop methods to conduct quantitative and reproducible rheological experiments on glass fiber filled polymeric fluids which allows one to correlate transient rheology with the evolution of fiber orientation and configuration.
- Conduct transient shear and extensional rheological studies on glass fiber-filled polypropylene (PP) systems in which fibers of various lengths (4-13 mm, diameter: 12.5 microns) and concentrations (10%, 30%, 50% wt.) are used to assess the effects of both fiber length and the viscoelastic nature of the matrix on the transient rheology.
- Experimentally characterize the relationship between the rheological behavior and the associated fiber microstructure.
- Identify the limitations of current approaches to predict the evolution of fiber orientation by comparing model predictions to experimental observations.

- Modify current theories for long fiber orientation and configuration to address these limitations.
- Define and evaluate specific rheological tests to determine the material parameters in the stress tensor which are unique and give consistent results when used in numerical simulations.
- Develop a finite element method simulation program capable of predicting fiber orientation of thermoplastic composite fluids containing long glass fibers in molding processes.
- Assess the performance of the simulation by comparing predicted fiber orientation against values determined experimentally from molded samples.

Accomplishments

- Rheological Characterization Technique: A fully functional sliding plate rheometer[1] incorporating a shear stress transducer has been designed and fabricated for the purpose of performing unbiased and reproducible steady shear rheological experiments on long glass fiber-filled polymeric fluids that are otherwise impossible to perform on rotational rheometers. Using this equipment, the rheological behavior of various fiber systems has already been analyzed. In addition to rheological studies, the rheometer has been used in tracking the transient evolution of long fiber orientation upon startup and cessation of shear flow.
- Fiber Orientation Measurements: A method[4] that uses optical microscopy was developed for acquiring orientation measurements. With this technique, we have initiated the characterization of fiber orientation in both rheometrical flows and complex flow geometries.
- Modeling: Various approaches to modeling flexible fibers have been investigated. These approaches include exploring an orientation model resulting from bead-rod theory, tracking individual fibers using Hinch's infinitely flexible fiber theory, and extending Hinch's equations for concentrated polymer solutions through the concept of mobility. The choice of approach is still not determined but will be the emphasis of future research.
- Simulations: The formulation of a finite element simulation package using a bead-rod orientation model is being written to simulate molding processes (such as compression molding and injection molding processes). Additionally, a program capable of utilizing an extension of Hinch's equation for concentrated polymer melts, through the use of a mobility tensor, has also begun.
- Molding Processes: Preliminary orientation visualization experiments have been completed for both injection molded samples and compression molded samples. Accurate orientation predictions of such molding processes continue to be the focus of this research.

Future Direction

- Focus our attention on characterizing the transient rheological behavior of long glass fiber suspensions using the sliding plate rheometer, and begin looking into the possibility of studying the rheology of these suspensions in a complex flow such as squeeze flow.
- Use the sliding plate rheometer to gain an understanding of long fiber orientation development in simple shear experiments.
- Use the sliding plate rheometer to gain an understanding of fiber mobility in concentrated fiber suspensions and to assess the performance of Hinch's equation and its extensions.
- Assess the performance of the bead-rod model with various long fiber lengths by comparing model predictions to fiber orientation obtained in molded parts (both injection molded and compression molded).

- Use modeling parameters determined from sliding plate experiments to predict the orientation evolution in molding processes.

Introduction

The overall goal of our research is to be able to accurately predict the orientation of long fibers suspended in polymer melts generated during molding processes using a finite element analysis. To accomplish this goal we first have to establish a model capable of predicting both the stress response to deformation of a composite fluid and the associated microstructure. As will be discussed, our approach to accomplish this goal begins with comparing model predictions to both the rheological behavior and experimentally determined microstructure in the startup of simple shear flow experiments. Furthermore, unique material parameters for a specific composite fluid are established by fitting to these rheological measurements. Once established, the stress tensor will be used with unique model parameters coupled with the equations of motion to then be implemented into a finite element code designed to simulate complex flow simulations associated with molding processes (ie. injection molding and compression molding).

We will highlight our advancements in the following order. First, we will discuss a unique method to accurately quantify the transient rheological behavior of long glass fiber-filled composite fluids and show some preliminary results. After this, we will discuss current theories used for the dynamic simulation of long/flexible fibers. Lastly, we will show some preliminary results obtained from orientation visualization experiments for the startup and cessation of simple shear flow and from compression molding.

Sliding Plate Rheometer (Characterization of Long Fiber Composite Fluids)

After numerous attempts at characterizing suspensions containing long glass fibers, we concluded that the conventional melt rotational rheometers were inadequate. These problems were found to be due to curvilinear streamlines and insufficient rheometer gap size. As a result, we initiated the design and fabrication of a sliding plate rheometer incorporating a wall shear stress transducer (Figure 1) with the primary purpose of being able to perform unbiased and reproducible steady shear rheological experiments on long glass fiber-filled polymeric fluids that are otherwise impossible to perform on rotational rheometers. The sliding plate rheometer imposes a rectilinear velocity field (Equation 1) and thus a homogenous shear field, where $\dot{\gamma}$ is the shear rate, and y is the vertical distance from the stationary plate.

$$v_x(y) = \dot{\gamma}\, y \quad (1)$$

After completion, the device was calibrated, and its behavior was verified. A viscosity standard and a commercial polymer, Equistar Petrothene NA 952, a LDPE with no processing aids or antiblock agents, were both used as reference materials to assess the performance of the sliding-plate device.

Localized shear stress measurement and a homogenous shear field with rectilinear streamlines are two key improvements the sliding plate rheometer offers over rotational rheometers. While localized stress measurement eliminates the problems arising due to edge effect, the homogenous shear field insures removal of unrealistic transient behavior. Moreover, theoretically it has no restriction on the gap size. Though the main purpose of sliding plate rheometer is to perform rheological measurements on long glass fiber composites, it will also be used in tracking the transient evolution of long fiber orientation upon startup and cessation of shear flow.

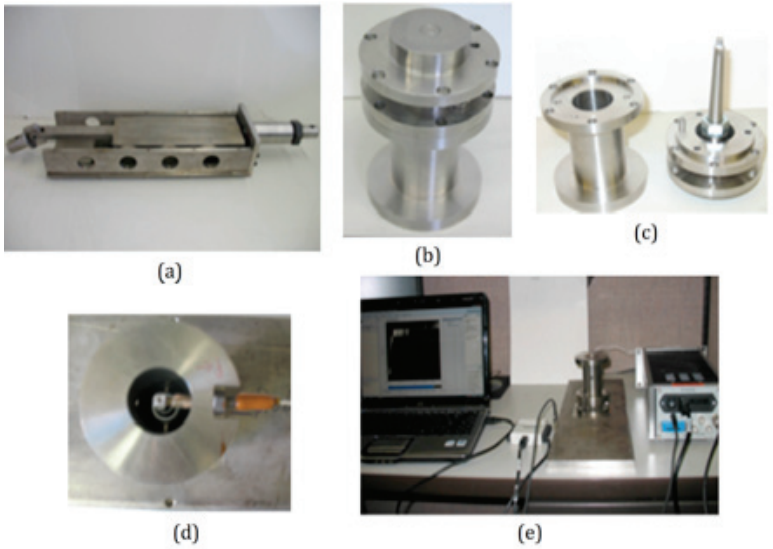

Figure 1. Sliding plate rheometer. (a) Sliding plate, (b) wall shear stress transducer, (c) disassembled shear stress transducer showing rigid beam, (d) shear stress transducer with capacitance probe, (e) complete assembly with all electrical components.

The rheological experiments conducted so far suggest that the transient viscosity is very sensitive to characteristics such as fiber concentration, initial orientation, and shear rate. For example, in (Figure 2) one can see that the magnitude of the shear rate greatly affects the magnitude of the stress overshoot. As the shear rate is increased, the stress overshoots decreases. This is indicative of a behavior known as fiber-fiber flocculation, whose effects are reported to be more easily disrupted with higher shearing force[2]. Such phenomena are unique to long fiber systems.

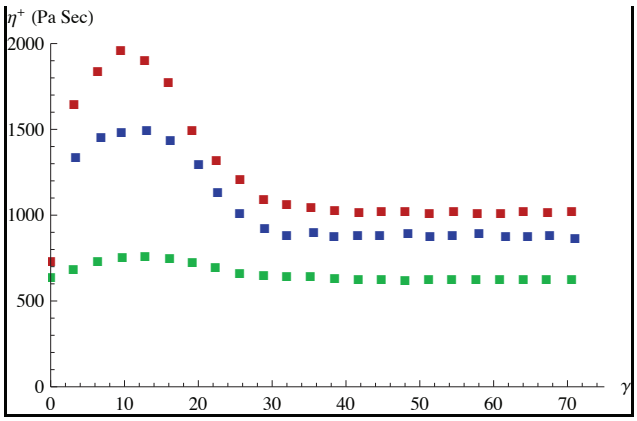

Figure 2. Experimentally measured transient viscosity vs. strain for 10% wt. (avg. length 4mm) long glass fibers initially oriented randomly in the shear plane, at various shear rates [■=0.4 sec-1, ■=1.0 sec-1, ■=4.0 sec^{-1}]

Transient rheology data of long fiber systems have not been published, to our knowledge, and presents itself an opportunity for a significant contribution. A full characterization of various fiber lengths, concentrations, initial fiber orientations, etc., is still being analyzed.

Theory: Model Development

An approach to modeling long/flexible fiber systems is to simulate the dynamic behavior of individual fibers. This can be done in various ways but the most “straight forward” approach is to begin with the theoretical work of Hinch[11] for an infinitely flexible fiber. In this theoretical development, the tension forces within the thread, T, are set equal to the viscous forces acting

on the thread. As a result, two equations are formed, one describing T at discretized points along the thread, Equation (2), and one defining the time rate of change of the nodal points as a function of T, Equation (3).

$$\frac{\partial^2 T}{\partial s^2} - \frac{1}{2}\left(\frac{\partial^2 \mathbf{x}}{\partial s^2}\right)\cdot\left(\frac{\partial^2 \mathbf{x}}{\partial s^2}\right)T = -\frac{\partial \mathbf{x}}{\partial s}\cdot\frac{\partial \mathbf{v}(\mathbf{x},t)}{\partial s} \tag{2}$$

$$\frac{\partial \mathbf{x}}{\partial t} = \mathbf{v}(\mathbf{x},t) + \frac{\partial T}{\partial s}\frac{\partial \mathbf{x}}{\partial s} + \frac{1}{2}T\frac{\partial^2 \mathbf{x}}{\partial s^2} \tag{3}$$

In Equations (2) and (3), s is the arc length, v is the velocity field, and x is the position vector. Given an initial fiber orientation, one can solve Equations (2) and (3) for the time rate of change of the fiber configuration. Model predictions for simple shear flow can be seen in Figure (3). The 'red' fiber relates to the initial fiber orientation and the 'blue' fibers show the evolution of orientation with a localized center of mass. This model predicts that, in simple flow, the fiber

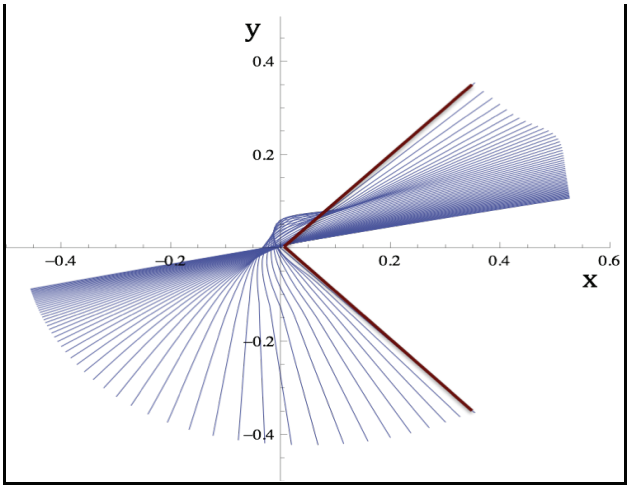

straightens and aligns itself with the flow direction.

Figure 3. Model predictions for the Hinch infinitely flexible fiber in simple shear flow (v_x = 1.0 y). Red fiber indicates the specified initial orientation and blue fibers indicate the orientation evolution with increasing strain.

Goddard and Huang[12] extended the work of Hinch, who described the motion of an individual perfectly flexible fiber in a dilute suspension, to concentrated suspensions by allowing the viscous drag to be represented by a mobility tensor. In the following Equations (4, 5), κ_T is the transverse mobility tensor while κ_L and κ_N are the lateral and normal components of the mobility tensor, respectively, and v is the velocity flow field. The system of equations is solved for the tension (T) and position vector (x) along the fiber arc length (s) in the following equations.

$$— - K_L\frac{\partial T}{\partial s}\frac{\partial \mathbf{x}}{\partial s} = T\mathbf{K}_T\cdot\frac{\partial^2 \mathbf{x}}{\partial s^2} + \mathbf{v}(\mathbf{x},t) \tag{4}$$

$$\frac{\partial}{\partial s}\left(K_L\frac{\partial T}{\partial s}\right) - \left(\frac{\partial^2 \mathbf{x}}{\partial s^2}\right)\cdot\left(\frac{\partial^2 \mathbf{x}}{\partial s^2}\right)K_N T = -\frac{\partial \mathbf{x}}{\partial s}\cdot\frac{\partial \mathbf{v}(\mathbf{x},t)}{\partial s} \tag{5}$$

The mobility tensor provides insight into the kinematic restrictions of a fiber caused by the presence of its neighbors. This restricted motion affects the orientation development of the fibers. Therefore, our future work will be to assess these equations and their ability to predict fiber orientation and configuration during flow.

Lastly, an orientation model that has been presented as a first approximation to capture the flexibility of long fibers in a dilute suspension is one suggested by Strautins and Latz[6]. Similar to the treatment of Jeffrey's Equation for a rigid rod, Strautins and Latz determine the evolution equations for two rigid rods (each rod of length l_B) connected by a joint. The joint and spring allow the two rigid rods to bend and exhibit flexibility as shown in (Figure 4) below.

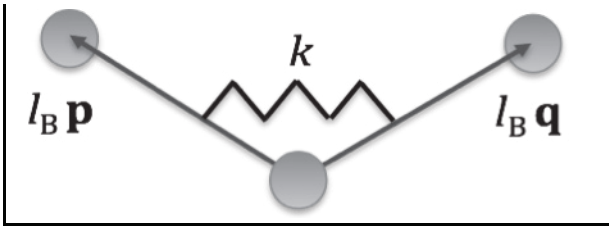

Figure 4. Bead-Rod model consists of two rigid rods connected to a pivoting bead.

In this figure, p and q are unit vectors associated with each of the rods of the flexible fiber. This is analogous to the u vector found in rigid fiber theory. However, for the case of a Bead-Rod fiber, there exists to two rigid rods, each with an orientation dictated by either p or q. The spring gives the modeled fiber a flexibility to which it resists bending (spring stiffness coefficient k). The beads, on the other hand, provide surface area for hydrodynamic drag to be exhibited on the fiber. This model is used in the formulation of a continuum model that describes the motion of fibers that can bend about its center of mass. In the treatment provided by Strautins and Latz, they allow their model to explore small bending angles.

$$= \int\int \mathbf{pp}\ \psi(\mathbf{p},\mathbf{q},t)d\mathbf{p}d\mathbf{q} \tag{6}$$

$$\mathbf{B} = \int\int \mathbf{pq}\ \psi(\mathbf{p},\mathbf{q},t)d\mathbf{p}d\mathbf{q} \tag{7}$$

$$\mathbf{C} = \int \mathbf{p}\,\psi(\mathbf{p},\mathbf{q},t)\,d\mathbf{p} \tag{8}$$

Two orientation tensors and one orientation vector exist within this model. One orientation tensor, similar to what exists in rigid rod theory, describes the second moment of any one of the rods with respect to the orientation distribution function (Equation 6). Another orientation tensor describes the mixed product of both rigid rod vectors with the orientation disturbing function (Equation 7). Lastly, the first moment of the distribution function, using either rod's orientation vector (Equation 8), is also formed. The equations that describe how a given flow field affects the orientation functions are given in the following equations:

$$\frac{D\mathbf{A}}{Dt} = (\mathbf{W}\cdot\mathbf{A} - \mathbf{A}\cdot\mathbf{W}) + (\mathbf{D}\cdot\mathbf{A} + \mathbf{A}\cdot\mathbf{D} - (2\mathbf{D}:\mathbf{A})\mathbf{A}) + \\ \ldots\frac{l_B}{2}[\mathbf{Cm} + \mathbf{mC} - 2(\mathbf{m}\cdot\mathbf{C})\mathbf{A}] - 2k[\mathbf{B} - \mathbf{A}\ \mathrm{tr}(\mathbf{B})] \tag{9}$$

$$\frac{D\mathbf{B}}{Dt} = (\mathbf{W}\cdot\mathbf{B} - \mathbf{B}\cdot\mathbf{W}) + (\mathbf{D}\cdot\mathbf{B} + \mathbf{B}\cdot\mathbf{D} - (2\mathbf{D}:\mathbf{A})\mathbf{B}) + \\ \ldots\frac{l_B}{2}[\mathbf{Cm} + \mathbf{mC} - 2(\mathbf{m}\cdot\mathbf{C})\mathbf{B}] - 2k[\mathbf{A} - \mathbf{B}\ \mathrm{tr}(\mathbf{B})] \tag{10}$$

$$\frac{D\mathbf{C}}{Dt} = \nabla \boldsymbol{v}^t \cdot \mathbf{C} - (\mathbf{A} : \nabla \boldsymbol{v}^t)\mathbf{C} + \frac{l_B}{2}[\mathbf{m} - \mathbf{C}(\mathbf{m} \cdot \mathbf{C})] - k\mathbf{C}[1 - \mathrm{tr}(\mathbf{B})] \tag{11}$$

$$m_i = \frac{\partial^2 v_i}{\partial x_i \partial x_k} A_{jk} \tag{12}$$

Within these equations D/Dt is the substantial time derivative, $\nabla v = \partial_{vj}/\partial_{xi}$ is the velocity gradient, W = [(∇v) t -∇v]/2 is the vorticity, D = [∇v + (∇v)^t]/2 is the rate of strain tensor, and tr() represents the trace of a specified tensor. In this model, m is a vector formed whose i-th component is found by the summation over the indicies j, k in Equation 12. One interesting consequence of fiber flexibility is that it can retard the rate of orientation of the end-to-end orientation vector, R. This effect is compared with the predictions of Folgar-Tucker[1,2,3] model in sliding plate flow of long glass fibers at 10% wt. in polypropylene with an initial random in-plane orientation (Figures 5 and 6).

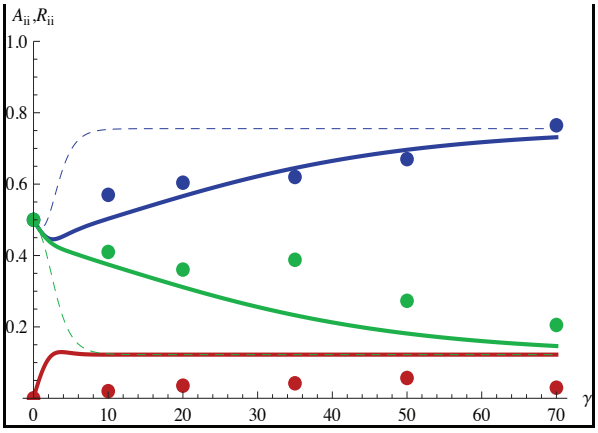

Figure 5. Flexibility retards orientation evolution. Experimentally determined data and model predictions for the orientation evolution of the trace components of the orientation tensor (A_{ij} for Folgar-Tucker and Data, and Rii for the Bead Rod model) versus strain at a shear rate of 1.0 sec^{-1}. System is 10% wt. glass fibers initially random in the shear plane. C_I =0.038, k =0.012. [Data=Points, FT=Dashed, BR=Solid, ●=A_{11},R_{11}, ●=A_{22},R_{22}, ●=A_{33},R_{33}]

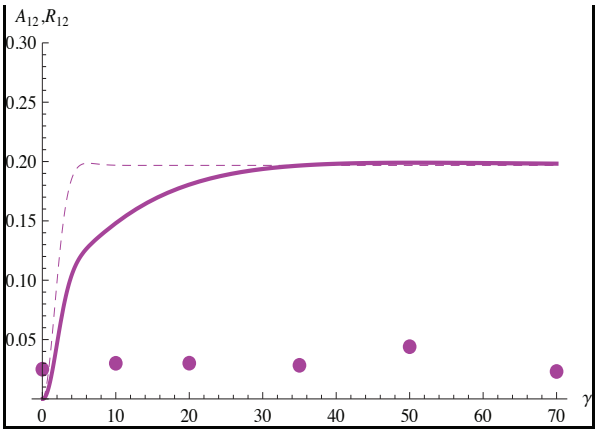

Figure 6. Flexibility retards orientation evolution. Experimentally determined data and model predictions for the orientation evolution of the 1-2 component of the orientation tensor (A_{12} for Folgar-Tucker and Data, and R_{12} for the Bead Rod model) versus strain at a shear rate of 1.0 sec^{-1}. System is 10% wt. glass fibers initially random in shear plane. C^I =0.038, k =0.012. [Data=Points, FT=Dashed, BR=Solid, ●=A_{12},R_{12}]

Future Work

Our future work will center on determining how well the Bead-Rod model describes long fiber orientation. Currently, the Bead-Rod model is also being explored for the case of an injection molded center-gated disk. We have also begun looking at squeeze flow samples as well (Figure 7). We have begun looking at the orientation profile of compression molded plaques (Figure 8) donated by Oak Ridge National Laboratory (ORNL), where they are experimenting with processing combinations of injection/compression molding. Because squeeze flow possess strong elongational effects, we believe this flow field is an important one to study. It is believed that these efforts will greatly enhance our understanding of long fiber orientation and configuration evolution.

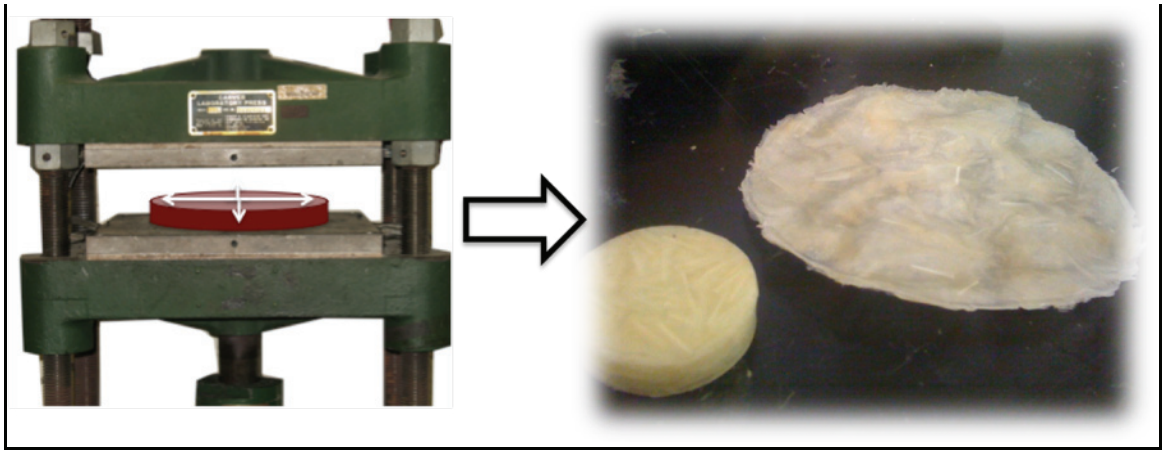

Figure 7. Figure depicting our initial methods of studying the orientation changes of a disk in squeeze flow.

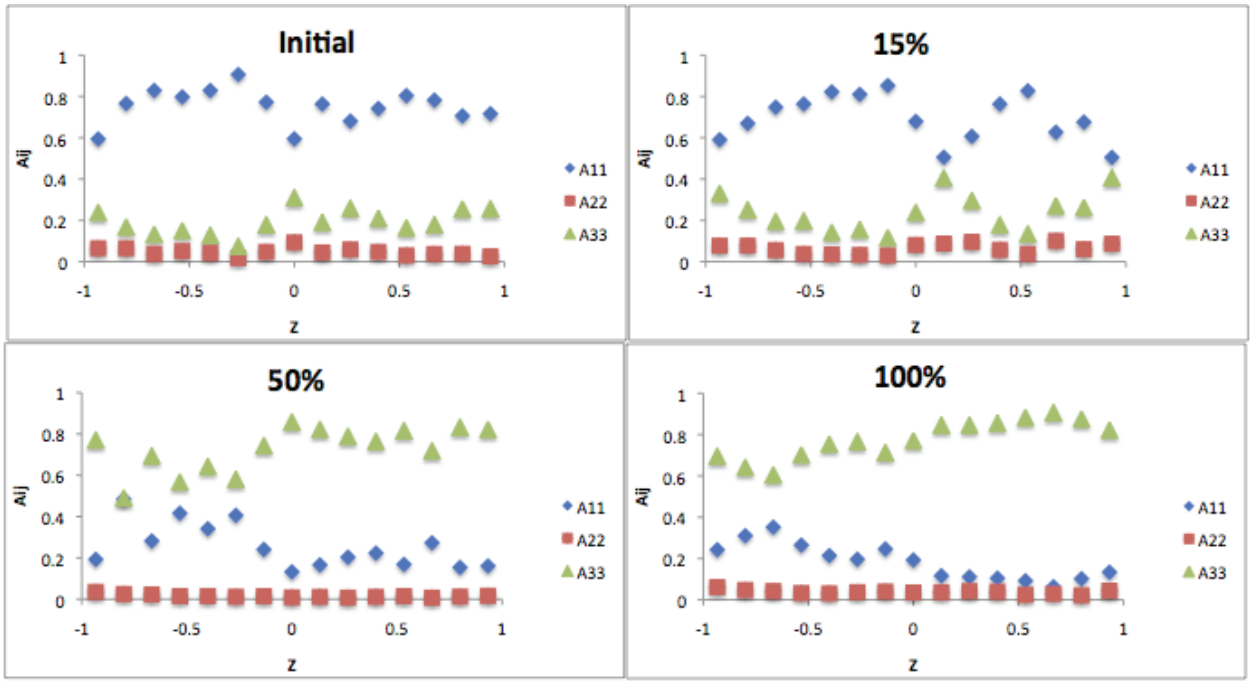

Figure 8. Orientation visualization experiments for ORNL plaques. Samples were extruded and compression molded into a square plaque (1 ft.^{2}). The orientations were measured along the length of the molded plaque starting at the center (initial) and working outwards to various length percentages, all the way to the square's edge (100%). It is seen that elongational effects become more prevalent (larger A_{33} component) nearer the square's edge (100%). '1'=length direction, '2'=width direction, '3'=thickness direction of the square plaque.

Summary

We have designed and fabricated a sliding plate rheometer primarily for the purpose of performing unbiased and reproducible rheological experiments on long glass fiber-filled polymeric fluids that are otherwise impossible to perform on rotational rheometers. It is with this device that we have also begun to understand orientation changes in simple flow. The Bead-Rod model presented within this research was shown to produce retarded orientation kinetics, a characteristic that preliminary results show to be consistent with our long fiber experiments. The Bead-Rod model is currently being assessed to see if it can correctly explain the dynamics of long fibers in complex flow. Lastly, an extension of Hinch's equation was written for tracking single fibers in concentrated polymer solutions. The use of this model in cooperation with sliding plate experiments will be used to gain further knowledge of long fiber dynamics through the use of mobility. The thrust of the future efforts will be on predicting orientation and configuration of long fibers during molding (compression and injection molding).

References

1. Advani, S.G., and Tucker EEE C.L., J. Rheol. 31, 751-84 (1987).
2. Advani S.G. and Tucker EEE C.L., J. Rheol. 34, 367-386 (1990).
3. Folgar, F. P. and Tucker III, C. L., J. Reinf. Plast. Comp. 3, 98-119 (1984).
4. Hine, P.J., Davidson, N., Duckett, R.A., Poly. Comp. 17, 720–729 (1996).
5. Bay R. S. and Tucker III, C. L., Polym Eng Sci. 32, 240-253 (1992).
6. Strautins, U. and Latz, A., Rheol. Acta. 46. 1057-1064 (2007).
7. Lipscomb, G., et al., J. Non-Newt. Fluid. Mech. 26, 297–325 (1988).
8. Kolitawong, C. and Giacomin, A.J., J. Non-Newt. Fluid. Mech. 102, 71-96 (2002).
9. Keshtkar, M., et al., J. Rheol., 2009. 53: p. 631-650.
10. Wang, J., O'Gara, J., and Tucker III, C. L., J. Rheol. 52(5), 1179-1200 (2008).
11. Hinch, E.J., J. Fluid Mech. 74, 317-333 (1976).
12. Goddard, J. D., and Huang, Y.H., J. Non-Newt. Fluid Mech. 13, 47-62 (1983).

L. Structural Nanocomposite Design of the Southern Regional Center for Lightweight Innovative Design (SRCLID)

Principal Investigator: Thomas E. Lacy
Associate Professor, Department of Aerospace Engineering,
P.O. Box A
Mississippi State University (MSU)
Mississippi State, MS 39762
(662) 325-2754; e-mail: Lacy@AE.MsState.edu

Participants: H. Toghiani, C.U. Pittman, Jr., S. Roy - University of Alabama,
S. Jeelani - Tuskegee University

Technology Area Development Manager: Dr. Carol Schutte
(202) 287-5371; e-mail:carol.schutte@ee.doe.gov

Project Manager: Magda Rivera
e-mail: magda.rivera@netl.doe.gov

Contractor: Mississippi State University
Contract No.: DE-FC-26-06NT42755

Objective

- Design of low-cost nanoreinforced composite systems for automotive structural applications.

Approach

- A multiscale design methodology is being employed to investigate the effects of nanoreinforcements on the mechanical properties of fiber-reinforced composites for automotive structural applications. This work addresses the following critical issues: selection of key combinations of continuous fibers, resin materials, and relatively low-cost nanoreinforcements (vapor grown carbon nanofibers, nanoclay particles, etc.); fabricating coupon scale samples for static and dynamic testing; and development of a multiscale materials modeling strategy for assessing high-performance nanocomposites subjected to static and dynamic loadings.

Milestone, Metrics and Accomplishments

- A full factorial experimental design/response surface methodology was employed to identify the combination of formulation and processing parameters that led to optimal nanocomposite dynamic mechanical and flexural properties, as well as to tailor the fabrication of nanocomposites accordingly. In addition, combinations of split Hopkinson pressure bar and crush tube tests were performed to investigate the high strain rate behavior and energy absorption characteristics of the structural nanocomposites.
- A synergistic multiscale modeling approach has been developed using molecular dynamics, micromechanics, and progressive failure simulations to predict the effective properties and nonlinear material response of structural nanocomposites.

Future Direction

- Response surface models will be developed to optimize nanocomposite formulations for enhanced performance under quasi-static and dynamic compression, as well as impact loading. Additional experiments will be performed to investigate the failure mechanisms at elevated strain rates.
- Continuous fiber composites with nanoreinforced resins will be fabricated. Compression, tension, and flexural tests will be performed to assess the effects of nanofibers on structural performance.
- A synergistic multiscale modeling methodology will be used to simulate the nonlinear material response and progressive failure of continuous fiber composites with nanoreinforced resins.

Introduction

The use of nanoreinforced composites in automotive structural applications is becoming increasingly attractive with improvements in nanomaterials technology (cf. Odegard et al. (2001); Ghoniem et al. (2003); Thostenson et al. (2004); Buryachenko et al. (2005); Gates et al. (2005); Odegard et al. (2005); Valavala and Odegard (2005); Hussein et al. (2006); Liu and Brinson (2006); Fisher et al. (2007)). The successful utilization of nanocomposites, however, requires a thorough understanding of the underlying chemical, physical, and mechanical aspects of the fabrication process and in-service performance. Furthermore, in order to predict the mechanical response, a multiscale design and modeling methodology is likely warranted. In this work, key aspects of nanocomposite fabrication, testing, modeling, and validation are addressed, including dispersion and interfacial adhesion of nanoreinforcements. A summary of year three accomplishments is included in the following discussion.

Determination of Composite Fiber-Matrix Systems and Nanoreinforcements

Because of their widespread use and relatively low cost, two commercially available thermoset resins (U.S. Composites, Inc. polyester and Ashland Co. vinyl ester) were selected as the primary matrix materials in this investigation (Lacy et al. (2008)); other polymer resins (e.g., epoxy and polypropylene) have also been investigated in this work (cf., Zhou et al. (2007); Ingram et al. (2008)). Two distinct vapor grown carbon nanofibers (VGCNFs) (typical diameters, 60-200nm; typical lengths, 20-100 μm) from Applied Science, Inc. were selected as nanoreinforcements in this examination: i) unmodified ("pristine") VGCNFs (PR-24-XT-LHT), and ii) surface-oxidized VGCNFs (PR-24-XT-LHT-OX). VGCNFs are relatively inexpensive and possess excellent mechanical properties. Table 1 contains a summary of materials used in nanocomposite preparation. Because of prevalent use in automotive applications, E-glass unidirectional and woven fabric plies are used as the primary traditional continuous fiber reinforcement phase in this investigation.

Table 1.List of materials

Material	Function	Manufacturer
Derakane 411-400	Epoxy vinyl ester resin	Ashland Co.
Cobalt naphthenate 6%	Promoter (catalyst)	North American Composites Co.
BYK-A515	Air release (antifoam) agent	BYK Chemie GmbH
BYK-A555	Air release (antifoam) agent	BYK Chemie GmbH
BYK-9076	Dispersing agent	BYK Chemie GmbH
PR-24-XT-LHT	Pristine VGCNF	Applied Sciences Inc.
PR-24-XT-LHT-OX	Oxidized VGCNF	Applied Sciences Inc.
MEKP	Curing agent (hardener)	U.S. Composites Inc.

Effects of Different Mixtures of Nanofibers/Polymer Matrices on Manufacturing

A general full factorial experimental design was established to study the effects of the type of VGCNF (A), use of dispersing agent (B), mixing method (C), and amount of VGCNF (D) on bulk thermal and mechanical nanocomposite properties. In the experimental design, the first three formulations and processing parameters (A, B, C) are treated as categorical (discrete) factors, whereas the amount of VGCNF (D) is treated as a continuous factor. A dispersing agent (DA) was used to facilitate nanocomposite dispersion. A combination of ultrasonication and/or high-shear mixing was used in specimen preparation (cf., Lacy et al. (2008)). Table 2 contains a summary of experimental factors and corresponding levels considered here.

Nanocomposite specimens were prepared using all possible combinations of formulation and processing factors for a total of 48 specimen configurations. Dynamic mechanical analysis (DMA) was performed for each configuration to measure storage and loss moduli (three repeat tests per configuration). In addition, four point bending tests were performed in accordance with ASTM Standard D-6272 to determine the flexural modulus and strength for each configuration (two replicates per configuration). The average values for storage, loss, and flexural moduli, as well as flexural strength, were used in the development of statistically-based response surface models (cf., Myers et al. (2009)) for identifying combinations of formulation and processing factors that lead to optimal nanocomposite properties.

Table 2. Design factors and their levels

Factor		Levels				
		1	2	3	4	5
A	Type of VGCNF	PR[1]	OX[2]	-	-	-
B	Use of DA	Yes	No	-	-	-
C	Mixing Method	US[3]	HS[4]	HS-US	-	-
D	Amount of VGCNF (phr[5])	0	0.25	0.50	0.75	1.00

[1]PR = pristine; [2]OX = oxidized; [3]US = ultrasonication; [4]HS = high-shear mixing; [5]phr = parts per hundred resin

Dynamic mechanical analysis (DMA)

Using DMA test results, statistically reliable response surface models for predicting storage and loss moduli as a function of experimental design factors (Table 2) were developed (Nouranian et al., 2009a, 2009b, 2009c). Based upon an analysis of variance, use of oxidized VGCNFs led to slightly improved material properties. Figure 1 shows predicted values for nanocomposite storage and loss modulus as a function of the amount of oxidized VGCNFs. In the figure, the moduli have been normalized by the corresponding moduli of the neat VE resin.

In general, the storage modulus can be regarded as a measure of the elastic stiffness of the material. The amount of VGCNF has a significant effect on nanocomposite storage modulus (Figure 1a). The predicted storage modulus increases with increasing nanofiber weight fraction until a maximum value is obtained at a weight fraction of roughly 0.5 phr. The storage modulus (e.g., stiffness) generally decreases at high VGCNF loadings. This suggests that nanofiber dispersion and agglomeration may be a concern at higher weight fractions of VGCNFs. Use of a DA in the nanocomposite formulation leads to an increase in predicted storage modulus for all configurations, arguably as a consequence of improved nanofiber dispersion. Similarly, configurations involving more aggressive high-shear (HS) mixing or coupled high-shear mixing/ultrasonication (HS-US) generally produced an improvement in predicted storage modulus for a given weight fraction of VGCNF. Nanofiber agglomeration is a major issue in the fabrication of VGCNF/VE nanocomposites. The use of DA in combination with the mechanical mixing facilitates the breaking of VGCNF agglomerates into individual nanofibers.

The loss modulus can be viewed as a measure of the toughness or energy dissipation capability of the material. The predicted loss modulus generally decreases with increasing nanofiber weight fraction (Figure 1b). This makes sense since an increase in stiffness (e.g., storage modulus) is typically accompanied by a corresponding decrease in toughness (loss modulus). Since the DA acts as a plasticizer, the use of a DA leads to a higher predicted loss modulus at all nanofiber weight fractions. In addition, less aggressive ultrasonication (US) mixing also led to higher predicted loss moduli. This suggests that nanofiber agglomerates, while having a detrimental effect on nanocomposite strength due to local stress concentrations, may dissipate more energy during deformation than individual well dispersed nanofibers.

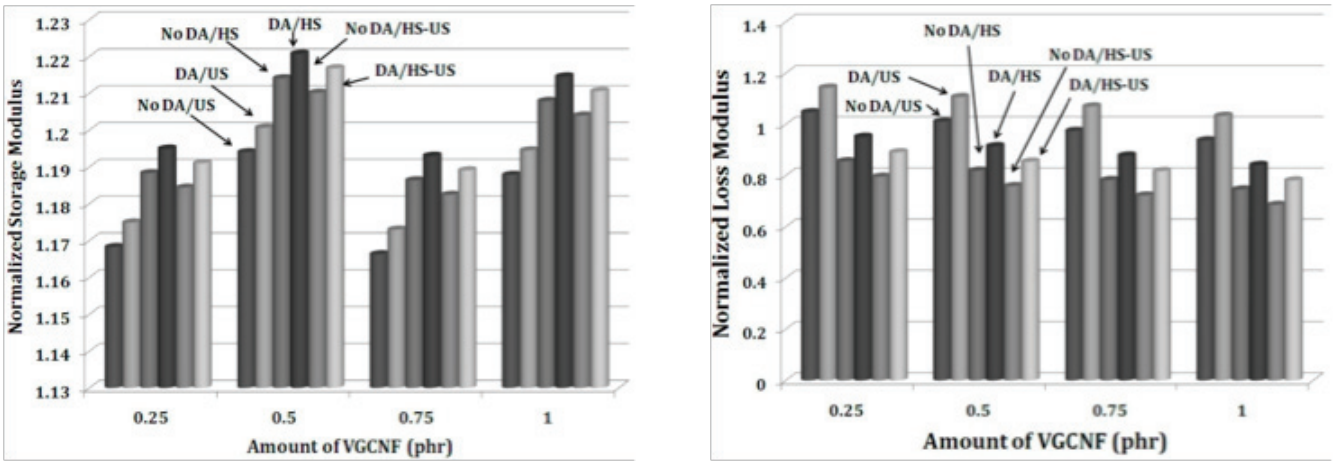

a) b)

Figure 1. Predicted a) storage modulus and b) loss modulus of oxidized VGCNF/VE nanocomposites.

Using the experimental design and response surface methodology implemented in this study, a numerical optimization procedure was employed to identify the combination of experimental factors that optimize a desired nanocomposite response (cf. Myers et al. (2009)). For example, Table 3 contains a summary of the combination of type of VGCNF, use of DA, amount of VGCNF, and mixing method that will maximize the storage modulus. The table also contains the combination of factors that maximize both storage and loss moduli, as well as those that maximize storage modulus while simultaneously minimizing loss modulus. Essentially, based upon the set goals and other factors (cf. Myers et al. (2009)), this procedure maximizes an objective (desirability) function that ranges from zero to a target value of unity.

Table 3.Numerical optimization results

		Goals		
		1: Max. Storage Modulus	**2: Max. Storage & Loss Modulus**	**3: Max. Storage Modulus/ Min. Loss Modulus**
Optimal Condition	A: Type of VGCNF	OX[1]	OX	OX
	B: Use of DA[2]	Yes	Yes	No
	C: Mixing Method	HS[2]	HS	HS/US[3]
	D: Amount of VGCNF	0.43 phr[4]	0.42 phr	0.46 phr
Normalized Storage Modulus		1.22	1.22	1.21
Norm. Loss Modulus		0.92	0.93	0.76
Desirability		0.839	0.848	0.867

[1]OX = oxidized; [2]HS = high-shear mixing; [3]US = ultrasonication; [4]phr = parts per hundred resin

These results suggest that it may be possible to tailor the fabrication and processing of nanocomposites to produce optimal macroscopic properties. Note that the addition of very small amounts of VGCNFs (<1 phr) to a thermosetting VE resin can lead to a substantial increase in storage modulus (stiffness). The mechanical properties can be further improved with better VGCNF dispersion by the use of DA, surface-oxidized nanofibers, and aggressive mixing.

Flexural testing and modeling

Using four point bending test results, statistically reliable response surface models for predicting flexural modulus and strength as a function of experimental design factors (Table 2) were developed. Similar to DMA test results, use of oxidized VGCNFs led to slightly improved flexural properties. Figure 2 shows predicted values for nanocomposite flexural modulus and strength as a function of the amount of oxidized VGCNFs, where the moduli and strengths have been normalized by the corresponding properties of the neat VE resin.

The predicted flexural modulus increased with increasing nanofiber weight fraction until a maximum value was obtained at a weight fraction in the range 0.5-0.75 phr (Figure 2a); here the predicted flexural modulus exceeded that of the neat resin by roughly 15%. The stiffness generally decreased at high VGCNF weight fractions. Similar to the storage modulus predictions, these results suggest that nanofiber dispersion and agglomeration may be a concern at higher weight fractions of VGCNFs. Use of a DA in the nanocomposite formulation led to a notable increase in predicted flexural modulus for specimens prepared using ultrasonication (US) mixing alone. For specimens prepared using a more aggressive high-shear (HS) mixing, use of a DA resulted in a slight decrease in estimated flexural properties for a given weight fraction of VGCNF. This may be due to the plasticizing effect of the DA on the VE resin, as well as breaking (shortening) of VGCNFs during high-shear mixing. Scanning electron microscopy (SEM) is being used to investigate the issues of nanofiber shortening during mixing.

The effect of fabrication and processing has a profound impact on predicted flexural strengths.

For example, Figure 2b shows that the predicted flexural modulus for specimens prepared using sonication mixing fell below that of the neat VE resin, i.e., the inclusion of VGCNFs has a detrimental effect on strength. This is likely due to relatively poor dispersion of nanofibers and the presence of VGCNF agglomerates. SEM images of the fracture surface of failed flexural specimens suggest that failure typically initiates from agglomerated nests of nanofibers (Figure 3). Conversely, specimens prepared using high-shear (HS) mixing showed an improvement in predicted strengths relative to the neat VE resin. The use of a DA led to a slight improvement in strength; this is likely attributable to somewhat better dispersion of nanofibers as well as the plasticizing (toughening) effect of the DA on the VE resin.

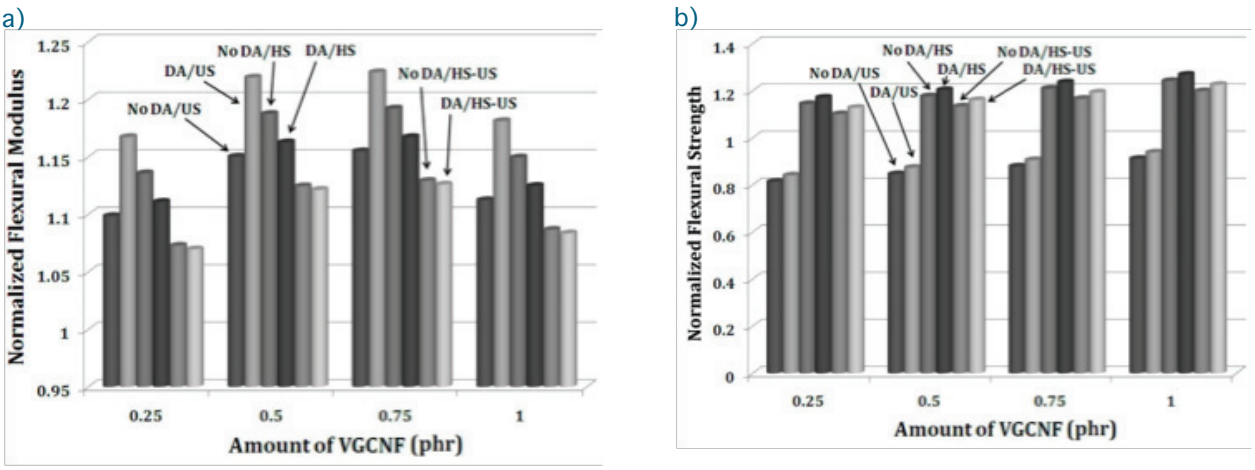

Figure 2. Predicted flexural a) modulus and b) strength of oxidized VGCNF/VE nanocomposites.

These results underscore the crucial role fabrication and processing have on bulk nanocomposite properties. Using a design of experiments approach, it is possible to isolate the coupled influence of various combinations of material, processing, and fabrication factors that lead to improved nanocomposite performance. For example, a numerical optimization procedure (cf. Myers et al. (2009)) was employed to identify the combination of experimental factors that simultaneously maximize storage modulus, flexural modulus, and flexural strength, while minimizing loss modulus. Based upon the optimization results, the nanocomposite configuration leading to the desired material properties corresponds to a specimen prepared with oxidized nanofibers, DA, high-shear mixing, and a nanofiber weight fraction of ~0.60 phr. Such results can guide the selection of additional nanocomposite configurations for future study and can drastically reduce the number of analyses and tests required to determine an optimal configuration.

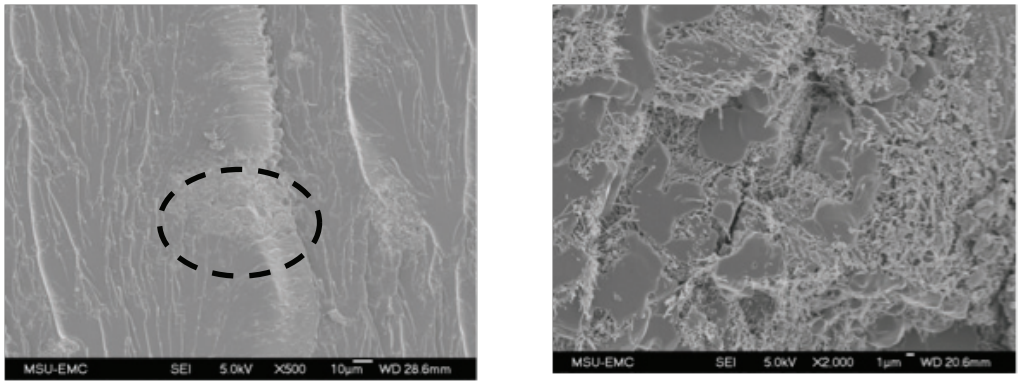

a) b)

Figure 3: SEM fracture surface images from flexure specimen: a) VGCNF agglomeration (500X), and b) VGCNF clusters within the agglomeration (2000X).

Nanocomposite Failure Modes and Energy Absorption Characteristics

Strain rate-dependent mechanical response of VGCNF/VE nanocomposites

Split Hopkinson Pressure Bar (SHPB) testing was performed to investigate the dynamic uniaxial compressive response of pristine VGCNF/ VE nanocomposites (Hutchins et al. (2009)). Four different material configurations were considered: 1) pure VE resin (neat VE), 2) neat VE with 1.00 phr DA (neat VE-DA), 3) VE with 0.50 phr VGCNF (VE-0.50CNF), and 4) VE with 1.00 phr VGCNF (VE-1.00CNF). VGCNFs/DA were mixed at a 1:1 ratio by weight. The neat VE-DA configuration was tested to assess the plasticizing effect of the DA on the bulk properties of the resin. Nanocomposite specimens were prepared using coupled high-shear mixing/ ultrasonication. A minimum of five repeat tests were performed for each material configuration at strain rates of 750 s^{-1}, 1550 s^{-1}, and 2350 s^{-1}; such strain rates arguably span the range of values experienced during automotive crashes.

The dynamic compressive stress-strain behavior was determined for each specimen, and the effect of loading rate on the apparent elastic modulus, yield strength, ultimate strength, and ultimate strain were determined. For example, Figure 4 shows the average elastic modulus and yield strength, respectively, from the tests. In the figure, the moduli and strengths have been normalized by corresponding values for the neat resin obtained at a quasi-static strain rate of 10^{-2} s^{-1}. In general, the apparent elastic modulus tended to increase significantly with increasing strain rate for a given configuration (Figure 4a). Note that the apparent moduli for neat VE specimens exceed those of the neat VE-DA specimens at all strain rates. This is likely due to the plasticizing effect of the DA on the VE resin as well as thermally induced softening at higher strain rates. Similarly, the inclusion of a nominal amount of nanofibers in the VE-0.50CNF specimens resulted in an improvement in apparent modulus in comparison to those of the neat VE-DA specimens. The relative decrease in apparent modulus for the VE-0.50CNF specimens at a strain rate of 2350 s^{-1} likely is attributable to thermal softening of the polymer resin. Note that the apparent moduli of the VE-1.00CNF specimens fell below those of any other configuration. SEM imaging of such specimens suggests that lack of nanofiber dispersion may be a key issue as the weight fraction of nanofibers is increased.

All configurations showed a significant increase in apparent yield strength over the range of strain rates (Figure 4b). For specimens prepared with a DA, however, the relative improvement in yield strength was not as pronounced at higher strain rates; the mechanism behind this observation is the topic of ongoing research. The reduction in stiffness properties (cf. Figure 4a) at higher VGCNF loadings is consistent with DMA and flexural test results, as well as results from the literature (Hussain et al. (2006); Plaseied et al. (2008); Lee et al. (2009)).

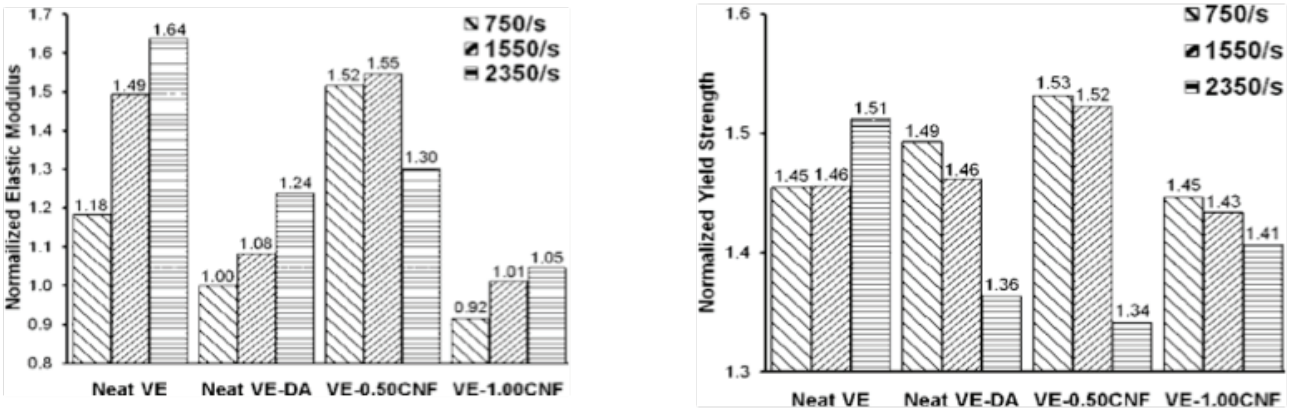

a) b)

Figure 4: Rate dependent nanocomposite a) elastic modulus and b) yield strength from SPHB testing.

Energy absorption characteristics of VGCNF-VE/E-glass composites

Flat platen compression testing of filament wound cylindrical E-glass crush tube specimens was initiated to investigate the energy absorption characteristics of continuous fiber composites reinforced with a VGCNF/VE resin (Figure 5). Five specimens were prepared using two different resin compositions: i) neat VE, and ii) VGCNF/ VE prepared using 0.38 phr oxidized VGCNFs, DA, and high-shear mixing. Continuous E-glass fiber tows were drawn through a liquid resin bath and filament wound around a one inch diameter mandrel in a [90°_2/+45°/-45°] layup and then cured (specimen preparation was performed by S. Roy at the University of Alabama).

Crush tube specimens were subjected to quasi-static compression under displacement control conditions. While the observed crush behavior of E-glass/VE specimens was superior to that of E-glass/VGCNF/ VE specimens, the disparity was attributable, in part, to poor E-glass fiber wetting due to the increased viscosity of the VGCNF/VE resin. This issue is currently being addressed.

Figure 5. Experimental setup for filament wound crush tube testing.

Nanocomposite Multiscale Modeling

Materials property data obtained from structure-property tests are being used in the development and validation of representative volume element (RVE) based multiscale models. One key issue is the establishment of an empirically validated material model (and appropriate homogenization technique) for predicting effective properties of the VGCNF/VE resin; a combination of molecular dynamics, micromechanics, and finite element (FE) simulations are currently being employed.

Coarse-grained molecular models for determining nanocomposite interphase properties

Coarse-grained molecular models (Shan et al. (2001); Clancy and Hinkley (2004); Chowdhury and Okabe (2007)) for simulating single nanofiber pullout from a cross-linked VE resin are being developed using the Materials Studio v4.4 software (Figure 6). VGCNFs are modeled as a series of concentrically stacked carbon nanocones and a robust energy minimization algorithm is used to identify the stable molecular configurations. Such models will be used to estimate the volume fraction, properties, and strength of the interphase region between VGCNF and VE resin, which can be passed on to higher length scale calculations.

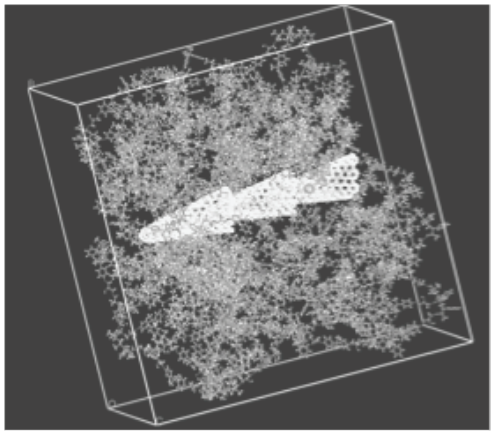

Figure 6.RVE model of 1.5wt% VGCNF and randomly distributed VE monomers.

Multiscale progressive failure models of nanoreinforced composites

Classical micromechanics approaches (Mori-Tanaka, self consistent, coated inclusion methods, etc.; cf. Mura (1991)) are being used to establish effective properties of the nanoreinforced matrix. These models are being used to assess the effect of the following: i) changes in VGCNF aspect ratio due to breakage during high-shear mixing, ii) different types, orientations, and volume fractions of nanoreinforcements (VGCNFs, nanoplatelets, nanospheres, etc.), and iii) VGCNF/VE interphase properties. Interphase properties will be determined from coarse-grained molecular simulations or by solving an inverse problem using bulk material properties.

Effective VGCNF/VE properties from micromechanics simulations and/or bulk structure property tests will be used in the development of computationally efficient material and geometric nonlinear FE models for predicting progressive failure of nanoreinforced continuous fiber composite structures. The NASA special purpose multiscale composite failure analysis code MAC/GMC (Micromechanics Analysis Code with Generalized Method of Cells; Bednarcyk and Arnold (2002)) is being used in conjunction with the ABAQUS FE solver to predict failure of E-glass plain-weave woven fabric laminates. MAC/GMC uses a robust local-to-global iteration scheme where a hierarchy of repeating unit cells (RUCs) is used to explicitly model composite material structure and morphology over a range of length scales. The generalized method of cells (Paley and Aboudi (1992); Aboudi et al.(2001)) is used to predict local field quantities within each RUC; homogenized material properties are then calculated at each FE integration point. The effect of local damage or failure at the constituent level is automatically propagated at each load or time step to the global FE scale through the change in homogenized stiffness properties. Figure 7 shows an ABAQUS finite element mesh of a filament wound composite crush tube and its corresponding MAC/GMC representation. Modeling and simulation activities will continue into the upcoming year.

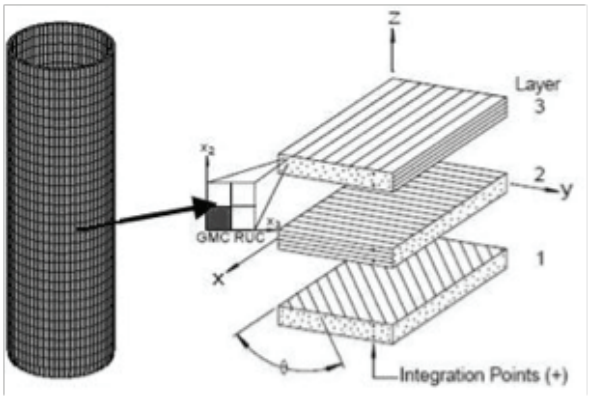

Figure 7.FE mesh of a filament wound crush tube with corresponding MAC/GMC representation.

Conclusions

The goal of this investigation is to exploit expertise in polymer chemistry, composite materials processing, and computational solid mechanics to design, synthesize, test, and analyze cost-effective multiscale engineered nanocomposites for automobile primary structural applications. One key challenge is to establish empirically validated multiscale methodologies, based on the morphologies and geometries of real heterogeneous materials, to obtain structure-property relationships over a wide range of length scales.

A crucial aspect of the work is that structure-property relations will be experimentally validated using a combination of fine-scale and macroscale tests. This study should facilitate the development of engineered multiscale materials design by providing insight into relationships between nanomaterial fabrication/processing, chemical and physical characteristics, and interaction and evolution of structure across disparate spatial scales that lead to improved macroscale performance.

2009 Presentations/Publications/Patents (5)

1. Hutchins, JW; Sisti, J; Lacy, TE; Nouranian, S; Toghiani, H; and Pittman Jr, CU. High Strain Rate Behavior of Carbon Nanofiber Reinforced Vinyl Ester. In: Proceedings of the 50th AIAA/ ASME/ ASCE/ AHS/ ASC Structures, Structural Dynamics, and Materials Conference; 2009 May 4-7; Palm Springs, CA.

2. Nouranian, S; Toghiani, H; Lacy, TE; and Pittman Jr, CU. Experimental Study of the Dynamic Mechanical Properties of Vapor-Grown Carbon Nanofiber/Vinyl Ester Nanocomposites Fabricated Using Coupled High-Shear Mixing and Ultrasonication. In: Proceedings of the 2009 Annual Meeting of the AIChE; 2009 Nov 8-13; Nashville, TN. (2009a).

3. Nouranian, S; Toghiani, H; Lacy, TE; and Pittman Jr, CU. Response Surface Study of Vapor-Grown Carbon Nanofiber/Vinyl Ester Nanocomposites Fabricated Using High-Shear Mixing. In: Proceedings of the 24th Annual Technical Conference of the American Society for Composites; 2009 Sept 15-17; Newark, DE. (2009b).

4. Nouranian, S; Toghiani, H; Lacy, TE; and Pittman Jr, CU. Viscoelastic Properties of Vapor-Grown Carbon Nanofiber/Vinyl Ester Nanocomposites. In: Proceedings of the International SAMPE Symposium and Exhibition, SAMPE'09; 2009 May 18-21; Baltimore, MD. (2009c).

5. Zhou, Y; Jeelani, S; and Lacy, T. Fabrication and Characterization of Vapor Grown Carbon Nanofiber Reinforced Polyester. In: Proceedings of the 24th Annual Technical Conference of the American Society for Composites; 2009 Sept 15-17; Newark, DE.

References

ABAQUS 6.7, 2009, Simulia, Inc.

Aboudi, J; Pindera, MJ; and Arnold, SM. 2001 Linear Thermoelastic Higher Order Theory for Periodic Multiphase Materials. J Appl Mech 68:697-707.

ASTM D6272. Standard Test Method for Flexural Properties of Unreinforced and Reinforced Plastics and Electrical Insulating Materials by Four-Point Bending. ASTM, Philadelphia, PA, 2002.

Bednarcyk, BA and Arnold, SM. 2002. Micromechanics Analysis Code With Generalized Method of Cells (MAC/GMC), User's Manual: Version 4.0. NASA-TM-2002-212077.

Buryachenko, VA; Roy, A; Lafdi, K; Anderson, KL; and Chellapilla, S. 2005. Multi-Scale Mechanics of Nanocomposites Including Interface: Experimental and Numerical Investigation. Comp Sci Tech. 65:2435-65.

Chowdhury, AC and Okabe, T. 2007. Computer Simulation of Carbon Nanotube Pull-Out from Polymer by the Molecular Dynamics Method. Comp: Part A 38:747-54.

Clancy, TC and Hinkley, J. 2004. Coarse-Grained and Atomistic Modeling of Polyamides. NASA/TM-2004-213030.

Fisher, FT; Bradshaw, RD; and Brinson, LC. 2007. Fiber Waviness in Nanotube-Reinforced Polymer Composites: I. Modulus Predictions Using Effective Nanotube Properties. Submitted: Comp Sci Tech.

Gates, TS; Odegard, GM; Frankland, SJV; and Clancy, TC. 2005. Computational Materials: Multi-Scale Modeling and Simulation of Nanostructured Materials. Comp Sci Tech 65:2416-34.

Ghoniem, NM; Busso, EP; Kioussis, N; and Huang, H. 2003. Multiscale Modelling of Nanomechanics and Micromechanics: An Overview. Phil Mag 83(31–34):3475-3528.

Hussain, A; Hojjati, M; Okamoto, M; and Gorga, RE. 2006. Review article: Polymer-Matrix Nanocomposites, Processing, Manufacturing, and Application: An Overview. J Comp Matl 40(17):1511-75.

Ingram, J; Zhou, Y; Jeelani, S; Lacy, T; and Horstemeyer, MF.2008. Effect of Strain Rate on Tensile Behavior of Polypropylene and Carbon Nanofiber Filled Polypropylene. Matl Sci Eng A 489(1):99-106.

Lacy, TE; Pittman Jr, CU; Toghiani, H; Nouranian, S; Hutchins, J; Zhou, Y; Jeelani, S; and Carpenter, JA. 2008. Structural Nanocomposite Design. DOE SRCLID FY 2008 Progress Report.

Lee, HN; Paeng, K; Swallen, SF; Ediger, MF. 2009. Direct Measurement of Molecular Mobility in Actively Deformed Polymer Glasses. Sci 323:231-34.

Liu, H and Brinson, LC. 2006. A Hybrid Numerical-Analytical Method for Modeling the Viscoelastic Properties of Polymer Nanocomposites. J Appl Mech 73:758-68.

Materials Studio v4.4, Accelrys, Inc., San Diego, CA, 2001.

Mura, T. 1991. Micromechanics of Defects in Solids. 2nd ed. The Hague: M. Nijhoff Publ.

Myers, RH; Montgomery, DC; and Anderson-Cook, CM. 2009. Response Surface Methodology: Process and Product Optimization Using Designed Experiments. New York: John Wiley & Sons. p. 261.

Odegard, GM; Gates, TS; Nicholson, LM; and Wise, KE. 2001. Equivalent-Continuum Modeling of Nano-structured Materials. NASA/TM 210863 p. 1-30.

Odegard, GM; Clancy, TC; and Gates, TS. 2005. Modeling of the Mechanical Properties of Nanoparticle/Polymer Composites. Polym. 46:553-62.

Paley, M and Aboudi, J. 1992. Micromechanical Analysis of Composites by the Generalized Cells Model. Mech Matl 14:127-39.

Plaseied, A; Fatemi, A; and Coleman, MR. 2008. Influence of Carbon Nanofiber Content and Surface Treatment on Mechanical Properties of Vinyl Ester.Polym Polym Comp 16(7):405-13.

Shan, L; Robertson, CG; Verghese, KNE; Burts, E; Riffle, JS; Ward, TC; and Reifsnider, KL. 2001. Influence of Vinyl Ester/Styrene Network Structure on Thermal and Mechanical Behavior. J Appl Polym Sci, 80(7):917-27.

Thostenson, ET; Li, C; and Chou, TW. 2004. Nanocomposites in Context. Comp Sci Tech 65:491-516.

Valavala, PK and Odegard, GM. 2005. Modeling Techniques for Determination of Mechanical of Polymer Nanocomposites. Rev Adv Matl Sci 9:34-44.

Zhou, Y; Akanda, SR; Jeelani, S; and Lacy, TE. 2007. Nonlinear Constitutive Equation for Vapor-Grown Carbon Nanofiber-Reinforced SC-15 Epoxy at Different Strain Rate. Matl Sci Eng A 465 (1):238-46.